Synthesis and characterization of phosphino nickel(II) complexes and their silica immobilized versions for the hydrogenation of furfural to furfuryl alcohol

Menala Kalumpha

A dissertation submitted in fulfilment of the requirements for the degree

Master of Science in Chemistry

UNIVERSITY OF JOHANNESBURG

Department of Chemical Sciences

Supervisor: Dr. Banothile C.E. Makhubela

Co-supervisor: Dr. Leah C. Matsinha

December 2020

DECLARATION

I hereby declare that the thesis: Synthesis and characterization of phosphino nickel(II) complexes and their silica immobilized versions for the hydrogenation of furfural to furfuryl alcohol: is my original work and has never been presented for the award of any degree in any other university. All information, references and sources used have been duly acknowledged by means of complete references.

I grant the University of Johannesburg free license to reproduce the dissertation in whole or in-part for the purpose of research.

Name: Menala Kalumpha

Signature..... Date.....

DEDICATION

This dissertation is dedicated to my family and best friend who supported me throughout my academic career.

ACKNOWLEDGEMENTS

To my rock Jesus Christ, thank you Lord for your faithfulness.

My greatest appreciation goes to my supervisors Dr Banothile Makhubela and Dr Leah Matsinha for their guidance and constant encouragement throughout the project.

To Dr C Rono, Mr J Lamola and Ms P Moyo for their assistance and advices.

To Mr Mutshinyalo Nwamadi (Spectrum staff, University of Johannesburg) for his assistance in NMR studies.

Many thanks to the Organometallic research group members at the University of Johannesburg for their invaluable advices and encouragement.

My heartfelt appreciation to my family and best friend Flarity for their support and unconditional love will forever be grateful.

Finally, I acknowledge the financial support provided by Royal Society (FLAIR) and African Academy of Sciences (ASA) and National Research Foundation (NRF).

TABLE OF CONTENTS

LIST OF FIGURES

LIST OF TABLES

LIST OF SCHEMES

ABSTRACT

Two phosphino ligands, **L1** which is a siloxane ligand and **L2** which is a schiff base ligand were synthesized and characterized using nuclear magnetic resonance spectroscopy. Complexation reactions of purchased ligands (triphenylphosphine, Bis(cyclopentadienyl) nickel(II)) , **L1** and **L2** gave half-sandwich and tridentate O^N^O Ni(II) complexes. The ligand **L1** was used in the synthesis of complex **C2** and **C3** while the ligand **L2** was used in the synthesis of complex **C4**, **C5** and **C6**. The molecular complexes (**C1**, **C2**, **C4**, **C5**) were characterized using spectroscopic and analytical techniques. The heterogenized complexes **C3** and **C6** were characterized using surface techniques such as BET, PXRD, ICP-MS, SEM, TEM and infrared spectroscopy.

All the complexes were evaluated as pre-catalysts in the hydrogenation of furfural using molecular hydrogen and all the catalysts showed activity and selectivity towards formation of furfuryl alcohol. The complex **C1** showed excellent catalytic activity up to three cycles. Catalyst poisoning was observed in the mercury poisoning experiments with pre-catalysts **C1**, **C4** indicating that some of the catalytic activity observed might be due to nanoparticles activity.

Complexes **C1** and **C4** were also evaluated as pre-catalysts for the hydrogenation of furfural using formic acid as hydrogen donor. Both catalytic systems displayed good activity and selectivity towards furfuryl alcohol. The highest turnover number obtained was 1859 using pre-catalyst **C1** at 4 hours. Pre-catalyst **C1** also proved to be recyclable and could be recycled four times with a drop in conversion of furfural in the fourth cycle. Catalytic transfer of cinnamaldehyde and 2-thiophenecarboxaldehyde was also explored using pre-catalysts **C1** and **C4** to determine whether these complexes were selective towards the aldehyde or the ring. Both pre-catalysts **C1** and **C4** displayed activity in the conversion of cinnamaldehyde and selectivity towards cinnamyl alcohol. The pre-catalysts also displayed activity in the conversion of 2-thiophenecarboxaldehyde and selectivity towards 2-thiophenemethanol.

LIST OF ABBREVIATIONS AND MEANING OF SYMBOLS

g	gram (s)
mg	milligram (s)
mL	millilitre (s)
m	mole (s)
mmol	millimole (s)
^{o}C	degrees Celsius
MHz	mega hertz
H	hour (s)
m/z	mass to charge ratio
rt	room temperature
v	wavenumber
MP	melting point
EA	elemental analysis
ẟ	chemical shift
S_{BET}	specific surface area

V_p	pore volume
D_p	pore diameter
$CDCl_3$	deuterated chloroform
NMR	nuclear magnetic resonance
^{1}H NMR	proton nuclear magnetic resonance
$^{13}C\{^{1}H\}$ NMR	carbon -13 decoupled nuclear magnetic resonance
$^{31}P\{^{1}H\}$ NMR	phosphorus- 31 decoupled nuclear magnetic resonance
$^{29}Si\{^{1}H\}$ NMR	silicon- 29 decoupled nuclear magnetic resonance
COSY	correlation spectroscopy
HSQC	heteronuclear single quantum correlation
ESI-MS	electrospray ionisation-mass spectrometry
FTIR	Fourier transform infrared spectroscopy
EDX	Energy dispersive x-ray spectroscopy
SEM	scanning electron microscopy
TEM	transmission electron microscopy
PXRD	powder x-ray diffraction

ICP-MS	Inductively coupled plasma mass-spectroscopy
BET	Brunauer-Emmett-Teller
FF	furfural
FA	furfuryl alcohol
MF	methylfuran
THF	tetrahydrofuran
THFA	tetrahydrofurfuryl alcohol
EtOH	ethanol
MeOH	methanol
PPh_3	triphenylphosphine
TON	turnover number
TOF	turnover frequency

Chapter one

Literature review on the origin of furfural and its valorisation using different catalysts

1.1 Introduction

The demand for both petrochemical products and fossil fuels is increasing rapidly as a result of industrialization and population increase therefore the world needs sustainable, energy efficient fuels and chemicals.[1,2] The conversion of biomass into valuable chemicals has become increasingly popular since biomass serves as a green substitute.[3] The use of biomass instead of petroleum derived chemicals is advantageous because it is carbon neutral and there is an abundance of biomass particularly lignocellulosic biomass.[4] Energy from biomass has been reported to reduce the accumulation of carbon dioxide in the atmosphere and as a result can be used to substitute fossil fuels which accumulate carbon dioxide.[5,4]

1.2 Biomass composition and conversion into valuable building blocks

Biomass can be regarded as organic material usually obtained from plants.[6] Agricultural waste is a common source of biomass used for the production of bio-fuels and bio-chemicals which help reduce carbon dioxide emission into the atmosphere.[7] There are different types of biomass namely wood, crops, old newspapers and garbage.[8] The highest source of renewable biomass is lignocellulosic material which includes cellulose (40-50 %), hemicellulose (25-35 %) and lignin (15-20 %).[9] Hemicellulose is more unstable than cellulose hence it is easily converted to xylose through hydrolysis and can further be converted to furfural.[8] Moreover, hemicellulose is more soluble in hot water compared to cellulose because of its crystalline structure and hence can be easily hydrolysed into the desired product.[10]

1.2.1 Cellulose

Cellulose is the major component of lignocellulosic biomass that can be regarded as a homo-polysaccharide that is made up of glucose units linked by (1-4)-glycosidic bonds.[11]

It is made up of straight chains which enable the formation of intra and inter molecule hydrogen bonds as shown in Fig 1.1. In addition, cellulose can be produced through the removal of lignin and hemicellulose from the lignocellulosic material by enzymatic hydrolysis since it is insoluble.[12] Cellulose is used to manufacture cardboard and paper in

the pulp and paper industry and also for the production of commercial products such as carboxymethyl cellulose and rayon.

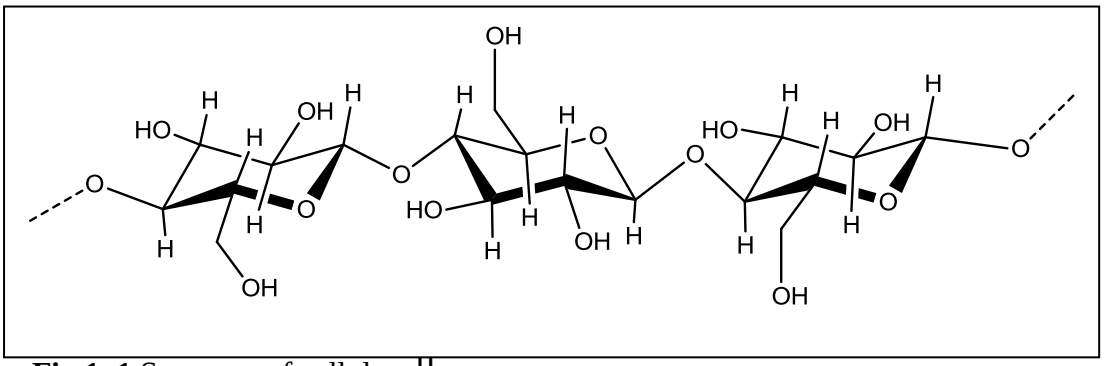

Fig 1. 1 Structure of cellulose[11]

1.2.2 Hemicellulose

It is the second most abundant polymer which is made up of mainly hexose and pentose sugars. It has a cell wall matrix that is well stabilized by hydrogen bonds as shown in Fig 1.2. Hemicellulose is amorphous in nature making it easy to attack by acids[11,13] to afford their monomeric components (monosaccharides) such as D-mannose, D-xylose and D-glucose.

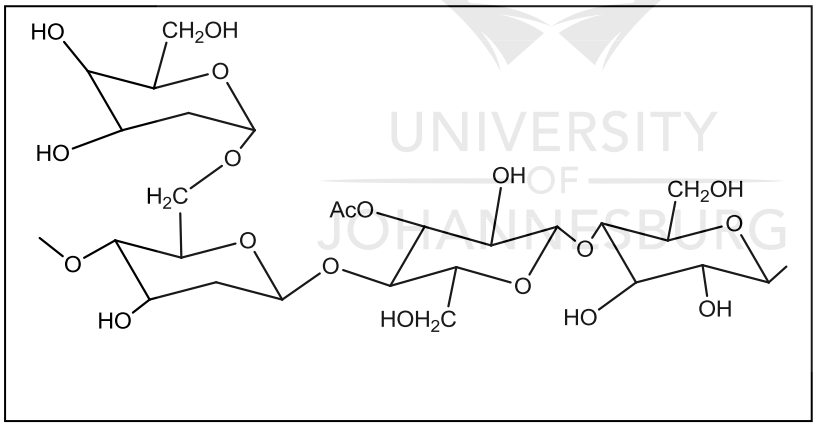

Fig 1. 2 Structure of hemicellulose[11]

1.2.3 Lignin

Lignin is derived from phenylalanine as an amorphous polymer of aromatic subunits[14] as shown in Fig 1.3. Lignin is known to be the binding (glue) agent that strongly binds together cellulose and hemicellulose by filling the space between them and is made up of largely aryl ether groups[15,16].

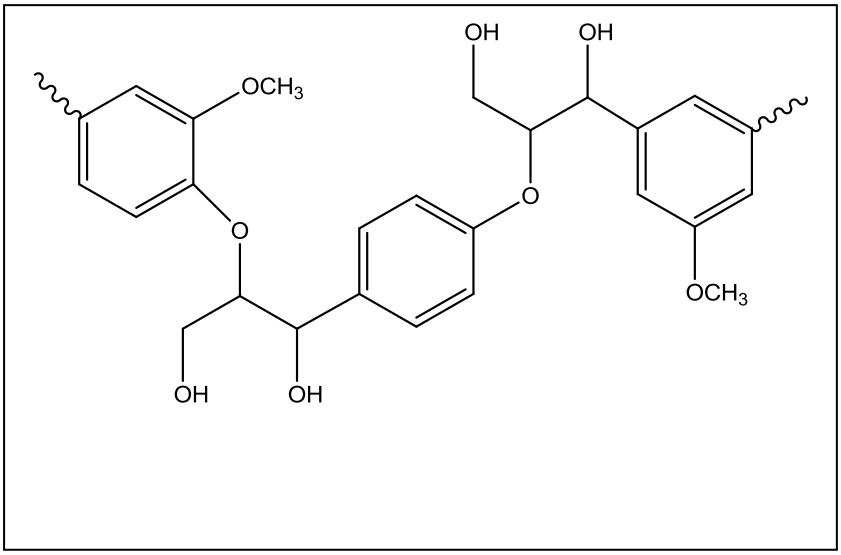

Fig 1. 3 Structure of lignin[16]

1.3 Bio-refinery

It is the concept of combining a series of technologies with the goal of converting biomass into value-added products such as liquid fuels, chemicals and thermal or electrical energy through biomass combustion and/or conversion (Fig 1.4).[17]

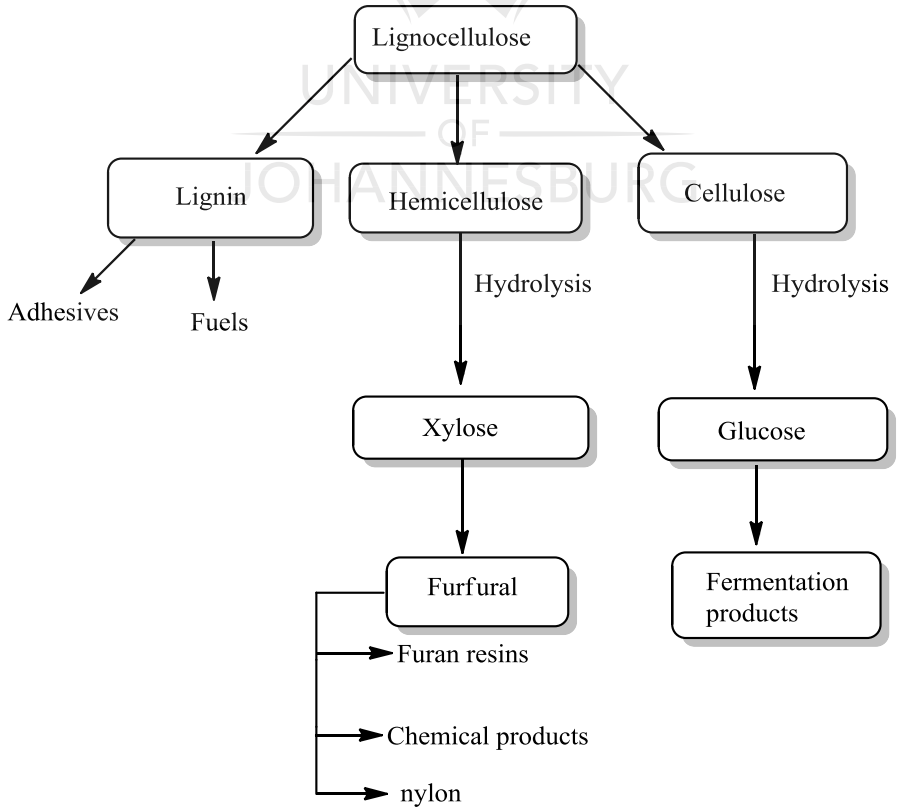

Fig 1. 4 Lignocellulosic- feedstock biorefinery[17]

Conversion of lignocellulosic biomass into fuels and chemicals can be done using processes such as gasification, pyrolysis, liquefaction and hydrolysis.[12,18]

1.3.1Gasification

Gasification is a thermo-chemical process used in biomass treatment where the reactants diffuse through gas films resulting in the formation of gaseous fuels.[19] This process is known to be economical hence most researchers have shown interest in production of energy from biomass using gasification. During heating of the biomass, there is activation of the sites on the ash catalyst causing the oxygen, hydrogen and carbon molecules chemisorbed on the ash sites to react to form carbon monoxide, carbon dioxide, hydrogen hydrocarbons and methane.[19,5] This process is compatible with the known cola to liquids process that uses coal as a feedstock to produce monoxide, hydrogen and carbon dioxide which are then subjected to Fischer-Tropsch synthesis (also known as coal-to-liquids, CTL) leading to gaseous and liquid hydrocarbons. In the latter case where biomass is used as a feedstock in gasification, the process is termed biomass-to-liquids (BTL). Biomass gasification can also be used to produce electricity, raw materials for chemicals production and heat as shown in Fig 1.5.

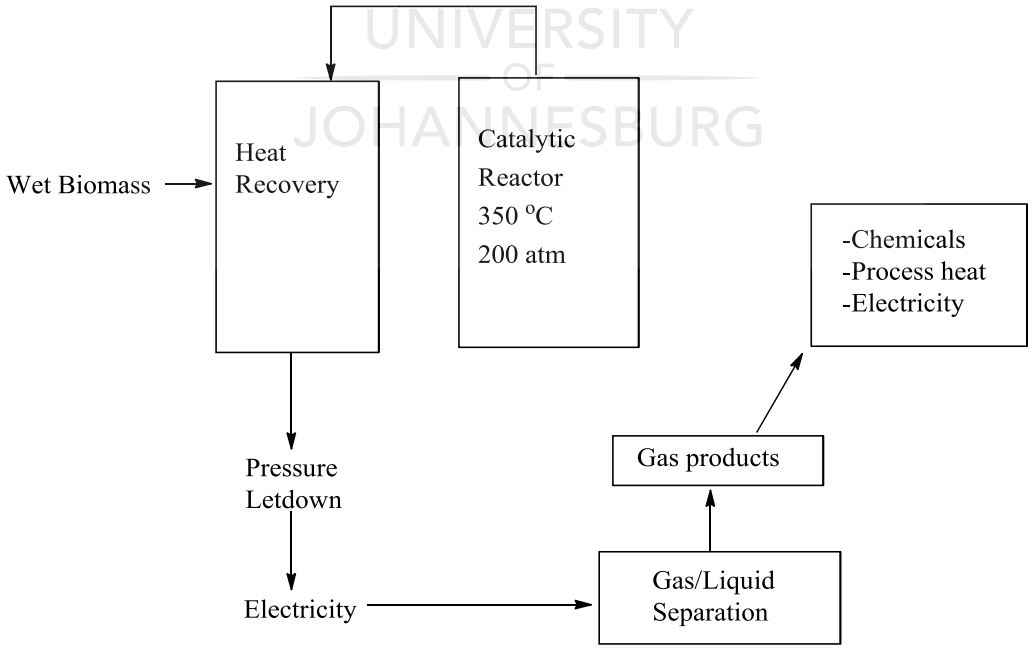

Fig 1. 5 Biomass gasification[20]

1.3.2 Pyrolysis

Biomass pyrolysis is a direct thermal process where the biomass organic matrix is decomposed in the absence of oxygen to obtain solid, liquid and gaseous products.[14] Pyrolysis is divided into two methods; namely fast and slow pyrolysis. Fast pyrolysis causes the biomass to decompose quickly forming a high percentage of gas products whilst slow pyrolysis results in homogenous liquid. Researchers are investigating the effect of pyrolysis conditions and residence time since they have been reported to have an effect on the final products obtained in biomass upgrading.[21] One of the solid products obtained from biomass pyrolysis is biochar which is used as activated carbon for various applications, such as metal catalysts (supports) and even directly as an activated carbon catalyst, in for example decarboxylation reactions.[22] The liquid products are used for the manufacture of fertilizers and adhesives.[14]

1.3.3 Liquefaction

Hydrothermal liquefaction is used to produce water insoluble products such as biocrude which is a liquid used in the production of bio-fuels. The liquid products obtained from biomass liquefaction often include aqueous solution of dissolved organic materials and biocrude of interest to most researchers in bio-refinery.[23] Unlike in pyrolysis of biomass, in biomass liquefaction there is no formation of char or ash.[23,24] Liquefaction is used in the paper industry for splitting black liquor.

1.3.4 Hydrolysis

Hydrolysis of biomass can be differentiated into acid hydrolysis, alkaline hydrolysis and enzymatic hydrolysis.[13] Concentrated acid is introduced into the cellulose structure which causes the cellulose to swell leading to breakage of the glycosidic bonds to give glucose units and oligomers, also known as industrial sugars.[25] The use of concentrated acids consumes low energy and as a result it was highly used in industry. However due to disadvantages encountered during industrial operations such as equipment corrosion, formation of biochar (humans) and large amounts of acidic effluent and therefore adverse environmental impact. Instead of acid hydrolysis, enzymatic hydrolysis is an alternative, the latter has been practised in a cost-effective way on a commercial scale to avoid the use of acids which increase the cost of operation.[26,27] Once hydrolysis has been achieved to release the valuable sugars from the cellulosic materials, various platform chemicals can be generated from the sugars. A top twelve list of promising platform chemicals for the future

has been reported and these are shown in the table below.[28] Among these furanics including furfural are seen as promising bio-based chemicals.

Table 1. 1 Promising Bio-based chemical targets as assessed in 2004 and 2010**.**[28]

Bio-based chemical opportunities

2004	**2010**
1,4-Dicarboxylic acids(Succinic,fumaric and malic)	Succinic acid
2.5-Furan dicarboxylic acid	Furanics
3-Hydroxy-propionic acid	Hydroxypropionic acid/ aldehyde
Glycerol	Glycerol and derivatives
Sorbitol	Sorbitol
Xylitol/ Arabinitol	Xylitol
Levulinic acid	Levulinic acid
Aspartic acid	-
Glucaric acid	-
Glutamic acid	-
Itaconic acid	-
3-Hydroxybutyrolactone	-
-	Biohydrocarbons
-	Lactic acid
-	Ethanol

1.4 Biomass derived platform chemicals

1.4.1 Furfural (FF)

Furfural (FF) is a C_5 carbohydrate which is obtained as a product in acid hydrolysis of biomass,[29] which has an almond scent and is oily, colourless but turns dark yellow when exposed to air. The structure of FF is shown below in Fig 1.6:

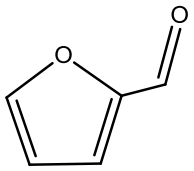

Fig 1. 6 Structure of FF [30]

FF was first discovered as a yellow oily substance in 1831 by J. Dobereiner after he used sulphuric acid to treat carbohydrates.[31] In 1845 G. Fownes also obtained FF from acid digestion of bran which is a Latin word for furfur.[32] Lignocellulosic biomass has been found to be a promising alternative to replace diminishing fossil fuels to produce FF.[8] A number of products can be derived from FF hence it has been considered the main building block for the upgrading of the hemi-cellulosic biomass fraction.[33] FF has two functionalities namely an aldehyde group and an aromatic ring which influence its high chemical reactivity. The carbonyl group on FF has a high electron withdrawing effect and as a result the furan ring of FF is less susceptible to hydrolytic ring cleavage.

FF can undergo different chemical reactions such as hydrogenation, acylation, reduction to alcohols, halogenation, reductive amination to amines, oxidation to carboxylic acids etc. Currently FF is produced from agricultural wastes as illustrated in Fig 1.7. However, most production plants are using homogenous catalysts in their reactions which makes it difficult to recycle and re-use the catalyst. Auto-hydrolysis of biomass feedstock is usually performed in a digester and the solid material is separated from the liquid material after cooling down the reactor. The liquid part is the one used for FF production and the maximum yield for FF was 73%.[34]

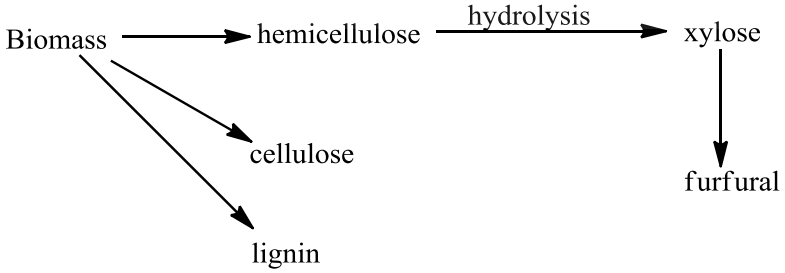

Fig 1. 7 Production of furfural from biomass[35]

FF has multi-functional groups such as C=C, C=O and C-O which make it possible to form various products upon its hydrogenation.[36] FF can be used for extracting aromatics from lubricating oils, it can also be used as a chemical feedstock for the synthesis of derivatives that contain furan.[32] FF can be converted into various compounds some are shown in

scheme1.1 namely furfuryl alcohol (FA), tetrahydrofurfuryl alcohol (THFA), tetrahydrofuran (THF), methyl furan (MF) and methyltetrahydrofuran (MTHF).[37,38] There are also other products produced in hydrogenation of FF where the furan ring opens and these include 4-oxo-pentanal, 5-hydroxy-2-pentanone and 1,4-pentanediol among others.[8,34] Catalytic hydrogenation of FF has been done using alcohol or formic acid hydrogen source and has proved to be an alternative greener synthetic route for the hydrogenation of carbonyl compounds such as in the hydrogenation of FF to FA.[39]

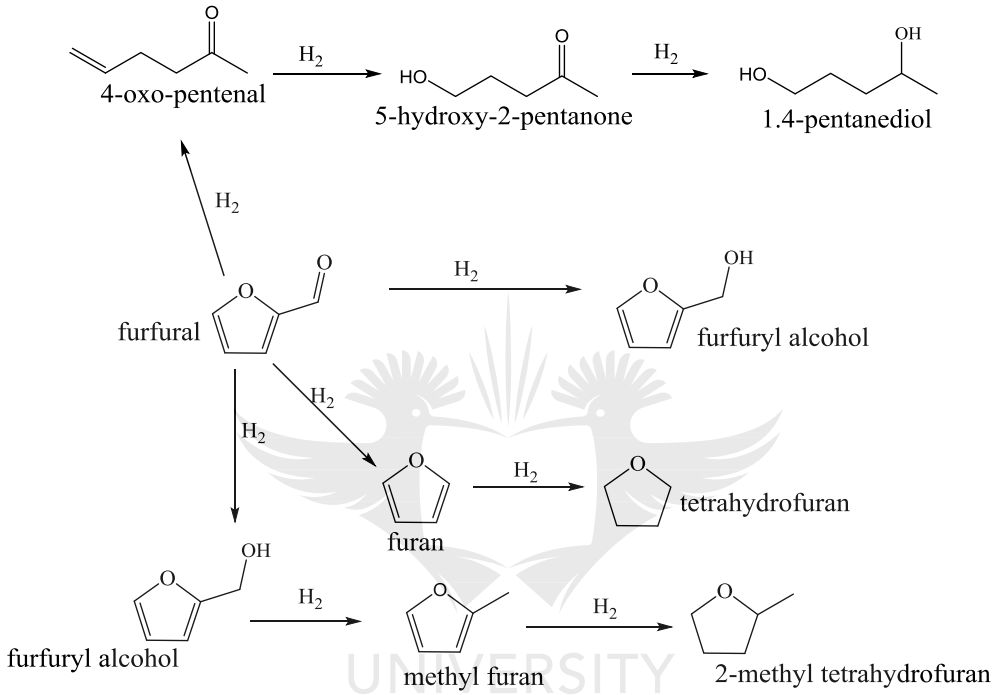

Scheme 1. 1 Various derivatives of FF[40,41]

1.4.2 Furfuryl alcohol (FA)

FA ($C_5H_6O_2$) is a colourless or yellow liquid with mild odor which can be produced by acid catalyzed reactions. It can also be formed from a hydrogenation reaction of FF in the presence of a catalyst as shown in Scheme 1.2 .

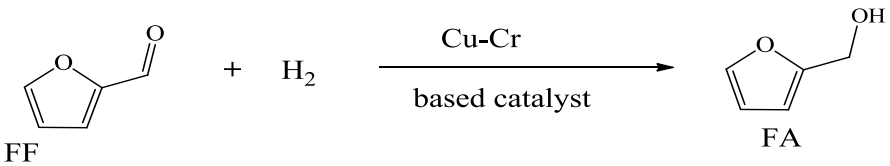

Scheme 1. 2 Conversion of FF to FA.[33]

The most commonly used catalyst is copper chromite, However, this catalysts leads to leaching of chromium (that can form toxic hexavalent Chromium) into the environment when spent, and is unsafe to the environmental and humans. There is therefore a need to

come up with eco-friendly catalysts which will not cause any negative health and environmental effects.[42] The hydrogenation of the carbonyl group of FF to FA proceeds through a Lewis acid mediated intermolecular hydride transfer.[43] In hydrogenation, C=O of the aldehyde functional group in FF breaks while the addition of the hydrogen to the oxygen results in an alcohol group O-H with an additional hydrogen bond to the exocyclic carbon of the furan based structure giving FA.[44,9] Industrial applications of FA include rubber production in polymer industry, drug synthesis pharmaceutical industry and also the metal casting industry for its anti-corrosion properties.[33] One useful chemical that can be in turn produced from FA is tetrahydrofurfuryl alcohol (THFA).

1.4.3 Tetrahydrofurfuryl alcohol (THFA)

THFA is a transparent liquid with mild odor and has been produced from FF using nickel and cobalt mono catalysts.[45] Traditionally THFA can be produced by hydrogenation of FF using commercial Cu-Cr catalyst as shown in Scheme 1.3:

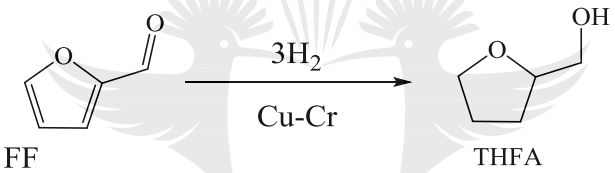

Scheme 1. 3 Production of THFA from FF.[33]

FF is first converted to FA which is further converted into THFA,[46] however, the above reaction consumes a lot of energy and requires long reaction times. In addition, the Cu-Cr catalyst is toxic and poses a lot of environmental concerns.[45] THFA has also been reported to have been produced from FF hydrogenation using hydroxyapatite (HAP) supported Pd catalyst in 2-propanol as the solvent.[47] Liu and co-workers reported that, FF is first reacted with 2-propanol to form 2-(isopropoxymethyl) furan as an intermediate through etherification and this intermediate is then converted to THFA. THFA is used in making industrial solvents, printing inks, organic synthesis and also it is used as a bio-fuel additive.[33]

Alternatively, FF can be hydrogenated to give FA as a primary product, which then undergo C-O bond hydrogenolysis in the presence of H_2 and a suitable catalyst to afford 2-methylfuran (MF).

1.4.4 Methylfuran (MF)

During FA hydrogenolysis, the atomic hydrogen adsorbed onto the metal sites on the

catalyst cleaves the C-OH bond and the hydrogen (H) is added.[43] The production of MF from FF has been recorded as 80% yield using monometallic copper metal and bimetallic catalysts in a stripping reactor as reported by Telleria and co-workers.[48] The bimetallic catalysts were made using copper metal and nickel, cobalt or tin due to their inexpensive cost.[48] MF is used as a solvent and feedstock for production of anti-malaria drugs known as chloroquine.

The high octane number (103)[49] of MF has enabled it to be used as a motor fuel.[50] Other investigations have shown that copper chromite has also been used as a catalyst in hydrogenation of FF to MF as shown in scheme 1.4. It has been reported that FF was successfully converted to MF on a bi-functional catalyst $Ru/RuO_x/C$ using isopropyl alcohol as the hydrogen donor[43] and the bi-functional nature of the catalyst is very efficient in hydro-deoxygenation of furan compounds. MF is used as a gasoline blend in vehicles, medical industry in synthesis of chloroquine and also used in making pesticides.[51]

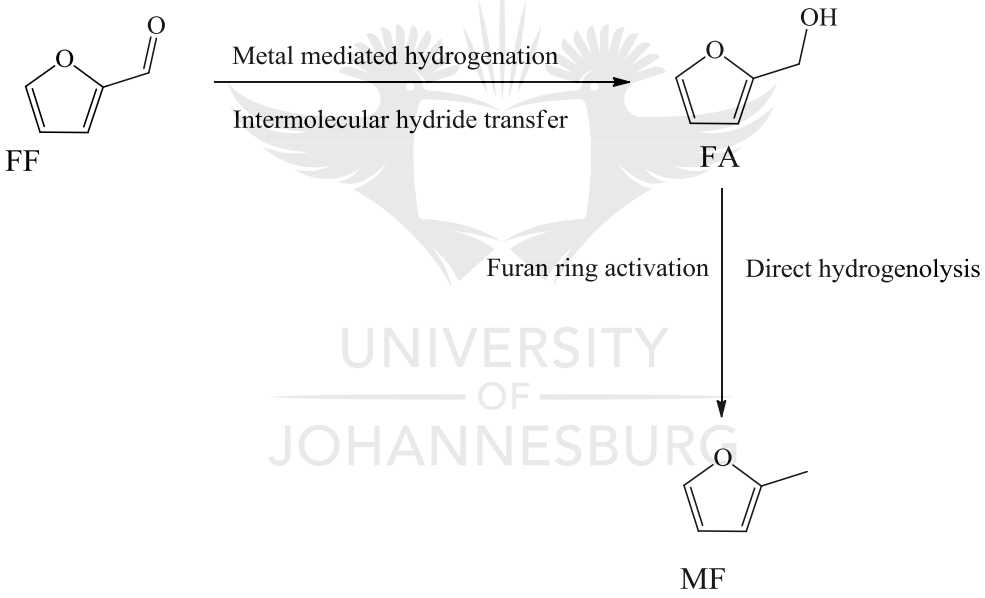

Scheme 1. 4 Proposed reaction pathway for hydrogenation of FF to MF.[43]

1.4.5 2-Methyl tetrahydrofuran (2-MTHF))

Further hydrogenation of FA leads to the formation of MF which when hydrogenated forms THMF furan as shown in scheme 1.5 below:

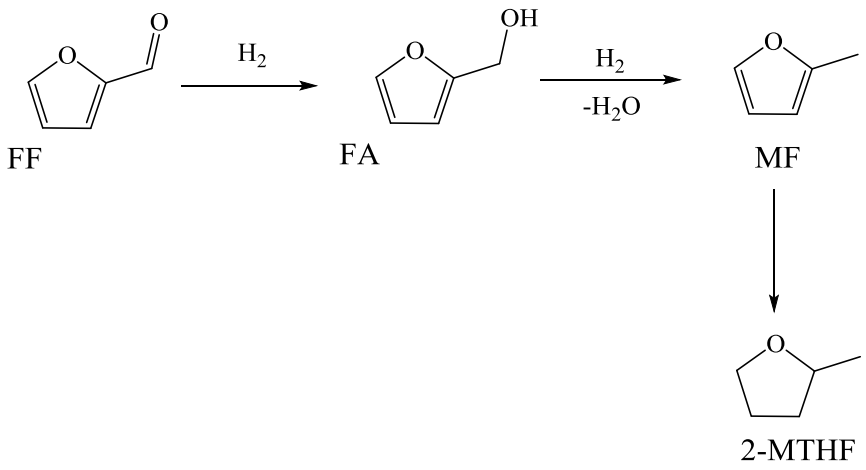

Scheme 1. 5 Production of THMF.[51]

THMF was obtained from FF hydrogenation using Ni/AC-SO_3H catalyst[49]. The obtained yield was very high (96 %) and the high yield was attributed to the catalytic activity enhanced by activated.

1.5 Describing the types of catalysts used in transformation of FF

1.5.1 Catalysts

Catalysts can be defined as chemical compounds that can increase the rate of a reaction by lowering the activation energy required to reach the transition state and is not consumed in the reaction process.[52] Catalysts are divided into two types namely homogeneous and heterogeneous catalyst depending on the reaction phase that they occupy.

1.5.1.1 Homogenous catalysis for biomass conversion

This is a reaction where the catalyst is in the same phase as the reactants.[52] The catalyst can access the linkages of lignocellulosic material easily since they decompose in the solvent system and as a result it is difficult to separate the catalyst from the products. The use of homogenous catalysts in industry has decreased to a greater extent due to difficulties encountered in catalyst separation.[53] Also, homogenous catalysts bearing halides have been reported as the cause of equipment corrosion as well as environmental pollution.[53]

1.5.1.2 Heterogenous catalysis for biomass conversion

This is the reaction where the catalyst is in a different phase from the reactants.[52] The catalyst has difficulties in attacking the linkages of lignocellulosic material due to steric hindrances from the material which results in low selectivity of the aromatic compounds.

Heterogenous catalysts have the characteristic of easy separation hence the current studies are being carried out using heterogenous catalysts. This type of catalysis enables the various use of solvents such as ionic liquids and organic polar solvents.[53]

1.6 Hydrogenation of FF

The hydrogenation of FF to its derivatives can be modified with the addition of different acids such as solid acids, mineral acids and organic acids. [54,55,56] In this way once FA is formed, the acid catalyst can promote either ring opening to afford levulinic acid (LA) as shown in the scheme 1.6 or etherification to yield difurfural ether (DFE), all of which are interesting and useful chemicals. On the other hand, organic acids such as formic acid can act as hydrogen carriers during metal catalyse hydrogenation of FF.

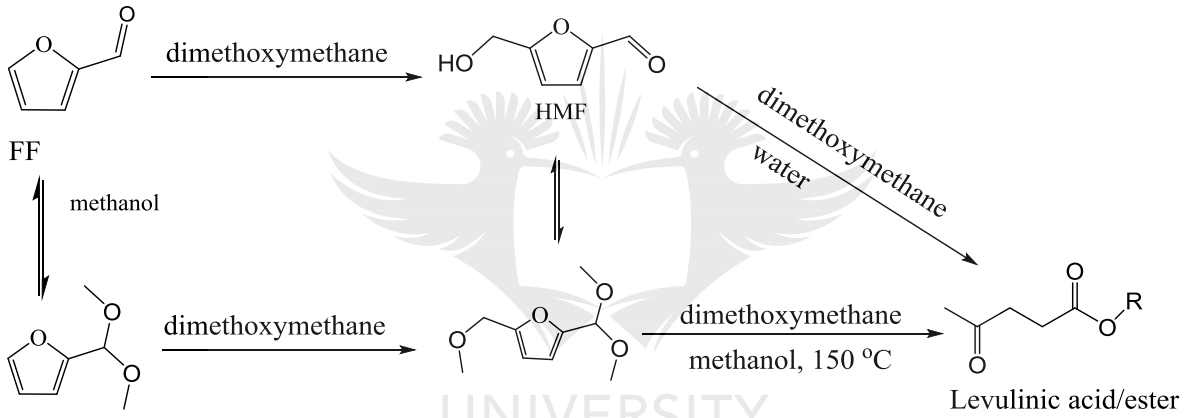

Scheme 1. 6 Conversion of FF to LA.[57]

1.6.1 Conversion of FF using metal catalyst in the presence of organic acids as hydrogen carriers

Formic acid is a liquid with low toxicity and has been reported as one of the promising hydrogen storage material.[58] It has a flash point well above room temperature and a hydrogen content of 4.4 wt%.[59] The production of formic acid has largely been from fossil feed stocks through reactions such as methanol carbonylation and partial oxidation of naphtha.[59] However, renewable sources such as biomass and carbon dioxide hydrogenation have been found to be the new storages for formic acid.[60] Researchers have been interested in use of formic acid because it is a co-product in the conversion of HMF to obtain LA.[61] Therefore the use of formic acid as a hydrogen source has been suggested as a sustainable potential route for hydrogen production which can be used for synthesis of furan

derivatives.[62]

Homogenous and heterogenous catalysts have been used to test the decomposition of formic acid and both catalysts selectively decompose formic acid to hydrogen (H_2) and carbon dioxide (CO_2) as shown below in equation 1:

$HCOOH_{(l)} \rightarrow H_{2(g)} + CO_{2(g)} \quad \Delta G^0 = -32.9 kJmol^{-1}$ [58]..... (1)

Supported palladium (5% palladium/C) catalyst has been used for FF hydrogenation using molecular hydrogen source. The FF conversion was 100% with 90.3 % selectivity to 2.5bis(2-furylmethylidene) cyclopentan-1-one and FA as a by product.[63] Despite the high conversion of FF by 5% palladium/C there are some drawbacks associated with use of formic acid such as inhibition of the formic acid dissociation and immiscibility of formic acid with polar solvents. These drawbacks can result in loss of catalytic activity due to the strong adsorption of formic acid on the catalyst's active sites which hinders the competitive adsorption of FF molecules solvated with formic acid.[63]

The conversion of FF using non-noble metals is more cost-effective compared to the use of noble metals. However the conversion process requires the addition of a large amount of hydrogen gas resulting in operational safety challenges.[64] A safer alternative that does not require handling of hydrogen directly is the use of liquid hydrogen donors such as formic acid, methanol, ethanol, acetic acid and isopropanol.[58] Wang and co-workers reported on the high activity and selectivity of Ni-Cu/ Al_2O_3 catalyst in FF hydrogenation where formic acid was used as a hydrogen donor for the complete reduction of FF to MF (92 mol%).[65] The total FF conversion was said to have been a result of synergic effect of the bimetallic nature of the catalyst which resulted in an increase in affinity for carbonyl reduction.

1.6.2 Conversion of FF using solid acids

Many industries have been using strong mineral acids such as hydrochloric acid (HCl) and sulphuric acid (H_2SO_4) for the hydrogenation of FF.[66,55] However, these strong acids reacted strongly with the equipment used resulting in corrosion. Some difficulties were experienced in mineral acid catalyst recycling for reuse, hence solid acid catalysts such as zeolites and acidic ion-exchange resins (like amberlyst-15) have been reported as recyclable potential catalysts with improved performance in FF hydrogenation.[66] Solid acids have been tested and found to be insoluble in water hence they can be easily filtered off after catalysis which makes their recovery easier compared to mineral acids.[67]

The use of solid acids such as zeolites has improved the catalytic activity of non-noble metal catalysts in the transfer hydrogenation of FF, an example is nickel catalysts which have been reported by Liu et al where they used zeolite Y as a support for nickel based catalysts.[68] The FF conversion was 97 % and among the obtained products was cyclopentanone (CPON) with 87 % yield. The zeolite topology is said to have an effect on the hydrogenation of FF due to its ability to detect the basicity of functional groups adjacent to the metal center. Han and co-workers reported on the use of non-noble metals such as cobalt, nickel and TiO_2 which have been supported on mesoporous zeolite in different reactions such as FF hydrogenation, benzene hydrogenation and Fischer-Tropsch synthesis.[69] The conversion of FF (80 %) to γ-valerolactone (GVL) 44 % yield was performed using TiO_2/beta-NS catalyst and the high FF conversion was attributed to the presence of Lewis acid sites provided by the supported TiO_2 while the zeolite mesoporous support provided the Bronsted acid sites resulting in high catalytic activity.

1.6.3 Ion-exchange resins

Commercial ion-exchange resins such as sulphonated polystyrene frameworks have been reported to be active for FF hydrogenation.[66] FA was obtained as an intermediate with a selectivity of 90 %, ethyl levulinate (EL) and diethyl ether (DE) were obtained as the final products. The catalytic performance of zeolites (like ZSM-5) and acidic ion-exchange resin (Amberlyst 15) were tested for the hydrogenation of FF and the yield for EL was 65 % for the zeolite while the acidic ion-exchange resin gave 90 % EL as shown in scheme 1.7.[66] The zeolite gave less yield of EL compared to the resin which might have been as a result of the styrene rings which contains two sulphonic acid groups resulting in bulkiness which might have led to difficulties for the FF substrate to interact with the zeolite active sites. Moreover, the low activity of the zeolite has also been reported due to zeolites being known to exhibit weaker acid sites.[70]

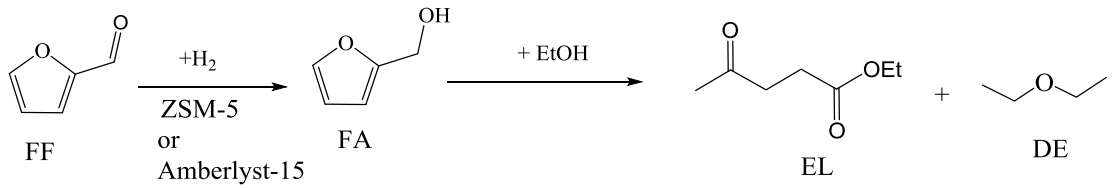

Scheme 1. 7 Conversion of FF into EL and DE.[66]

1.6.4 Immobilized transition-metal complexes and their use in hydrogenation of FF

The use of supported complexes has been of great interest in industry, this is because of the

ability of supported complexes to be recycled compared to homogenous catalysts which were difficult to recover after catalysis. [71] Complexes with a support system can be easily recycled and they have been reported to have high catalytic activity and product selectivity.[72] One of the greatest disadvantages of supported catalysts is the tendency of the catalyst to detach from the support (causing metal leaching) during catalysis usually as a result of insufficient binding.[73] It has been reported that catalyst design can be of great importance in order to avoid catalyst detaching from the support by making sure that there is strong binding of the metal. Catalysts obtained by sol-gel process have been reported to display great binding to the support hence they do not easily detach from the support.[74] Several supports can be used to immobilize the metal catalyst including silica (SiO_2), alumina (Al_2O_3) and various carbon supports like graphitic carbon nitrile. These are discussed in the next section. With specific examples where they were used to support metal catalysts for hydrogenation of FF.

1.6.4.1 FF hydrogenation by metal catalyst immobilized on nitrogen-doped –carbon supports.

Iron catalyst supported on nitrogen doped carbon has been reported to effectively hydrogenate FF to FA as shown in scheme 1.8.[75] The nitrogen-carbon support plays a major role in enhancing the catalytic activity which was evident in the reported study with 92 % FF conversion and 83 % FA selectivity shown in scheme 1.9.[76] The results obtained in catalyst characterization confirmed that the enhanced catalytic activity was attributed to the presence of iron cations which are coordinated by pyridinic nitrogen functionalities. Density functional theory (DFT) studies that were conducted displayed that transition metal sites can be stabilized by four pyridinic nitrogen atoms doped in grapheme resulting in the formation of structures of an M-N_x type (where M is the metal and N is the nitrogen specie) which is active in oxygen reduction reactions hence the nitrogen combination with the metal center gave high catalytic performance.

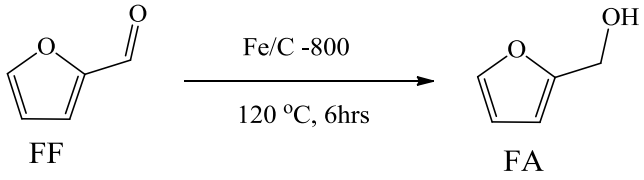

Scheme 1. 8 FF hydrogenation using iron catalyst supported on carbon.[75]

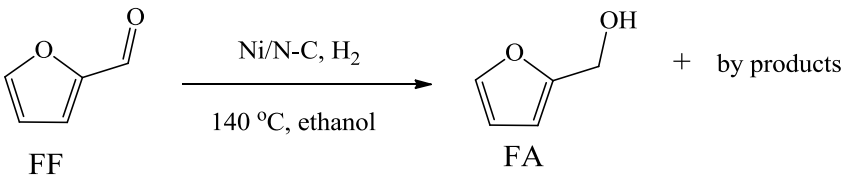

Scheme 1. 9 FF hydrogenation using Ni/C-N.[76]

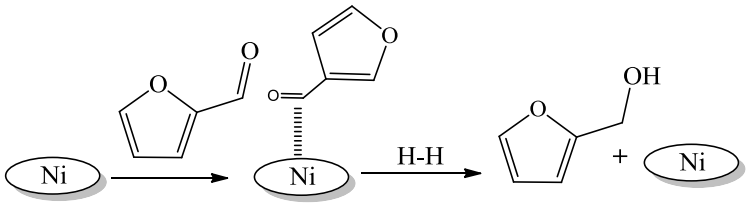

Scheme 1. 10 Possible mechanistic pathway for FF hydrogenation using Ni/N-C.[76]

Hydrogenation of FF to FA using a nickel catalyst has been reported by Panda and co-workers and mechanistic pathway by which the reaction proceeds was provided by the authors in scheme 1.10. There is interaction of the nickel(0) metal with the FF which was initially adsorbed on the surface of the nickel catalyst through the C=O bond.[76] The nitrogen support enhanced the decomposition of molecular hydrogen used in the reaction to hydrogen atoms. The C=O was selectively hydrogenated forming FA through attack by activated hydrogen atoms, which is followed by FA leaving the catalytic site after formation. Here too the nitrogen support was reported to have formed a good combination with nickel(0) and hence there was high catalytic activity which was attributed to the nitrogen carbon support.[76]

1.6.4.2 FF hydrogenation by metal catalysts immobilized on silica support.

Silica is the most commonly used support, this is because silica has been reported to be resistant to elevated temperatures and can hence be used in hydrogenation reactions that require high temperatures.[3] Infrared spectroscopy has been reported to be one of the characterization techniques used to investigate the molecular nature of silica surfaces.[77] Yaroslaysky and Terenin reported that silica surfaces contain hydroxyl groups which act as centers of molecular adsorption thus allowing the formation of hydrogen during interaction with adsorbates. [78] There are different types of surface hydroxyl groups which can be either isolated free (SiOH) or bridged.

Nickel supported on silica have been reported as better performing catalyst in

hydrogenation of FF and among the products was FA, MF, THFA and F.[41] Peterson and co-workers reported on FF hydrogenation using silica supported bimetallic nanoparticles (Fe-Ni/SiO_2),[79] the authors considered Fe and Ni because they are abundantly available and less expensive. In addition, Fe is poorly active and unstable, on the other hand Ni has been reported to be active in hydrogenation of aldehydes however it experiences deactivation by carbon hence they combined the two metals in order to improve their chemical properties. The FF conversion using Fe-Ni/SiO_2 catalyst was 100 % and FA yield was 0.14 mmol but when they used Ni/SiO_2 no FA was obtained among the products which were MTHF and THFA and hence the bimetallic catalyst supported had better catalytic performance in FF hydrogenation. X-ray Diffraction (XRD) and X-ray photoelectron spectroscopy (XPS) characterization techniques were used to confirm the stability of Fe-Ni/SiO_2 catalyst and it was stable. The stability of the catalyst was based on comparison of the used catalyst which showed similar surface and structural characteristics as that of the fresh catalyst.[79]

1.6.4.3 Effect of alumina support on the catalyst activity

It has been reported that the catalyst activity is dependent on the alumina used.[74] Fernandez and co-workers reported on the use of Cu-Co/γ-Al_2O_3 in FF hydrogenation, the FF conversion was 100 % and the main products obtained were MF (80 %), MTHF (12.6 %) and other products were FA and 1-pentanol.[48] The authors pointed out that the dispersion of the active metal is dependent on the chemical properties of the alumina support as well as the pore texture and can affect catalytic activity. The impregnation of the metal precursor on the alumina can be affected by the pore diameter of the alumina and this has an influence on the catalyst surface crystallinity.[80]

Alumina support has been reported to improve both FF conversion and product selectivity. As such the conversion of FF was 35 % over Cu/Ni whilst that of Cu-Ni-Al_2O_3 was 94 %.[81] The rapid increase in FF conversion was attributed to the presence of alumina support which enhanced the catalytic activity resulting in increase in FF conversion. FA and MF were obtained as products with selectivity of 36 % and 54 % respectively and by products such as MTHF and F which are products formed *via* saturation of the furan ring followed by hydrogenolysis and decarbonylation respectively.[81]

The choice of metal also has an impact on the product distribution when performing catalytic hydrogenation of FF. Various metals ranging from base metals (Fe, Co, Zn and Ni) to noble metals (Pt and Pd) have been studied for this reaction and these are discussed in the following section.

1.6.5 Nickel, cobalt, iron and zinc catalysed FF hydrogenation

Nickel is one of the active and cheap metals for the hydrogenation reactions in general hence its use in catalytic hydrogenation of FF is seen as the cost-effective option from an industry process perspective.[82] Nickel has been used in the hydrogenation of FF to FA as Ni@N/C, however the nickel nanoparticles were not stable hence they were stabilized by using a nitrogen rich support.[36] Firstly, FF was adsorbed onto the catalyst surface *via* the C=O bond and interacted with the Ni metal. The hydrogen molecules are adsorbed on the nitrogen rich support, the C=O bond was hydrogenated selectively by the activated hydrogen atoms forming FA. The Ni catalyst showed high activity towards desired products.[83]

In another report, a boron doped Ni catalyst was used in conversion of FF and the obtained yield was high (94 %). The high yields were attributed to the strong binding of boron to the octahedral subsurface of Ni(III) which causes surface reconstruction and as a result a corrugated surface is formed. This leads to the ease of activation of the furan ring due to enhanced adsorption energies of the reaction intermediate species as the surface is reconstructed.[35] Also, Ni nanoparticles supported on Al_2O_3 has been reported for FF hydrogenation with isopropanol as the hydrogen carrier. The catalytic activity of Ni/Al_2O_3-T catalyst was greatly influenced by temperature and as a result the catalyst showed potential in cleaving C-O bonds without external hydrogen.[36]

The bimetallic Ni-Co catalyst has been reported as toxic free catalyst and also due to their inexpensive prices they can be of high use in industry. The hydrogenation of FF was carried out using Ni-Co supported on SBA catalyst,[45] it showed better catalytic properties compared to mono-metallic catalysts. The FF conversion was 100 %, giving 92 % selectivity to THFA and the high conversion was attributed to the even distribution of active sites which effectively inhibited crystal growth which gave rise to a high surface area for the reaction.

The conversion of FF was investigated under methane environment and the obtained results revealed that Zn-Ga/ZSM5 catalyst has better catalytic properties. The high yield of aromatics was attributed to Zn and Ga having better dispersion on the zeolite used and also Zn^{2+} and Ga^{3+} were used which are known to be stable oxidation state of these metals. The use of metal species as catalysts have shown to help reduce the gas yield while increasing

aromatics yield.[84]

Catalytic transfer hydrogenation of FF to FA has been done using the metal Fe catalyst as shown in Scheme 1.11 below. Hydroxy-apatite was encapsulated with Fe_2O_3 to produce the catalyst.[85] Isopropanol was employed as the hydrogen donor, the results obtained revealed that isopropanol was the best H-donor giving a yield for FA as 92 % and a conversion of 96 %. The catalyst was easily removed after hydrogenation using a magnet and also it could be used for another six runs without losing its catalytic activity. The obtained results indicated that the alkaline HAP in the Fe_2O_3@HAP catalyst should be the active site for the hydrogenation of FF to afford FA.[85]

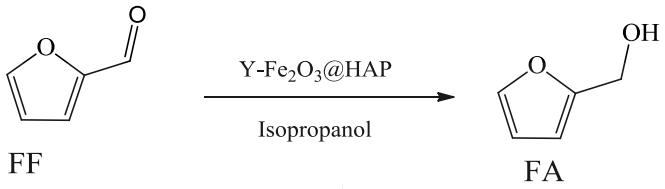

Scheme 1. 11 Catalytic hydrogenation of FF to FA using iron catalyst.[85]

1.6.6 Pd and Pt catalysed FF hydrogenation

Palladium catalyst has been used in transfer hydrogenation of FF to FA.[39,86,87] Nitrogen functionalized carbon (NPC) was used as a support to anchor Pd nanoparticles forming the Pd/NPC catalyst. The Pd/NPC catalyst was found to be re-usable without losing its catalytic activity, however palladium metal is expensive and hence there is still need for cheaper metals to use as catalysts. Palladium metal catalysts have also been used in hydrogenation of FF in the presence of high pressure hydrogen gas.[39,37] However, this process has its own draw backs such as high production of by products and consumes high energy which is not economically viable. Catalytic hydrogenation of FF was carried out using Pd/ NPC catalyst and gave a conversion of 68 %, the obtained results indicated that Pd/NPC possessed high catalytic activity which the authors attributed to the synergistic effect from both Pd and nitrogen sites to the carbon network.[39] Moreover, Pd metal has been used in combination with other metals like Iridium (Ir) to form bimetallic catalysts Pd/Ir. The obtained FA yield was 98 % which is very high and it was attributed to the fact the Iridium on the surface promotes adsorption at C=O site whilst the Pd metal interacts with the furan ring resulting in a higher conversion.[46]

FA has also been reported to have been obtained from FF hydrogenation using hydroxyapatite (HAP) supported Pd catalyst. The FA yield was 100 % with a conversion of

100 % which was attributed to outstanding catalytic performance of Pd-HAP. The quasicoordination effect between Pd and HAP gave rise to highly dispersed and stable Pd nanoclusters which improved the activation of hydrogen.[47] Also, Pd nanoparticles supported on activated carbon have been used as a catalyst for the hydrogenation of FF using formic acid as the hydrogen donor and also as a reactant to form the esterified intermediate. The FA yield and selectivity were 80 % and 90 % respectively.[88]

The hydrogenation of FF has been reported to be highly sensitive over platinum catalysts. However, FF adsorption onto Pt catalyst results in carbon deposition which is one of the draw backs of its application in most industrial reactions.[89] Conversion of FF to FA is governed by its coverage on the surface, hence there is hindrance of chemisorption when FF encounters a bare surface. Moreover, biochar supported Pt catalyst has been reported to have been used in the conversion of FF to FA in a batch reactor. A conversion of 80 % was obtained and selectivity was affected by variations in temperatures.[1] In addition, platinum nanoparticles were used in FF hydrogenation and the results showed highest conversion and selectivity to FA giving a yield of 87.4 %.[90] The use of bimetallic catalysts has shown to improve both catalytic activity and stability.

1.7 Summary

The depletion of fossil fuel reserves has become a concern to researchers and hence the need to look for renewable energy sources[12,25]. Also, the negative environmental impacts such as greenhouse gases, acid rain as a result of carbon dioxide emission into the atmosphere from fossil combustion has resulted in switching to the use of biomass. Biomass is a promising energy source which is available in abundance and also less expensive considering the fact that most of the biomass is obtained from agricultural wastes[53]. Biomass can be hydrolysed in the presence of a suitable catalyst to produce furfural which can further be hydrogenated to produce various chemicals[91,34.]

Precious metal catalysts such as osmium, platinum, palladium, ruthenium and iridium have been reported for effective hydrogenation of furfural to furfuryl alcohol and sometimes tetrahydrofurfuryl alcohol (THFA).[90] However, the cost of these precious metals is very high hence the need for research to investigate the potential of substituting precious metals with non-precious metals which costs less.[92] Non- precious metals such as Cu, Co, Ni and Fe have been reported as potential catalysts for the hydrogenation of furfural C=O bond forming furfuryl alcohol as the main product.[93,94] However, Ni among the non-precious

metals has been reported as a better catalyst compared to other non-precious metals especially supported heterogenous catalysts because of its excellent hydrogenation activity.[93]As a result modification of Ni catalysts is required in order to improve both the selectivity and the yield of the desired products. To the best of our knowledge no literature has been reported on the use of homogenous Ni(II) complexes for the hydrogenation of furfural.[71,72] Nickel-catalysed systems have been used in the hydrogenation of furfural into various valuable chemicals.[95,96,97] However, the yields for the desired product obtained so far are very low and at times the selectivity is compromised. One of the ways of improving the efficiency of nickel catalysts is involving a supporting system which is one of the aims of this research. The addition of a support system enhances both catalytic and chemical behaviour to the complexes hence improving the yield of the desired products.[9] Very few articles have been reported in literature on the application of half-sandwich and tridentate O^N^O nickel (II) complexes in the direct hydrogenation of furfural. In this work, we will investigate application of half-sandwich and tridentate O^N^O nickel(II) complexes in both direct and indirect hydrogenation of furfural.

1.8 Research aims and objectives

1.8.1General aims

The aim of this project is to design, synthesize and characterize nickel(II) molecular and supported molecular complexes and investigate their efficacy as catalyst precursors in hydrogenation of furfural , while gaining insight into the reaction pathway.

1.8.2 Specific objectives

- Synthesis and characterization of nickel(II) half-sandwich complex **C1**

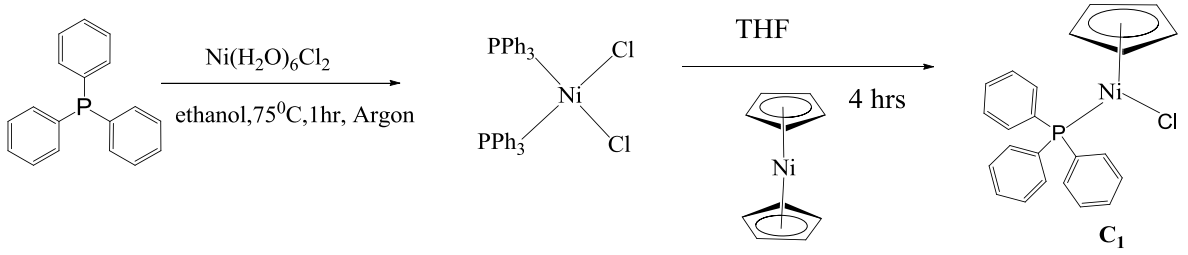

Scheme 1. 12 Synthesis of complex **C1**

- Synthesis and characterization of **L1** nickel(II) half-sandwich and supported

nickel(II) half-sandwich complexes **C2** and **C3**.

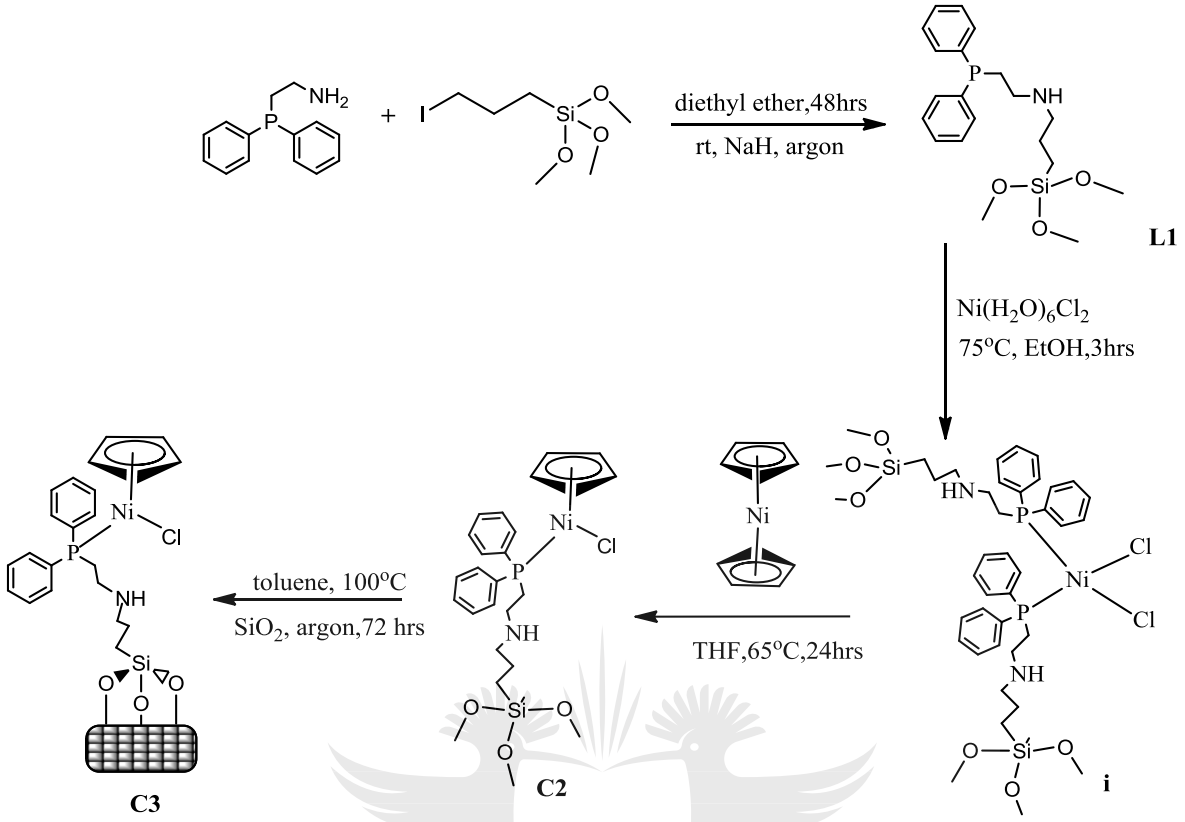

Scheme 1. 13 Synthesis of complexes **C2** and **C3**.

- Synthesis and characterization of homogenous tridentate O^N^O nickel(II) complex **C4**

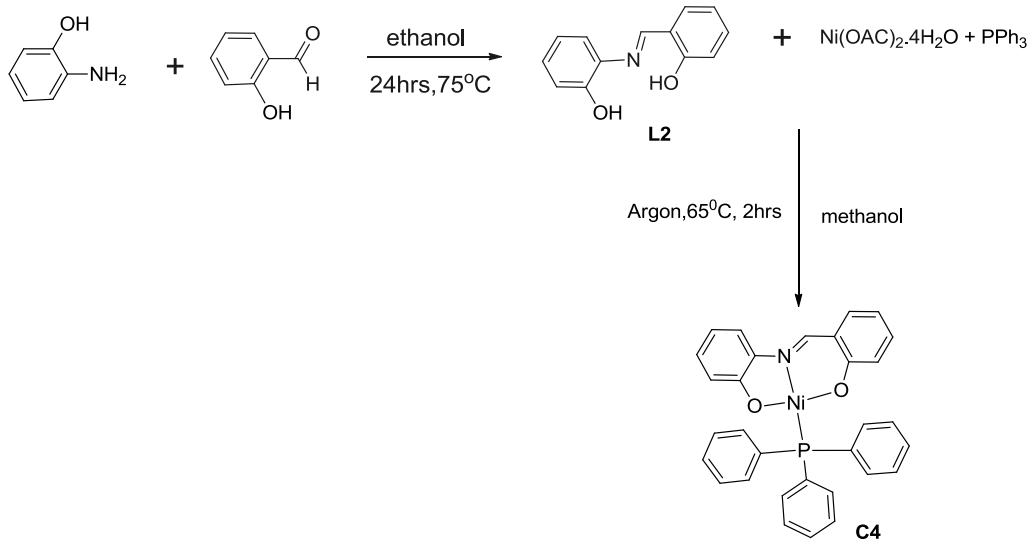

Scheme 1. 14 Synthesis of complex **C4**

- Synthesis and characterization of homogenous and supported tridentate O^N^O nickel(II) complexes **C5** and **C6**.

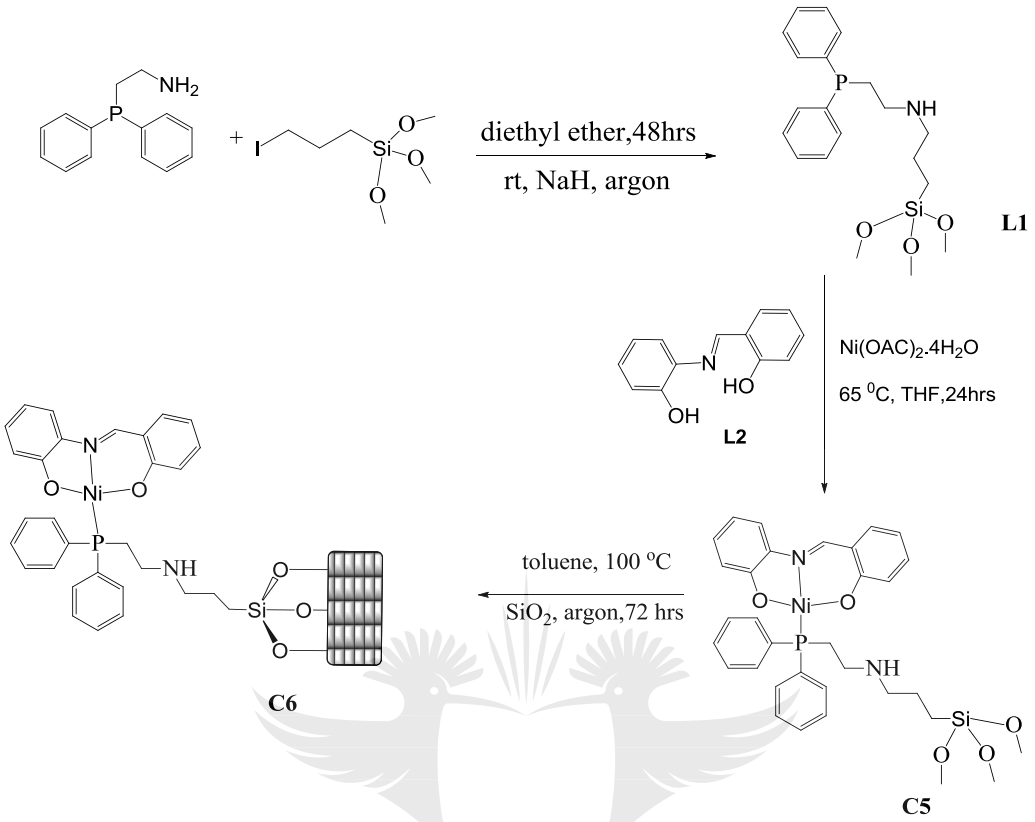

Scheme 1. 15 Synthesis of complexes **C5** and **C6**.

- To characterize the homogenous nickel(II) complexes using ^{1}H NMR, $^{13}C\{^{1}H\}$ NMR, $^{31}P\{^{1}H\}$ NMR, $^{29}Si\{^{1}H\}$ NMR, Infrared spectroscopy, High resolution mass spectroscopy, melting point and elemental analysis.
- To characterize the silica supported nickel(II) complexes using powder X-ray diffraction, BET, ICP-MS, SEM and TEM.
- To evaluate complexes **C1-C6** as catalyst precursors in both direct and transfer hydrogenation of furfural and conduct *in situ* NMR studies, of the catalytic reactions, in order to gain insight into the reaction pathway.

1.9 References

1 A. Fuente-Hernández, R. Lee, N. Béland, I. Zamboni and J.-M. Lavoie, *Energies*, 2017, **10**, 286.

2 N. S. Date, S. E. Kondawar, R. C. Chikate and C. V Rode, *ACS Omega*, 2018, **3**, 9860–9871.

3 Y. Nakagawa, H. Nakazawa, H. Watanabe and K. Tomishige, *ChemCatChem*, 2012, **4**, 1791–1797.

4 H. P. Winoto, Z. A. Fikri, J. Ha, Y. Park, H. Lee, D. J. Suh and J. Jae, *Appl. Catal. B Environ.*, 2019, **241**, 588–597.

5 H. Schmieder, J. Abeln, N. Boukis, E. Dinjus, A. Kruse, M. Kluth, G. Petrich, E. Sadri and M. Schacht, *J. Supercrit. Fluids*, 2000, **17**, 145–153.

6 V. Krzelj, J. van Kampen, J. van der Schaaf and M. F. Neira d'Angelo, *Ind. Eng. Chem. Res.*, 2019, **58**, 16126–16137.

7 Y. B. Huang, T. Yang, Y. J. Luo, A. F. Liu, Y. H. Zhou, H. Pan and F. Wang, *Catal. Sci. Technol.*, 2018, **8**, 6252–6262.

8 Y. Luo, Z. Li, X. Li, X. Liu, J. Fan, J. H. Clark and C. Hu, *Catal. Today*, 2019, **319**, 14–24.

9 O. Aldosari, , H. Alshammari, M. Alhumaimess, and I. Wawata, *Turkish J. Chem.*, 2019, **43**, 24–38.

10 L. Zhang, L. Tian, R. Sun, C. Liu, Q. Kou and H. Zuo, *Bioresour. Technol.*, 2019, **276**, 60–64.

11 S. S. Toor, L. Rosendahl and A. Rudolf, *Energy*, 2011, 36, 2328–2342.

12 J. Goffé and J.-H. Ferrasse, *Energy*, 2019, **170**, 438–458.

13 H. Wu, Q. Fu, R. Giles and J. Bartle, *Energy & Fuels*, 2008, **22**, 190–198.

14 S. Yaman, *Energy Convers. Manag.*, 2004, **45**, 651–671.

15 Y. Zhu, Z. Li and J. Chen, *Green Energy Environ.*, 2019, **4**, 210–244.

16 J. K. Saini, A. K. Patel, M. Adsul and R. R. Singhania, *Renew. Energy*, 2016, **98**, 29–42.

17 B. Kamm and M. Kamm, *Chem. Biochem.*, 2004, **18**, 1–6.

18 J. Long, W. Zhao, Y. Xu, W. Wu, C. Fang, H. Li and S. Yang, *RSC Adv.*, 2019, **9**, 3063–3071.

19 V. Kirubakaran, V. Sivaramakrishnan, R. Nalini, T. Sekar, M. Premalatha and P.

Subramanian, *Renew. Sustain. Energy Rev.*, 2009, **13**, 179–186.

20 D. C. Elliott and N. National, *Rev. Catal. hydrothermal Gasif. biomass*, 2008, 254–265.

21 A. V Bridgwater, *Biomass and Bioenergy*, 2012, **38**, 68–94.

22 W.-C. Wang, N. Thapaliya, A. Campos, L. F. Stikeleather and W. L. Roberts, *Fuel*, 2012, **95**, 622–629.

23 A. Kruse, A. Funke and M. M. Titirici, *Curr. Opin. Chem. Biol.*, 2013, 17, 515–521.

24 D. Castello, T. Pedersen and L. Rosendahl, *Energies*, 2018, **11**, 3165.

25 F. Guo, Z. Fang, C. C. Xu and R. L. Smith, *Prog. Energy Combust. Sci.*, 2012, 38, 672–690.

26 European Biofuels Technology Platform, 2016, 2.

27 Crescentino, 2013, 12.

28 E. de Jong, H. Stichnothe, G. Bell and H. Jørgensen, *IEA Bioenergy Task 42 - Bio-Based Chemicals: a 2020 Update*, 2020.

29 L. Grazia, A. Lolli, F. Folco, Y. Zhang, S. Albonetti and F. Cavani, *Catal. Sci. Technol.*, 2016, **6**, 4418–4427.

30 X. Li, P. Jia and T. Wang, *ACS Catal.*, 2016, **6**, 7621–7640.

31 M. Kabbour and R. Luque, in *Biomass, Biofuels, Biochemicals*, Elsevier, 2020, pp. 283–297.

32 R. Christoph, B. Schmidt, U. Steinberner, W. Dilla and R. Karinen, *Ullmann's Encycl. Ind. Chem.*, 1998, **16**, 67–82.

33 A. Mandalika, L. Qin, T. K. Sato and T. Runge, *Green Chem.*, 2014, **16**, 2480–2489.

34 L. Liu, H. Chang, H. Jameel and S. Park, *Bioresour. Technol.*, 2018, **252**, 165–171.

35 A. Banerjee and S. H. Mushrif, *J. Phys. Chem. C*, 2018, **122**, 18383–18394.

36 J. He, M. R. Nielsen, T. W. Hansen, S. Yang and A. Riisager, *Catal. Sci. Technol.*, 2019, **9**, 1289–1300.

37 W. Ouyang, A. Yepez, A. A. Romero and R. Luque, *Catal. Today*, 2018, **308**, 32–37.

38 N. Viar, J. M. Requies, I. Agirre, A. Iriondo and P. L. Arias, *Energy*, 2019, **172**, 531–544.

39 P. Puthiaraj, K. Kim and W.-S. Ahn, *Catal. Today*, 2019, **324**, 49–58.

40 K. E. Salnikova, V. G. Matveeva, Y. V. Larichev, A. V. Bykov, G. N. Demidenko, I. P. Shkileva and M. G. Sulman, *Catal. Today*, 2019, **329**, 142–148.

41 G. Giorgianni, S. Abate, G. Centi, S. Perathoner, S. Van Beuzekom, S. H. Soo-Tang and J. C. Van Der Waal, *ACS Sustain. Chem. Eng.*, 2018, **6**, 16235–16247.

42 X. Y. Zhang, Z. H. Xu, M. H. Zong, C. F. Wang and N. Li, *Catalysts*, 2019, **9**, 70.

43 M. J. Gilkey, P. Panagiotopoulou, A. V Mironenko, G. R. Jenness, D. G. Vlachos and B. Xu, *ACS Catal.*, 2015, **5**, 3988–3994.

44 R. Ma, X. P. Wu, T. Tong, Z. J. Shao, Y. Wang, X. Liu, Q. Xia and X. Q. Gong, *ACS Catal.*, 2017, **7**, 333–337.

45 S. Li, Y. Wang, L. Gao, Y. Wu, X. Yang, P. Sheng and G. Xiao, *Microporous Mesoporous Mater.*, 2018, **262**, 154–165.

46 Y. Nakagawa, K. Takada, M. Tamura and K. Tomishige, *ACS Catal.*, 2014, **4**, 2718–2726.

47 C. Li, G. Xu, X. Liu, Y. Zhang and Y. Fu, *Ind. Eng. Chem. Res.*, 2017, **56**, 8843–8849.

48 I. Gandarias, S. García-Fernández, I. Obregón, I. Agirrezabal-Telleria and P. L. Arias, *Fuel Process. Technol.*, 2018, **178**, 336–343.

49 Y. Wang, D. Zhao, D. Rodríguez-Padrón and C. Len, *Catalysts*, 2019, **9**, 796.

50 S. Srivastava, G. C. Jadeja and J. Parikh, *Chem. Eng. Res. Des.*, 2018, **132**, 313–324.

51 S. Srivastava, G. C. Jadeja and J. Parikh, *RSC Adv.*, 2016, **6**, 1649–1658.

52 S. B. Ötvös, I. Pálinkó and F. Fülöp, *Catal. Sci. Technol.*, 2019, **9**, 47–60.

53 F. Huang, Y. Su, Y. Tao, W. Sun and W. Wang, *Fuel*, 2018, **226**, 417–422.

54 E. I. Gürbüz, J. M. R. Gallo, D. M. Alonso, S. G. Wettstein, W. Y. Lim and J. A. Dumesic, *Angew. Chemie Int. Ed.*, 2013, **52**, 1270–1274.

55 T. Horvath, L. Qi, Y. F. Mui, S. W. Lo, M. Y. Lui and G. R. Akien, *ACS Catal.*, 2014, **4**, 1470–1477.

56 J. D. Lewis, S. Van de Vyver, A. J. Crisci, W. R. Gunther, V. K. Michaelis, R. G. Griffin and Y. Román-Leshkov, *ChemSusChem*, 2014, **7**, 2255–2265.

57 X. Hu, S. Jiang, L. Wu, S. Wang and C.-Z. Li, *Chem. Commun.*, 2017, **53**, 2938–2941.

58 M. Grasemann and G. Laurenczy, *Energy Environ. Sci.*, 2012, **5**, 8171.

59 Z.-L. Wang, J.-M. Yan, H.-L. Wang, Y. Ping and Q. Jiang, *Sci. Rep.*, 2012, **2**, 598.

60 J. Tuteja, H. Choudhary, S. Nishimura and K. Ebitani, *ChemSusChem*, 2014, **7**, 96–100.

61 W. De Jong and G. Marcotullio, *Int. J. Chem. React. Eng.*, 2010, **8**, 2–27.

62 M. G. Mura, L. De Luca, G. Giacomelli and A. Porcheddu, *Adv. Synth. Catal.*, 2012, **354**, 3180–3186.

63 K. Fulajtárová, M. Hronec, T. Liptaj, N. Prónayová and T. Soták, *J. Taiwan Inst.*

Chem. Eng., 2016, **66**, 137–142.

64 D. Shi, Q. Yang, C. Peterson, A.-F. Lamic-Humblot, J.-S. Girardon, A. Griboval-Constant, L. Stievano, M. T. Sougrati, V. Briois, P. A. J. Bagot, R. Wojcieszak, S. Paul and E. Marceau, *Catal. Today*, 2019, **334**, 162–172.

65 Z. Fu, Z. Wang, W. Lin, W. Song and S. Li, *Appl. Catal. A Gen.*, 2017, **547**, 248–255.

66 J.-P. Lange, W. D. van de Graaf and R. J. Haan, *ChemSusChem*, 2009, **2**, 437–441.

67 R. Sahu and P. L. Dhepe, *ChemSusChem*, 2012, **5**, 751–761.

68 C.-Y. Liu, R.-P. Wei, G.-L. Geng, M.-H. Zhou, L.-J. Gao and G.-M. Xiao, *Fuel Process. Technol.*, 2015, **134**, 168–174.

69 J. Han, J. Cho, J.-C. Kim and R. Ryoo, *ACS Catal.*, 2018, **8**, 876–879.

70 J. Lange and L. Petrus, *Appl. Catal. A Gen.*, 2001, **216**, 285–294.

71 L. Liu, H. Lou and M. Chen, *Int. J. Hydrogen Energy*, 2016, **41**, 14721–14731.

72 T. P. Sulmonetti, S. H. Pang, M. T. Claure, S. Lee, D. A. Cullen, P. K. Agrawal and C. W. Jones, *Appl. Catal. A Gen.*, 2016, **517**, 187–195.

73 P. G. Savva, K. Goundani, J. Vakros, K. Bourikas, C. Fountzoula, D. Vattis, A. Lycourghiotis and C. Kordulis, *Appl. Catal. B Environ.*, 2008, **79**, 199–207.

74 M. Zangouei, A. Z. Moghaddam and M. Arasteh, *Chem. Eng. Res. Bull.*, 2010, **14**, 97–102.

75 J. Li, J. L. Liu, H. J. Zhou and Y. Fu, *ChemSusChem*, 2016, **9**, 1339–1347.

76 S. Nandi, A. Saha, P. Patel, N. H. Khan, R. I. Kureshy and A. B. Panda, *ACS Appl. Mater. Interfaces*, 2018, **10**, 24480–24490.

77 E. Maarel, *Vegetatio*, 1975, **30**, 213–219.

78 H. Zou, S. Wu and J. Shen, *Chem. Rev.*, 2008, 108, 3893–3957.

79 D. Shi, Q. Yang, C. Peterson, A.-F. Lamic-Humblot, J.-S. Girardon, A. Griboval-Constant, L. Stievano, M. T. Sougrati, V. Briois, P. A. J. Bagot, R. Wojcieszak, S. Paul and E. Marceau, *Catal. Today*, 2019, **334**, 162–172.

80 M. Inoue, T. Miyake, Y. Takegami and T. Inui, *Appl. Catal.*, 1987, **29**, 285–294.

81 S. Srivastava, G. C. Jadeja and J. Parikh, *J. Mol. Catal. A Chem.*, 2017, **426**, 244–256.

82 S. Zhang, H. Ma, Y. Sun, Y. Luo, X. Liu, M. Zhang, J. Gao and J. Xu, *Green Chem.*, 2019, **21**, 1702–1709.

83 W. Gong, C. Chen, H. Wang, R. Fan, H. Zhang, G. Wang and H. Zhao, *Chinese Chem. Lett.*, 2018, **29**, 1617–1620.

84 A. Wang, D. Austin, H. Qian, H. Zeng and H. Song, *ACS Sustain. Chem. Eng.*, 2018, **6**, 8891–8903.

85 F. Wang and Z. Zhang, *ACS Sustain. Chem. Eng.*, 2017, **5**, 942–947.

86 C. Nguyen-Huy, J. S. Kim, S. Yoon, E. Yang, J. H. Kwak, M. S. Lee and K. An, *Fuel*, 2018, **226**, 607–617.

87 N. Cherkasov, A. J. Expósito, M. S. Aw, J. Fernández-García, S. Huband, J. Sloan, L. Paniwnyk and E. V. Rebrov, *Appl. Catal. A Gen.*, 2019, **570**, 183–191.

88 G. Sun, J. An, H. Hu, C. Li, S. Zuo and H. Xia, *Catal. Sci. Technol.*, 2019, **9**, 1238–1244.

89 M. J. Taylor, L. Jiang, J. Reichert, A. C. Papageorgiou, S. K. Beaumont, K. Wilson, A. F. Lee, J. V Barth and G. Kyriakou, *J. Phys. Chem. C*, 2017, **121**, 8490–8497.

90 L. Liu, H. Lou and M. Chen, *Appl. Catal. A Gen.*, 2018, **550**, 1–10.

91 N. Gupta, N. Dimitratos, D. Su and A. Villa, *Energy Technol.*, 2019, **7**, 269–276.

92 Y. Li, X. Guo, D. Liu, X. Mu, X. Chen and Y. Shi, *Catalysts*, 2018, **8**, 193.

93 P. Guo, S. Liao and X. Tong, *ACS Omega*, 2019, **4**, 21724–21731.

94 X. Zhou, Z. Feng, W. Guo, J. Liu, R. Li, R. Chen and J. Huang, *Ind. Eng. Chem. Res.*, 2019, **58**, 3988–3993.

95 A. Guerrero-Torres, C. P. Jiménez-Gómez, J. A. Cecilia, C. García-Sancho, F. Franco, J. J. Quirante-Sánchez and P. Maireles-Torres, *Top. Catal.*, 2019, **62**, 535–550.

96 X. Meng, Y. Yang, L. Chen, M. Xu, X. Zhang and M. Wei, *ACS Catal.*, 2019, **9**, 4226–4235.

97 S. A. Khromova, M. V Bykova, O. A. Bulavchenko, D. Y. Ermakov, A. A. Saraev, V. V. Kaichev, R. H. Venderbosch and V. A. Yakovlev, *Top. Catal.*, 2016, **59**, 1413–1423.

Chapter two

Synthesis and characterization of homogenous and supported Ni(II) half-sandwich complexes

2.1 Introduction

Nickel catalysts have gained extensive attention due to their potential application as less expensive alternatives when compared to precious metals.[1] Some nickel based catalysts have been traditionally prepared using $Ni(COD)_2$ as the nickel source, however challenges have been encountered during synthesis due to the precursor being air and moisture sensitive which requires special handling. However, half-sandwich versions have been found to be air and moisture stable and can be prepared with easy handling under inert atmosphere. [2,3]

Nickel(II) half-sandwich complexes are currently of interest in the field of organometallic chemistry due to their versatile reactivity, application in a variety of catalytic reactions and also better performance in the presence of bases which activates the Ni(II) complex to produce catalytically active species.[2] Bis(cyclopentadienyl)nickel(II) commonly known as nickelocene is a unique 20 valence electron metallocene which forms 18 valence electron species when reacted with different ligands either by the Cp ring displacement or ligand addition and as such complexes generated from nickelocene have been reported to be active in catalysis.[4] Moreover, phosphine ligands are usually employed along with nickelocene in the synthesis of nickel complexes because of their ability to readily coordinate to metal centers through the lone pair of electrons on the phosphorus atom and their variety of coordination modes.[5]

The use of heterogenous catalysts supported or anchored on solid surfaces has been an active area of research.[6,7,8] It has been reported that Ni(II) can be anchored on to different solid surfaces such as porous silica through silane organic moiety taking advantage of the silanol groups which are usually on the surface[9] and complexes with such supports have been reported to have high catalytic activity and product selectivity.[10]

Herein, we discuss the synthesis of homogenous and supported half-sandwich nickel(II) complexes and their application in the conversion of furfural to furfuryl alcohol. The ligands and homogenous complexes have been characterized using nuclear magnetic resonance spectroscopy (^{1}H NMR,^{13}C{^{1}H} NMR, ^{31}P{^{1}H}, ^{29}Si{^{1}H} NMR, high resolution electrospray ionisation-mass spectrometry, elemental analysis and Fourier transform

infrared spectroscopy. The supported complex has been characterized using both analytical and spectroscopic techniques such as ICP-MS, PXRD, BET, TEM and SEM.

2.2 Synthesis and characterization of ligand L1

The Ligand **L1** was prepared by modified synthetic procedure from the literature.[20] The ligand was prepared by stirring 2-(diphenylphosphino)ethylamine with an equimolar amount of (3-Iodopropyl) trimethoxysilane in the presence of sodium hydride as a base at room temperature (Scheme 2.1). Ligand **L1** was obtained in good yield (75 %) as a colourless oil. The ligand is soluble in methanol, tetrahydrofuran, dichloromethane, chloroform and insoluble in hexane and water. Due to air and moisture sensitivity, the ligand could only be characterized by $^{31}P\{^{1}H\}$ NMR spectroscopy.

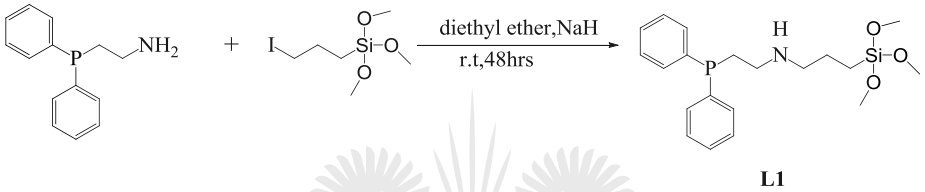

L1

Scheme 2. 1 Synthesis of ligand **L1.**

2.2.1 $^{31}P\{^{1}H\}$ NMR spectroscopy of ligand L1

The $^{31}P\{^{1}H\}$ NMR spectrum of ligand **L1** (Fig 2.1) shows two signals where the first signal appearing at -21.95 ppm was assigned to the ligand **L1** which slightly shifted from -21.98 ppm in the starting material, 2-(diphenylphosphino)ethylamine. However, this was expected as the alkylation reaction is taking place three bonds away from the phosphorus atom hence the effect might not be much. A second signal was observed at 30.44 ppm corresponding to phosphine oxide due to ligand air sensitivity. Several attempts to prevent oxidation of the ligand by working under an inert environment and using dry solvents still resulted in minute amounts of the phosphine oxide forming.

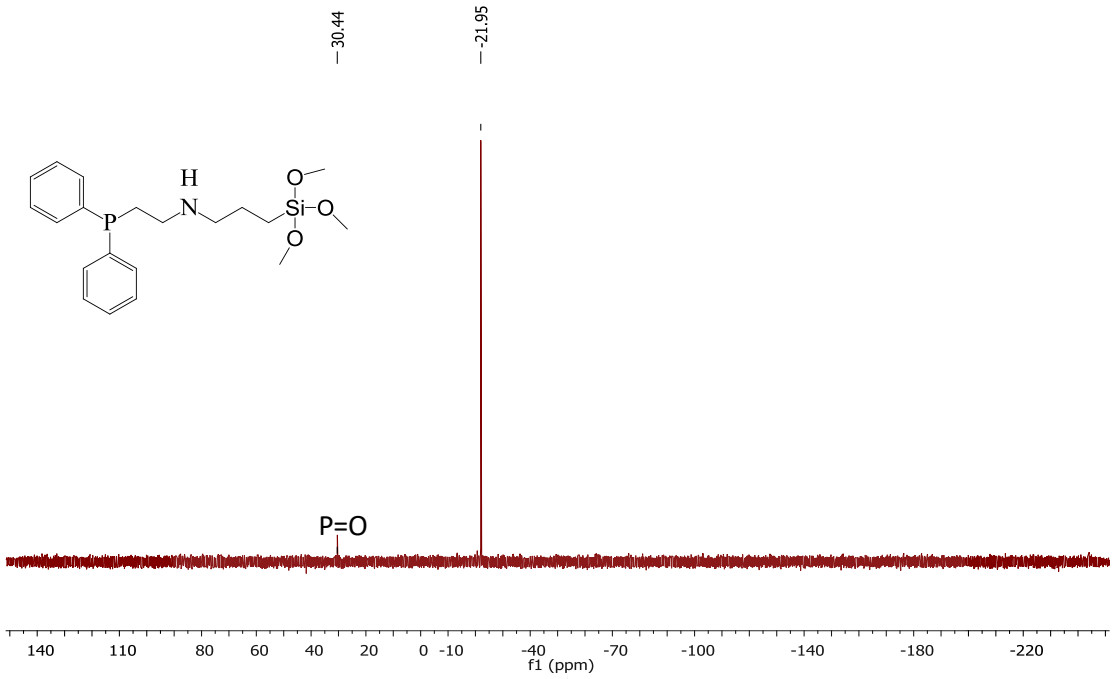

Fig 2. 1 $^{31}P\{^{1}H\}$ NMR spectrum for ligand **L1** in $CDCl_3$ (500 MHz).

2.3 Synthesis and characterization of $NiCl_2(PPh_3)_2$

The nickel(II) precursor $[NiCl_2(PPh_3)_2]$ was synthesized following a literature synthetic procedure as shown in Scheme 2.2.[11] Nickel chloride hexahydrate dissolved in ethanol was added to triphenylphosphine dissolved in ethanol and the reaction mixture was refluxed at 75 ^{o}C for 1 hour. A purple solid precipitated out and was filtered while hot, washed with minute amount of ethanol and dried under vacuum overnight (approx. 18 hours). The nickel(II) precursor, $[NiCl_2(PPh_3)_2]$, was obtained in good yield (89 %). It is soluble in dichloromethane, chloroform, acetonitrile, dimethyl sulfoxide and insoluble in hexane and diethyl ether. Due to failure of a solution of $[NiCl_2(PPh_3)_2]$, to shim no conclusive ^{1}H NMR spectrum was obtained due to the paramagnetic nature of the complex. It has been reported by Bridgeman that nickel(II) complexes can have temperature dependent magnetic moments which are usually higher than the spin which results in paramagnetism.[12] The The complex was therefore characterized using $^{31}P\{^{1}H\}$ NMR, $^{13}C\{^{1}H\}$ NMR, high resolution mass spectroscopy, elemental analysis and melting point.

2.3.1 $^{31}P\{^{1}H\}$ NMR spectroscopy of $[NiCl_2(PPh_3)_2]$

The $^{31}P\{^{1}H\}$ NMR spectrum of $[NiCl_2(PPh_3)_2]$, shown in Fig 2.2 shows a single peak appearing at -5.16 ppm which is a slight downfield shift from the triphenylphosphine (-6.28 ppm). This confirms the coordination of the phosphorus atom to the nickel center and this

downfield shift can be attributed to the fact that phosphorus is a σ-donor ligand hence the movement of electron density from the phosphorus towards the nickel center.

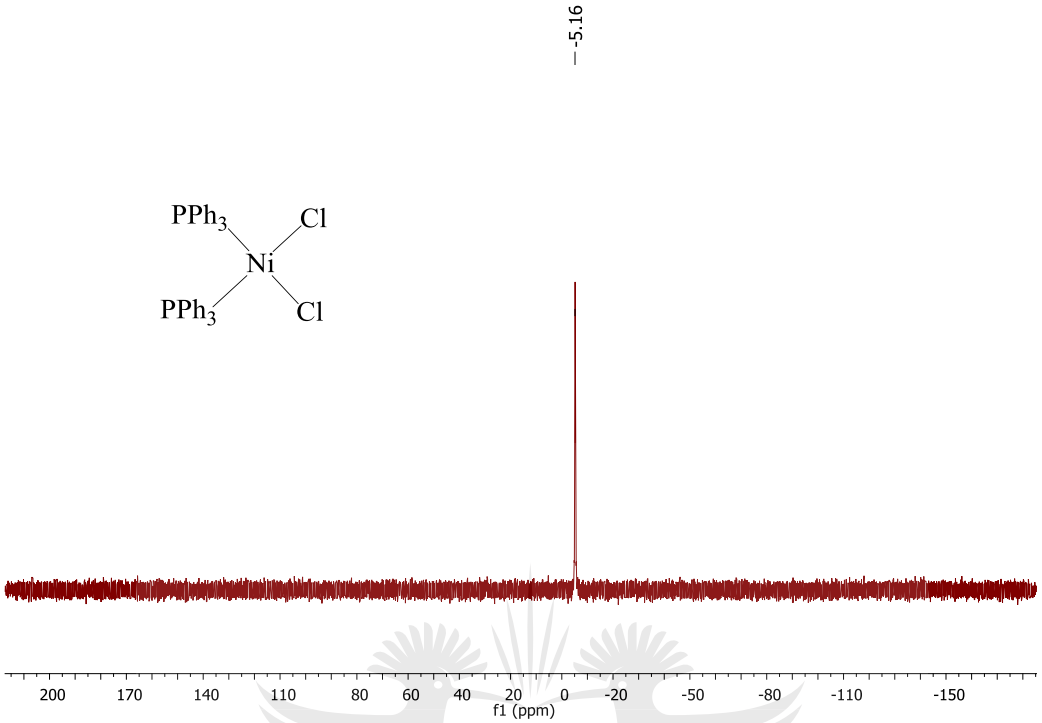

Fig 2. 2 $^{31}P\{^{1}H\}$ NMR spectrum for **$NiCl_2(PPh_3)_2$** in $CDCl_3$ (500 MHz).

The $[NiCl_2(PPh_3)_2]$ was further characterized by $^{13}C\{^{1}H\}$ NMR which was recorded using TMS as internal reference in $CDCl_3$.

2.3.2 $^{13}C\{^{1}H\}$ NMR spectroscopy of $NiCl_2(PPh_3)_2$

The $^{13}C\{^{1}H\}$ NMR spectrum (Fig. 2.3) shows carbon signals between 128.22- 137.43 ppm which is in agreement with the proposed structure of the complex.

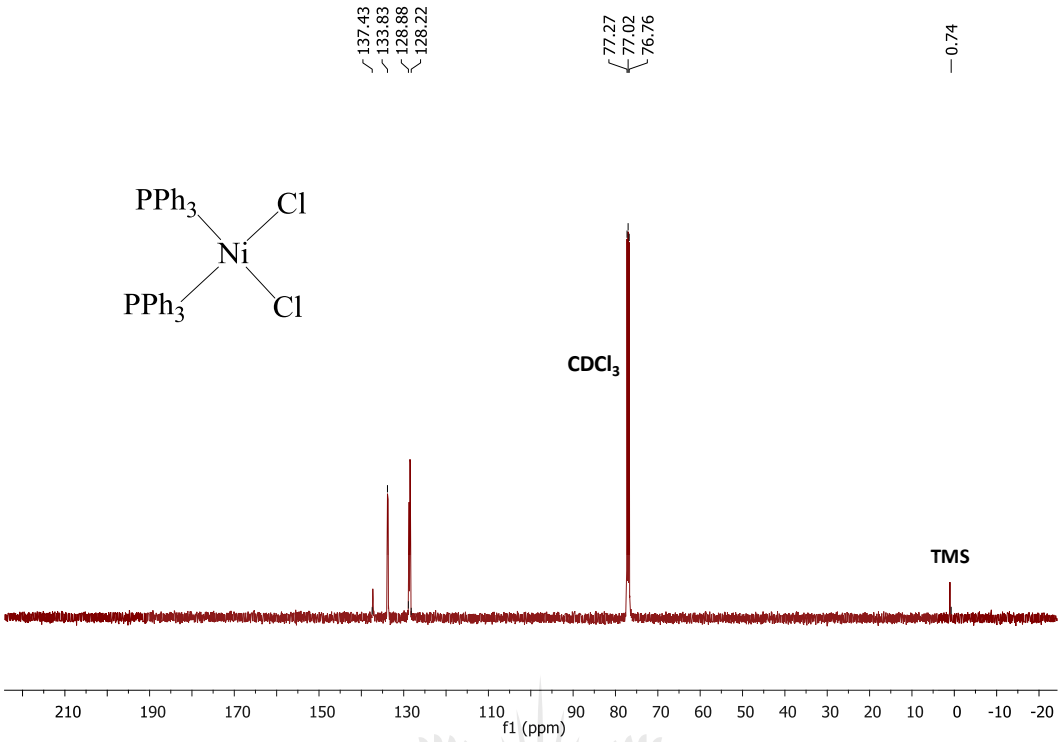

Fig 2. 3 $^{31}C\{^{1}H\}$ NMR spectrum for **$NiCl_2(PPh_3)_2$** in $CDCl_3$ (500 MHz).

In addition to NMR characterization, high resolution-mass spectroscopy was also used to characterize the nickel(II) precursor $[NiCl_2(PPh_3)_2]$.

The high resolution mass spectrum of $[NiCl_2(PPh_3)_2]$ showed a peak for *m/z* =619.0809 for $[M\text{-}Cl+H]^+$.

The purity of the synthesized $[NiCl_2(PPh_3)_2]$was determined using elemental analysis and melting point determination.

2.3.3 Elemental analysis and melting point of $NiCl_2(PPh_3)_2$

The elemental analysis of $[NiCl_2(PPh_3)_2]$ was calculated and found to be within the acceptable limits of the calculated value and the melting point range was 227- 231 ^{o}C which confirms the purity of the synthesized complex.

2.4 Synthesis and characterization of complex C1

The complex **C1** was synthesized by dissolving the nickel(II) metal precursor $[NiCl_2(PPh_3)_2]$ [11] and Bis(cyclopentadienyl) nickel(II) in tetrahydrofuran. The reaction mixture was refluxed at 60 ^{o}C for 6 hours (Scheme 2.2). Then the solvent was removed under reduced pressure and the residue dissolved in hot benzene followed by gravity

filtration. Excess hexane was added to the benzene filtrate and cooled to 0 ^{o}C. The complex **C1** was isolated as red purple crystals in good yield (82 %). Complex **C1** is soluble in chloroform, ethanol, methanol, toluene, dimethyl sulfoxide, acetonitrile and insoluble in hexane, diethyl ether and water. The complex **C1** was characterized using ^{1}H NMR, ^{13}C{^{1}H} NMR, ^{31}P{^{1}H} NMR, high resolution mass spectroscopy, elemental analysis and melting point.

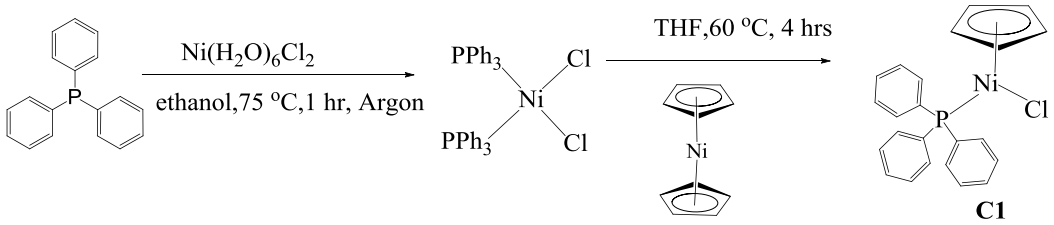

Scheme 2. 2 Synthesis of complex **C1.**

2.4.1 ^{1}H NMR spectroscopy of complex C1

The ^{1}H NMR spectrum (Fi.g 2.4) shows the characteristic cyclopentadienyl (Cp) ring protons which appear at 5.08 ppm intergrating for five protons. Two signals were observed in the aromatic region between 7.40- 7.79 ppm corresponding to the triphenylphosphine protons. The intergration accounts for all the expected protons in the proposed structure.

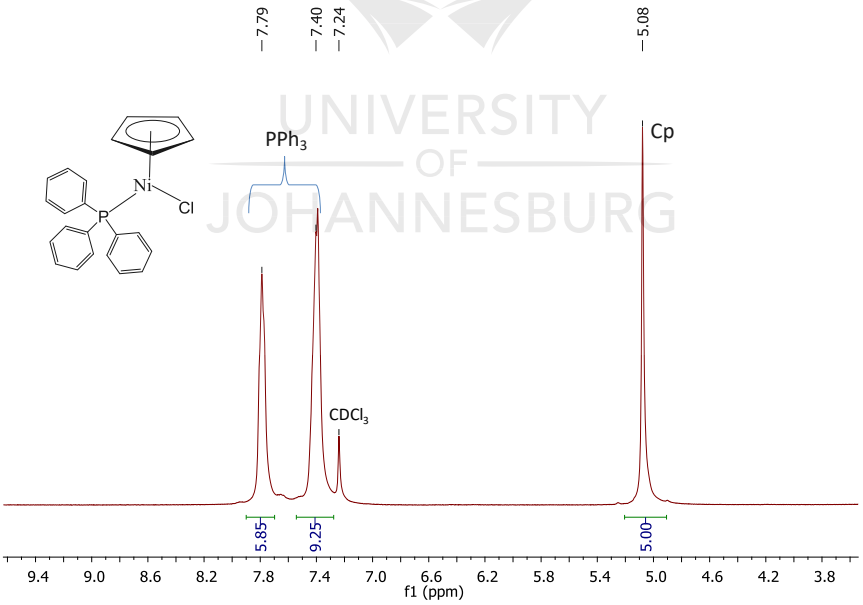

Fig 2. 4 ^{1}H NMR spectrum of complex **C1** in $CDCl_3$ (500 MHz).

The complex **C1** was further characterized using $^{13}C\{^{1}H\}$ NMR spectroscopy

2.4.2 $^{13}C\{^{1}H\}$ NMR spectroscopy of complex C1

The $^{13}C\{^{1}H\}$NMR spectrum of complex **C1** (Fig. 2.5) was analysed in deuterated chloroform. The spectrum shows the Cp ring carbon peaks appearing upfield at 94.66 pm and the aromatic carbons appeared in the region 128.53- 134.19 ppm. The number of carbon signals observed are in accordance with the expected carbons in the complex.

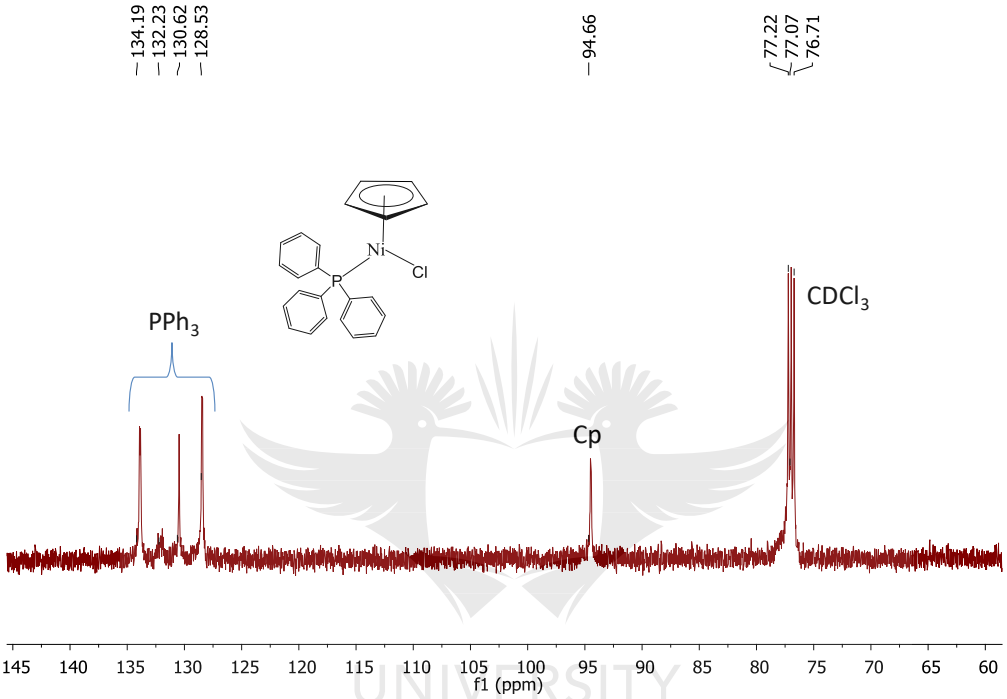

Fig 2. 5 $^{13}C\{^{1}H\}$ NMR of complex **C1** in $CDCl_3$ (500 MHz).

A $^{31}P\{^{1}H\}$ NMR experiment was also conducted to identify the phosphorus species in the complex.

2.4.3 $^{31}P\{^{1}H\}$ NMR spectroscopy of complex C1

The $^{31}P\{^{1}H\}$ NMR spectrum of complex **C1** (Fig. 2.6) shows a single peak at 28.88 ppm. This peak shifted downfield in comparison to the free triphenylphosphine ligand (-6.28 ppm),which confirms that the phosphorus atom is coordinated to the nickel center. The deshielding of the signal observed for complex **C1** can be attributed to the phosphorus ligand being a σ-donor and π acceptor, this results in the movement of electron density from the phosphorus atom towards the nickel atom upon complexation, leaving the phosporus less electron dense that in the free ligand.[13,14]

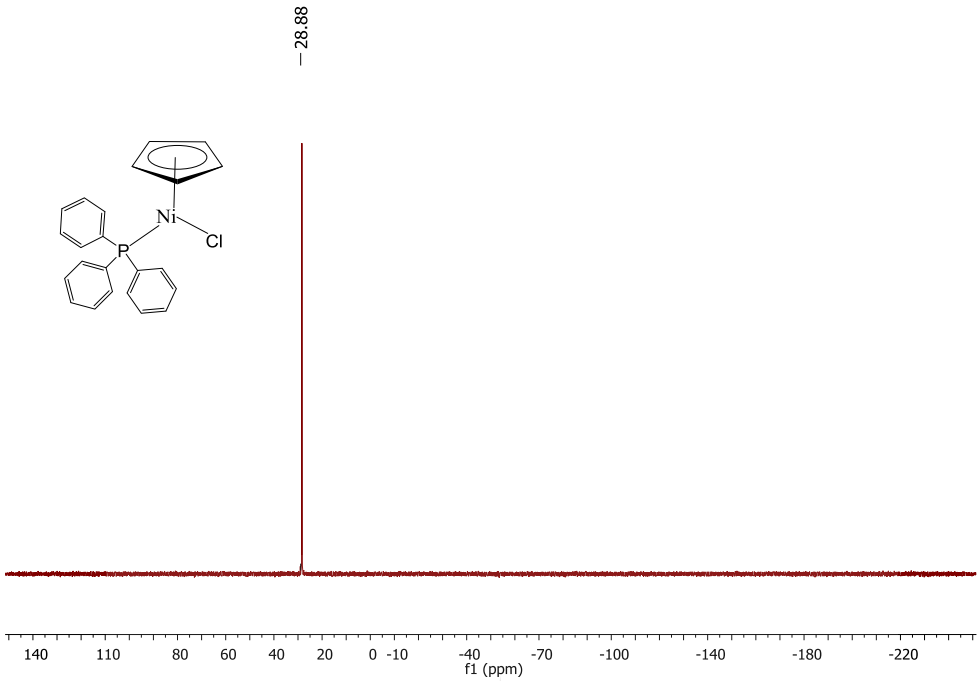

Fig 2. 6 $^{31}P\{^{1}H\}$ NMR of complex **C1** in $CDCl_3$ (500 MHz).

In addition to NMR characterization, HR-MS was also used to further characterize complex **C1**.

2.4.4 High resolution mass spectroscopy of complex C1

The high resolution mass spectrum of complex **C1** showed a peak for *m/z*= 385.0657 for $[M\text{-}Cl+H]^+$ which corresponds to the molar mass of the protonated complex **C1** as shown in Fig. 2.7.

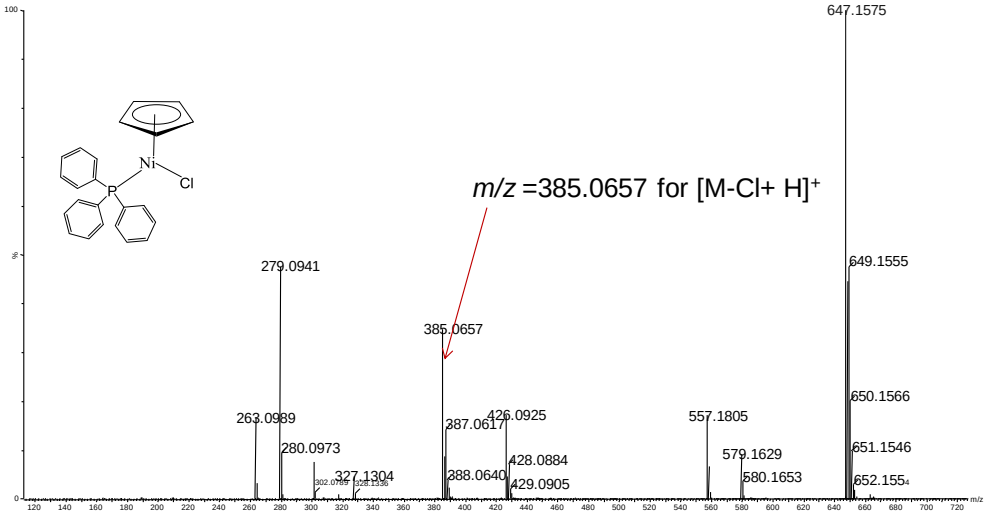

Fig 2. 7 Mass spectrum of complex **C1**

The complex **C1** was further characterized by elemental analysis to determine the elemental composition of the complex and to ascertain its purity.

2.4.5 Elemental analysis and melting point of complex C1

The elemental analysis of complex **C1** was calculated and found to be within the acceptable limits of the calculated value and the melting point range was 168- 170 ^{o}C.

2.5 Synthesis and characterization of compound (i)

The compound (i) was synthesized using a modified one pot synthetic procedure as shown in Scheme 2.3.[11] Ligand **L1** dissolved in ethanol was added to nickel chloride hexahydrate dissolved in ethanol and the reaction mixture was refluxed at 75 ^{o}C for 3 hours under argon. The solvent was removed using rotary evaporation and the product was obtained as green oil with good yield (67 %). Compound (i) is soluble in chloroform, THF, dichloromethane, dimethyl sulfoxide, acetonitrile and insoluble in hexane, pentane and diethyl ether. Due to failure of compound (i) to shim no conclusive ^{1}H NMR spectrum was obtained. The compound (i) was characterized using ^{31}P{^{1}H} NMR, ^{13}C{^{1}H} NMR, ^{29}Si{^{1}H}NMR and high resolution mass spectroscopy.

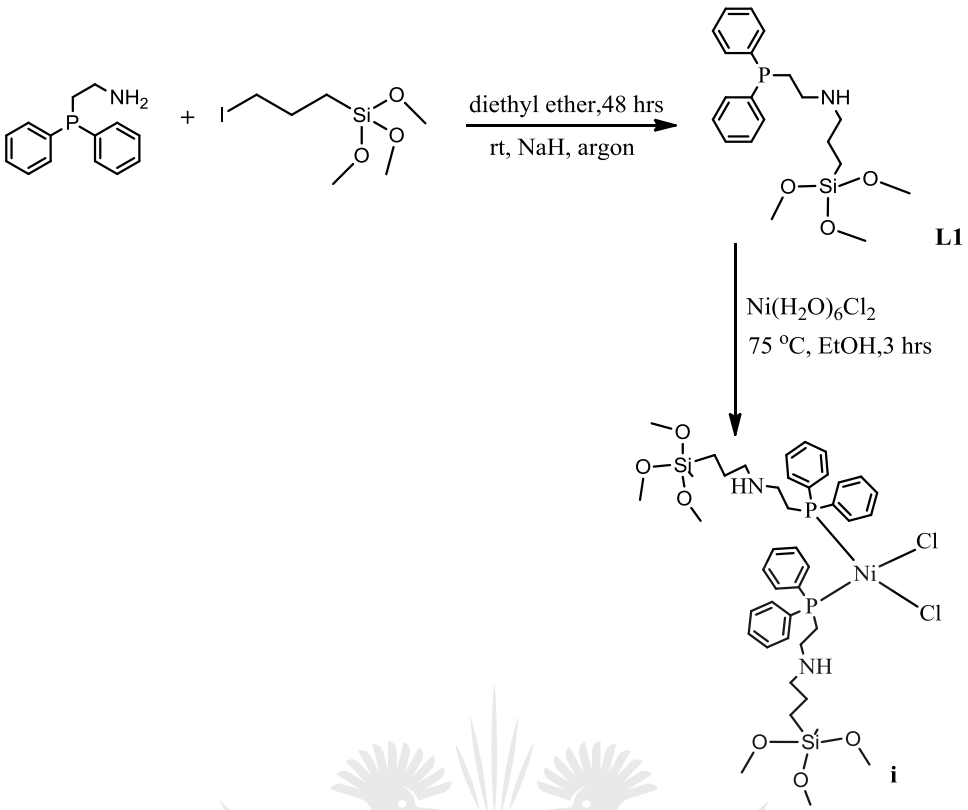

Scheme 2. 3 Synthesis of compound (i).

2.5.1 $^{31}P\{^{1}H\}$ NMR spectroscopy of compound (i)

The $^{31}P\{^{1}H\}$ NMR spectrum of compound (i) is shown in Fig 2.8, the ^{31}P signal for compound (i) is observed as a singlet appearing at 45.68 ppm which is a downfield shift compared to the ligand **L1** (-21.95 ppm), which confims that the phoshorus atom is coordinated to the nickel center.

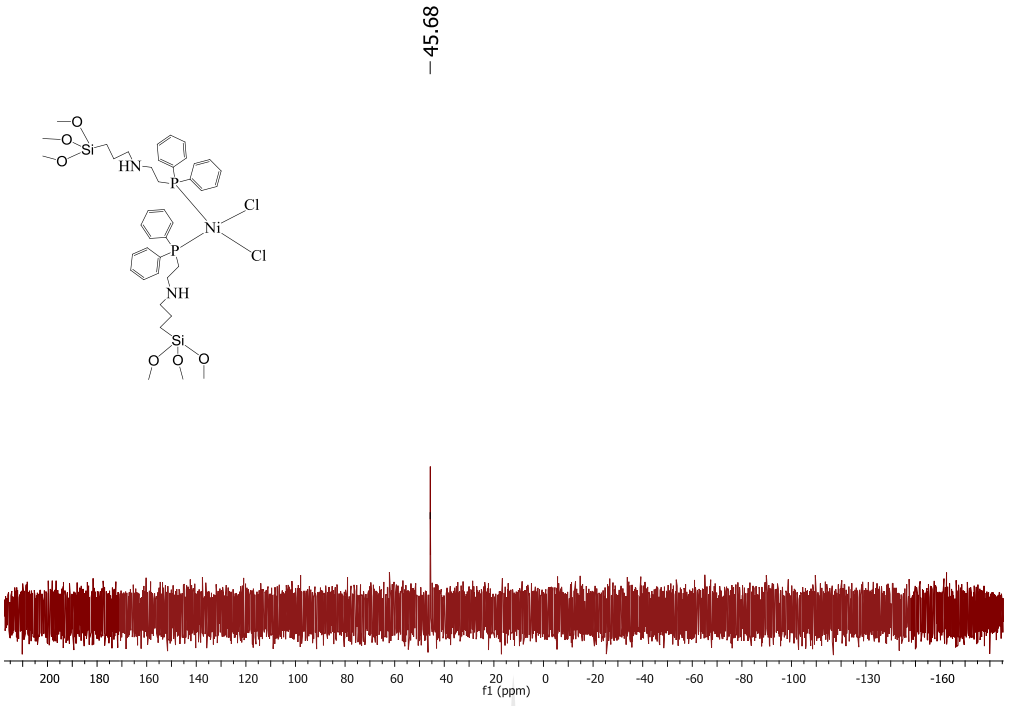

Fig 2. 8 $^{31}P\{^{1}H\}$ NMR spectrum of compound (i) in $CDCl_3$ (500 MHz).

The compound (i) was further characterized with $^{13}C\{^{1}H\}$ NMR spectroscopy to identify the compound.

2.5.2 $^{13}C\{^{1}H\}$ NMR spectroscopy of compound (i)

The $^{13}C\{^{1}H\}$ NMR spectrum of compound (i) (Fig 2.9) was recorded in deuterated chloroform, using TMS as internal reference. The spectrum shows aromatic carbon peaks appearing downfield in the region 124.39- 134.53 ppm and the methylene carbons appeared upfield in the region 18.21- 58.71 ppm. The observed number of carbon signals corresponds to the proposed structure.

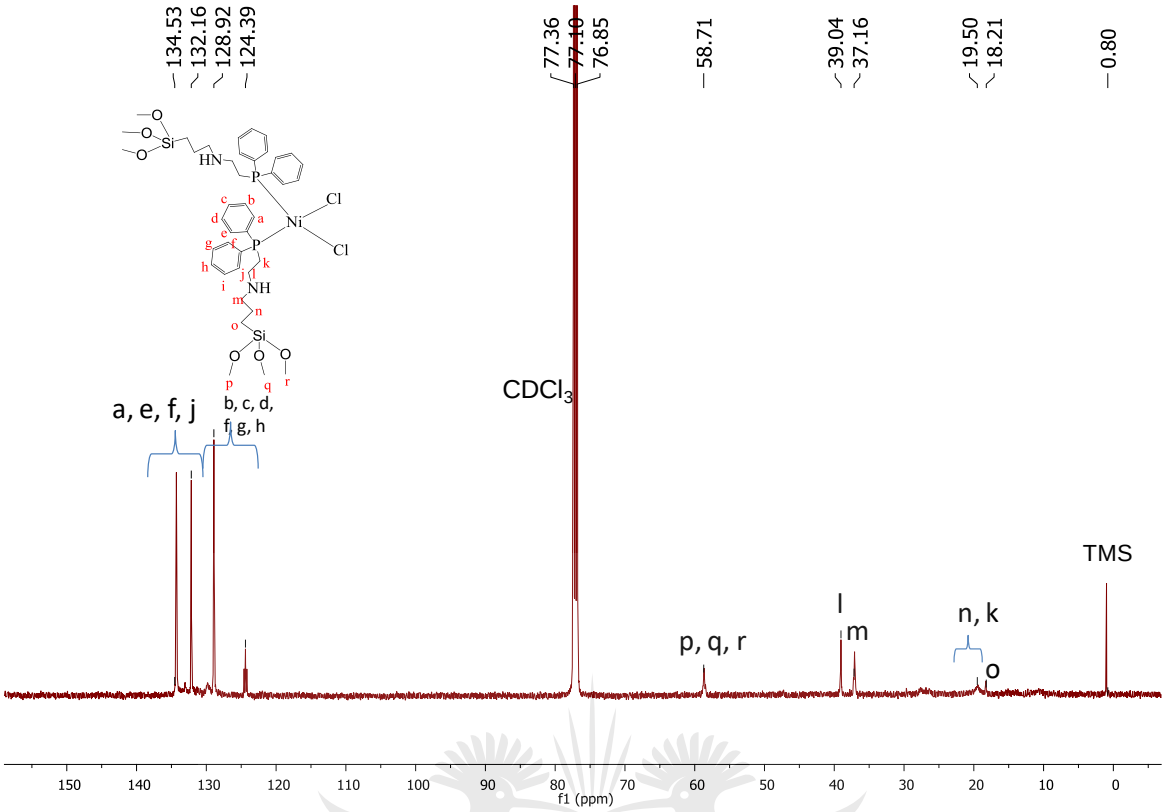

Fig 2. 9 $^{13}C\{^{1}H\}$NMR spectrum of compound (i) in $CDCl_3$ (500 MHz).

The compound (i) was further characterized by high resolution mass spectroscopy and the obtained mass spectrum showed a peak for *m/z* = 939.6956 for $[M+H]^+$ which corresponds to the molar mass of the compound (i).

2.5.3 ^{29}Si{^{1}H} NMR spectroscopy of compound (i)

The $^{29}Si\{^{1}H\}$ NMR spectrum of compound (i) in Fig 2.10 exhibits a broad peak at -107.81 ppm assigned to borosilicate glass of the NMR tube used during analysis. A second peak observed at -58.40 ppm is assigned to the compound (i) which is an upfield shift compared to ligand **L1**.

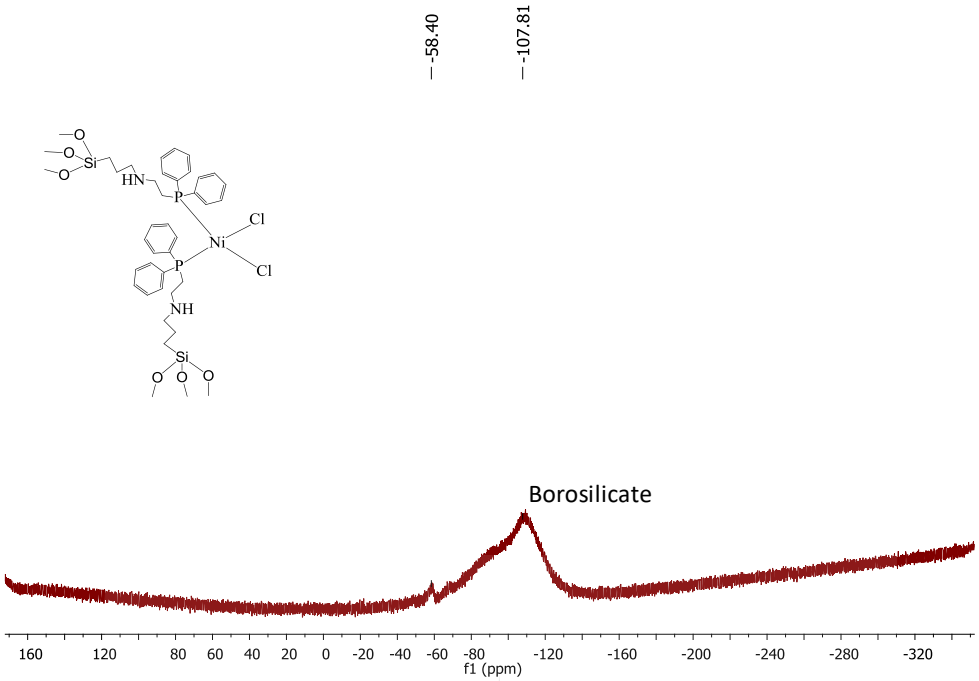

Fig 2.10 $^{29}Si\{^{1}H\}$NMR spectrum of compound (i) in $CDCl_3$ (500 MHz).

2.6 Synthesis and characterization of complex C2 and C3

The complex **C2** was synthesized using a one pot procedure (Scheme 2.4). The compound (i) dissolved in THF was added to bis(cyclopentadienyl)nickel(II) dissolved in THF and the reaction mixture was stirred under reflux at 65 ^{o}C for 24 hours following which time the solvent was removed using vacuum under reduced pressure. The complex **C2** was recovered as a brown oil in moderate yield (69 %). The complex **C2** is soluble in dimethyl sulfoxide, dichloromethane, THF, chloroform, acetonitrile, methanol and insoluble in hexane and diethyl ether. Due to failure to shim a solution of complex **C2**, no conclusive ^{1}H NMR spectrum was obtained, and this could is as a result of the paramagnetic nature of the complex. The complex **C2** was characterized using $^{31}P\{^{1}H\}$ NMR, $^{13}C\{^{1}H\}$ NMR, $^{29}Si\{^{1}H\}$ NMR, high resolution mass spectroscopy, thermal gravimetric and elemental analysis.

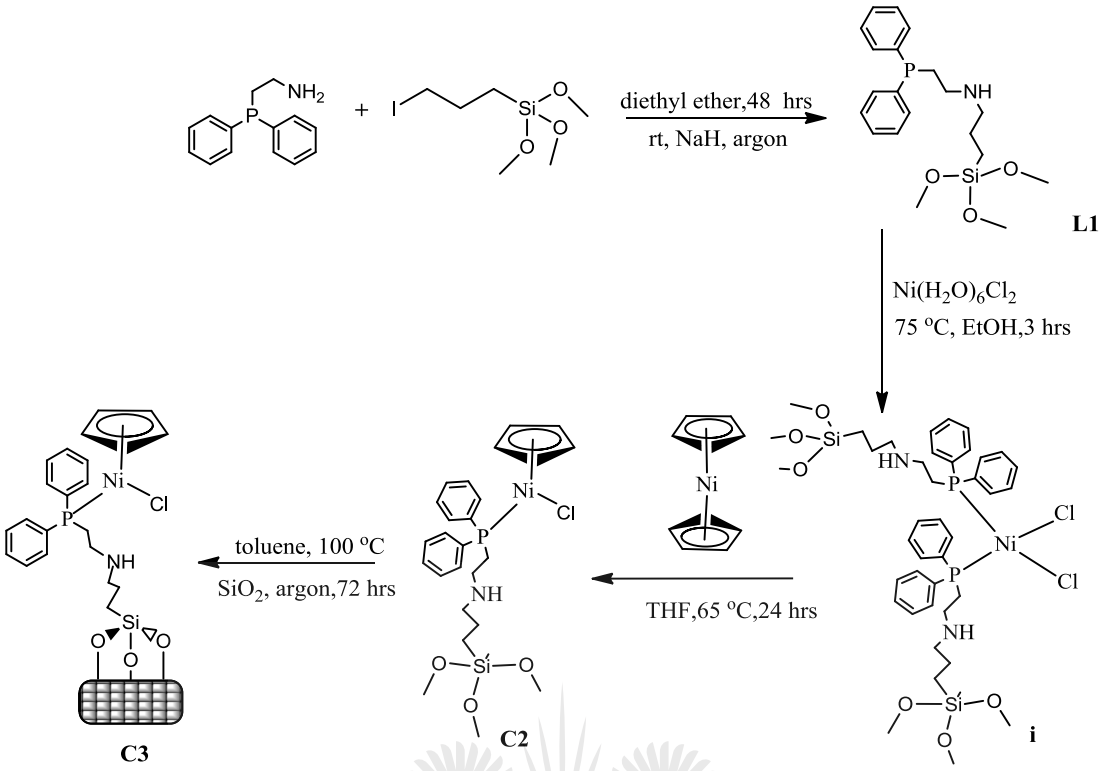

Scheme 2. 4 Synthesis of complexes **C2** and **C3.**

2.6.1 ^{31}P {^{1}H} NMR spectroscopy of complex C2

The ^{31}P{^{1}H} NMR spectrum of complex **C2** distinctly shows a broad peak at 34.00 ppm (Fig. 2.11) which shifted upfield compared to the compound (i) (45.68 ppm**)**, this confirms the coordination of the phosphorus atom to the nickel centre. The upfield shift of the ^{31}P signal on complexation with nickel center has been reported by Valarmathi *et al* and it was attributed to the mesomeric effect of electron density from the phosphorus towards the Ni center through the C-N bond.[13]

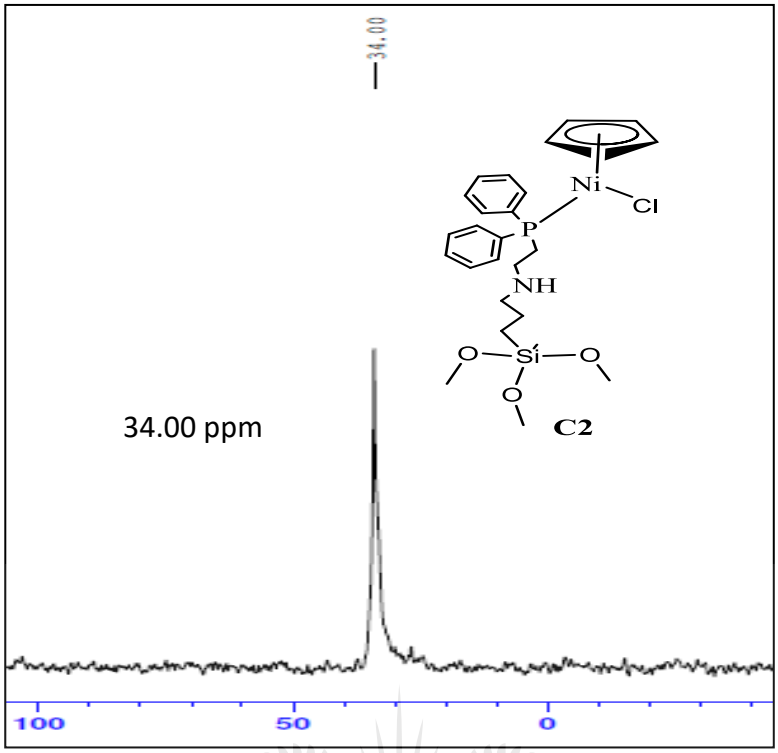

Fig 2. 11 $^{31}P\{^{1}H\}$ NMR spectrum of complex **C2** in $CDCl_3$ (500 MHz).

The $^{13}C\{^{1}H\}$ NMR spectroscopy was used to further characterize complex **C2.**

2.6.2 $^{13}C\{^{1}H\}$ NMR spectroscopy of complex C2

The $^{13}C\{^{1}H\}$ NMR spectrum of complex **C2** (Fig 2.12) was analysed in deuterated chloroform using TMS as internal reference. The spectrum shows the Cp ring carbons appearing upfield at 92.88 ppm and the aromatic carbons appeared in the region 129.26 - 132.61 ppm. The number of carbon signals observed show good agreement with the proposed structure of the complex.

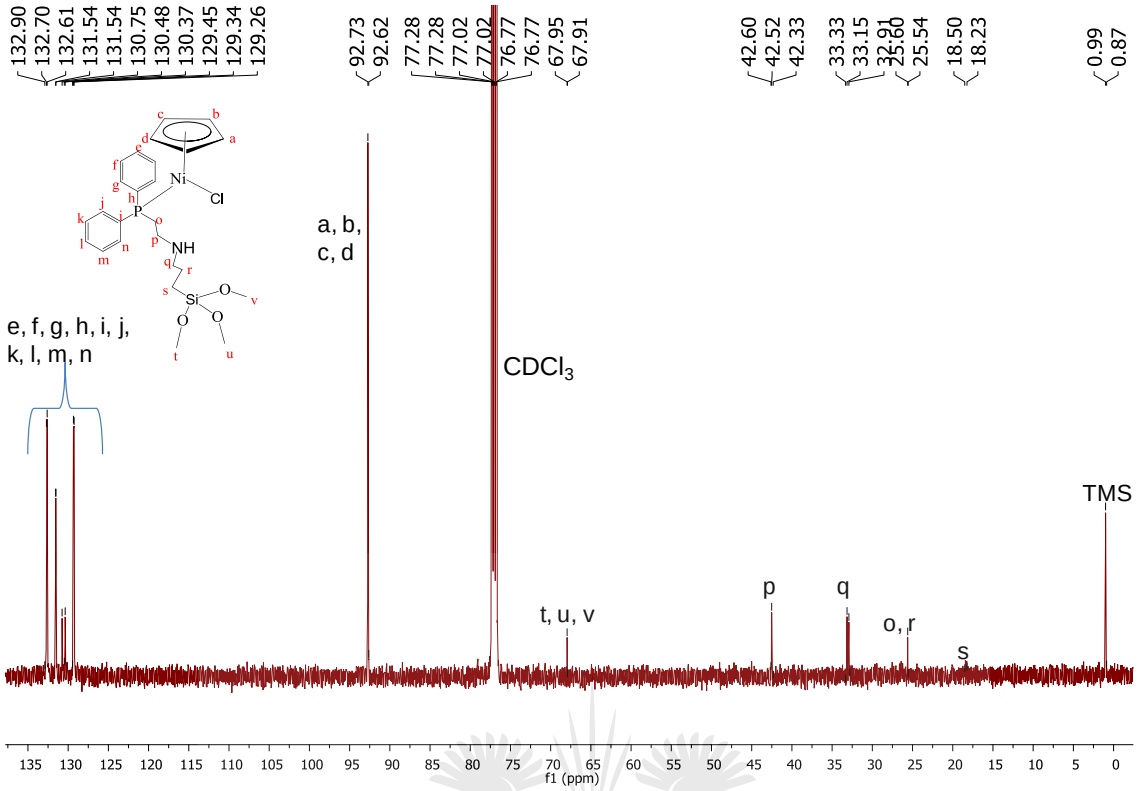

Fig 2. 12 $^{13}C\{^{1}H\}$ NMR spectrum of complex **C2** in $CDCl_3$ (500 MHz).

The complex **C2** was also characterized by $^{29}Si\{^{1}H\}$ NMR to confirm the presence of silicon species.

2.6.3 ^{29} Si{^{1}H} NMR spectroscopy of complex C2

The $^{29}Si\{^{1}H\}$ NMR spectrum of complex **C2** (Fig. 2.13) shows one signal at -43.80 ppm and a broad peak at -108.44 ppm which is due to the glass NMR tube. There was no observable shift in the $^{29}Si\{^{1}H\}$ NMR spectrum of complex **C2** compared to that of the metal precursor.

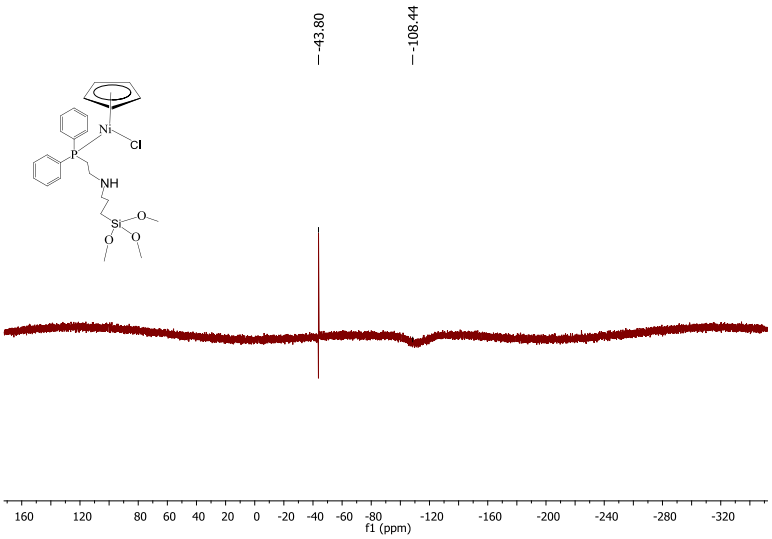

Fig 2. 13 $^{29}Si\{^{1}H\}$ NMR spectrum of complex **C2** in $CDCl_3$ (500 MHz).

The complex **C2** was further characterized by high resolution mass spectroscopy to determine the molecular weight of the complex **C2**.

2.6.4 High resolution mass spectroscopy of complex C2

The high resolution mass spectrum of complex **C2 (**Fig 2.14**)** showed a peak for m/z = 593.1252 for $[M-H]^-$ which corresponds to the molar mass of the proposed structure of complex **C2** and this confirms the successful synthesis of **C2**.

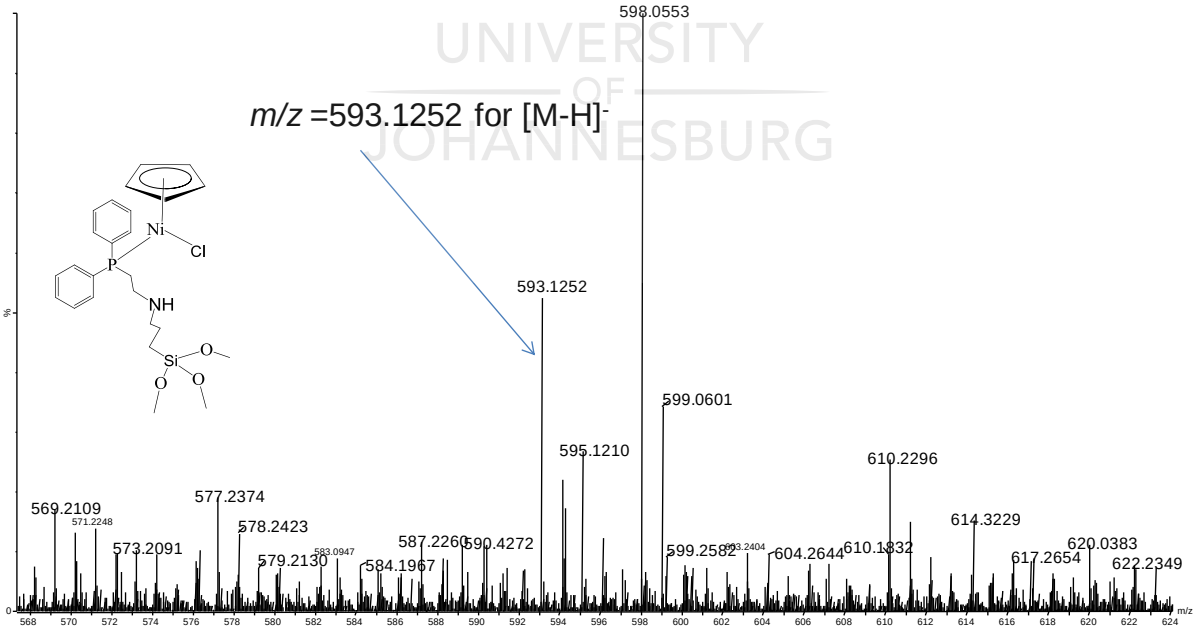

Fig 2. 14 Mass spectrum of complex **C2.**

The complex **C2** was further characterized by thermal gravimetric analysis in order to determine the thermal stability of the complex.

2.6.5 Thermal gravimetric analysis of complex C2

The TGA spectrum of complex **C2** (Fig 2.15) shows the first mass loss stage of 8.16 % from 46- 105 ^{o}C which might be due to the solvent used in synthesis. The second mass loss stage of 11.9 is observed from 176- 310 ^{o}C which might be due to decomposition of the complex.

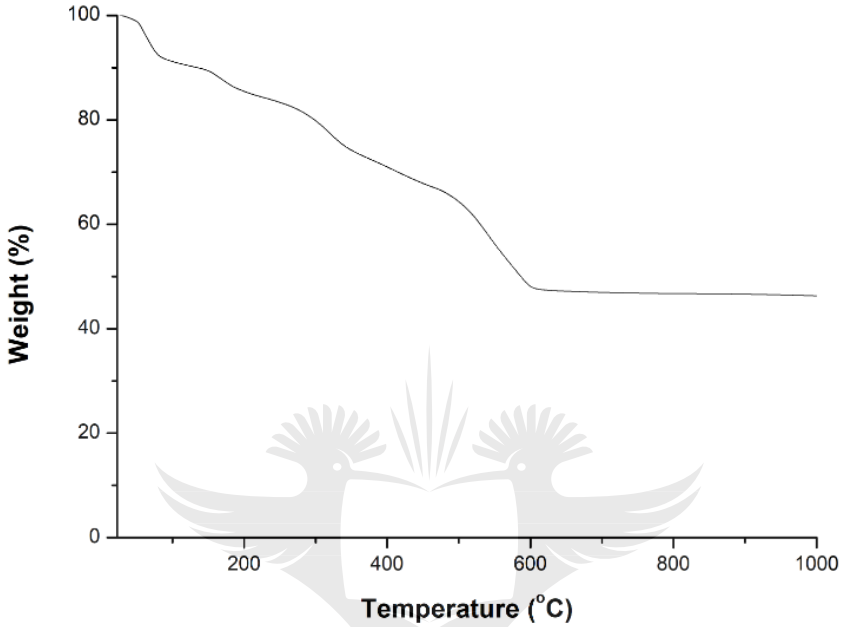

Fig 2.15 Thermal gravimetric analysis spectrum of complex **C2**

2.7 Synthesis and characterization of complex C3

The complex **C3** was synthesized using a literature synthetic procedure.[15] The complex **C2** was dissolved in dry toluene, the silica gel was dispersed in the reaction mixture and refluxed at 100 ^{o}C under dry argon atmosphere for 72 hours. The solid phase was filtered using gravity filtration and washed with equimolar amounts of toluene: ethanol and dried in the oven at 30 ^{o}C for 24 hours to afford a brown powder with good yield (71 %). The complex **C3** was characterized by BET, PXRD, ICP-MS, TGA, SEM and TEM.

2.7.1 Surface properties of complex C3

2.7.1.1 Nitrogen adsorption-desorption studies – The BET surface area, pore volume and pore size data of the silica supported complex **C3** is shown in Table 2.1 and Fig 2.16. It has been reported in literature by Venturelli and co-workers that the surface area of a catalyst plays a major role because the catalytic process takes place on the surface of the catalyst and as a result the surface area greatly affects the catalytic activity.[16]

The complex **C3** exhibited a high surface area of 258 m^2/g although it was lower compared

to that of SiO_2 (442 m^2/g) which might be as a result of the presence of the nickel metal as well as SiO_2 transformation during synthesis.[17]

In addition, the catalyst pore structure (volume and size) has an effect on its activity hence the pore volume and size was investigated. The pore volume decreased from 0.69 cm^3/g in prestine SiO_2 to 0.39 cm^3/g (in **C3**) which might be due to pores collapsing at elevated temperatures during synthesis. The physisorption isotherms (Fig 2.16a) are typical of type IV based on the literature reported IUPAC classification,[18] this confirms that the synthesized complex **C3** is mesoporous. The pore diameter of complex **C3** (4.63 nm) shown in Fig 2.14(b) falls within the range for mesoporous materials (2 nm < size < 50 nm)[16] which also confirms that complex **C3** is mesoporous.

Table 2. 1 The surface properties of silica gel and silica supported complex **C3**

Entry	Catalyst	S_{BET} (m^2/g)	Vp (cm^3/g)	Dp (nm)
1	SiO_2	442	0.69	5.13
2	$C3/SiO_2$	258	0.39	4.63

S_{BET} (BET specific surface area), Vp (pore volume), Dp (pore diameter)

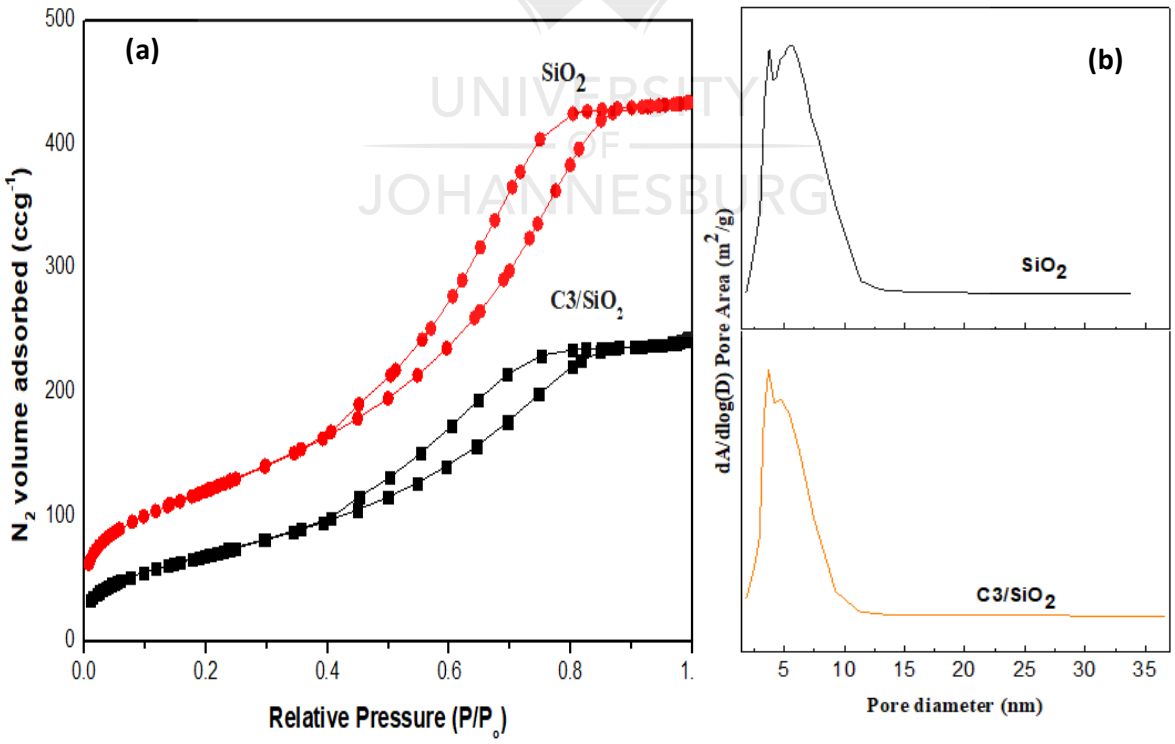

Fig 2. 16 (a) N_2 adsorption-desorption isotherms and (b) pore size distribution of the silica gel and complex **C3.**

The SiO_2 support and the complex **C3** were further characterized by X-ray powder diffraction to determine their phase composition.

2.7.1.2 X-ray Powder Diffraction - The XRD patterns presented in Fig 2.17 were obtained in order to determine the phase composition of the supported catalysts. It has been reported in literature that silica gel is amorphous and displays a broad band centred at $2\Theta = 22^{o}$.[6] The complex **C3** exhibits sharp (2Θ = 32^{o}, 36^{o}, 42^{o}) and broad (2Θ = 22^{o}) diffraction peaks which means that it could be a mixture of both crystalline and amorphous in nature. The broad peak around 2Θ = 22-24^{o} is a characteristic peak of amorphous silica, this confirms that complex **C3** is supported on silica. The diffraction pattern of complex **C3** shows the appearance of new peaks that are absent in pure silica support, which also indicates that the complex **C3** has been supported on SiO_2.

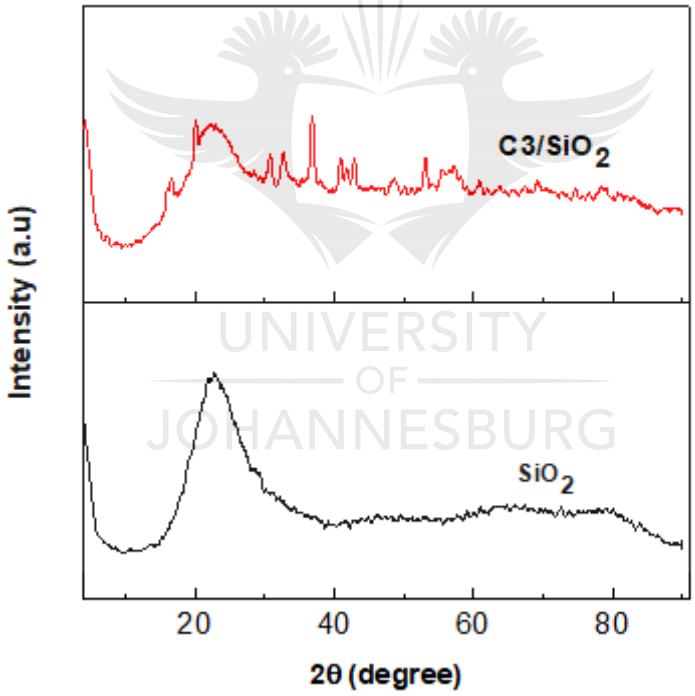

Fig 2. 17 XRD spectra of complex **C3** (top) and silica gel (bottom).

The complex **C3** was further characterized by ICP-MS to determine the metal loading.

2.7.1.3 Inductively Coupled Plasma-Mass Spectrometry- The metal loading on supported complexes plays an important role especially in catalytic reactions where there is need to determine the productivity per gram of metal[19], hence the Ni loading on complex **C3** was determined using ICP-MS and it was found that complex **C3** has 7.42 % Ni content.

The thermal stability of the complex **C3** was also determined using thermal gravimetric analysis.

2.7.1.4 Thermal gravimetric analysis of complex C3

The TGA spectrum of complex **C3** (Fig 2.18) shows a gradual decrease in weight compared to the version which is not supported on silica (complex **C2**) indicating that immobilization on silica improved the thermal stability of the complex **C3**. The first mass loss of 2.50 % from 80- 110 ^{o}C might be due to the toluene used as solvent during synthesis. The second mass loss of 16.81 % from 250- 550 ^{o}C was attributed to the condensation of silanol groups.

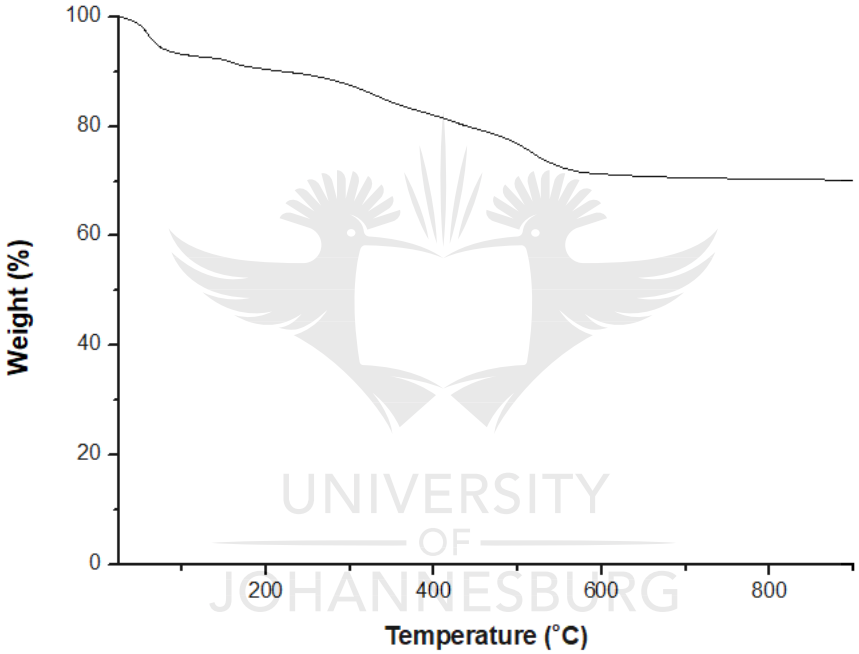

Fig 2.18 Thermal gravimetric analysis spectrum of complex **C3**

The SiO_2 support and the complex **C3** were also characterized by TEM.

2.7.1.5 Transmission Electron Microscopy- The TEM images of the silica support as well as the supported complex **C3** (Fig 2.19(a) and b) showed that the silica gel has pores which are retained even after complex **C3** was anchored on it although the pores are not so well defined. It was not possible to perform point scans along the diameter of the particles due to their small size and undefined pores.

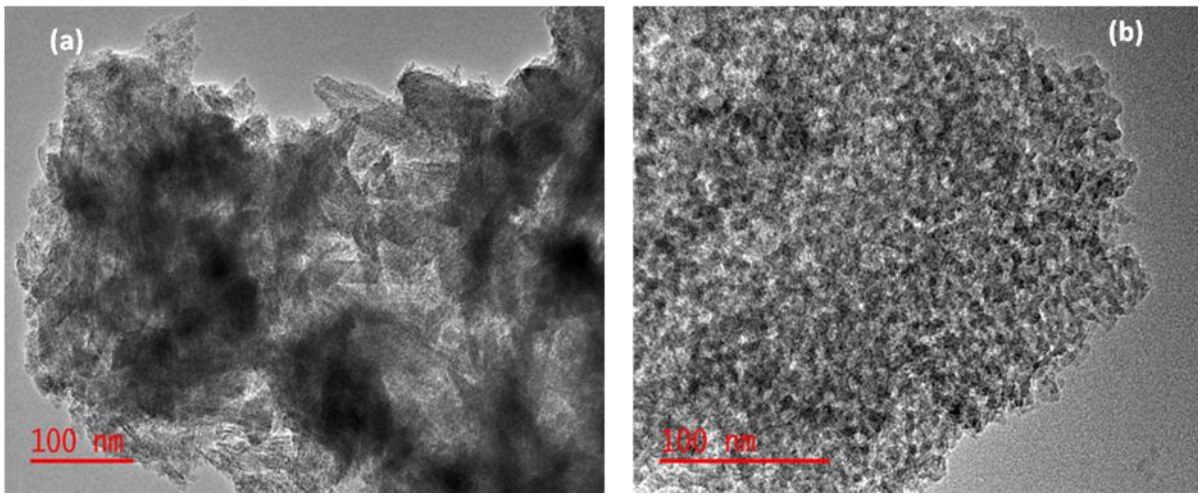

Fig 2. 19 TEM images of silica gel (a) and complex **C3** (b)

To understand the surface morphology of complex **C3** Scanning Electron Microscopy (SEM) characterization was performed.

2.7.1.6 Scanning Electron Microscopy- The obtained SEM images (Fig. 2.20) showed that the silica texture is retained in complex **C3** which results in complex **C3** to exhibit a porous texture that is similar to that of SiO_2 which was confirmed by the BET results**.** It has been reported in literature that the type of catalyst supported on silica can significantly alter the particle morphology.

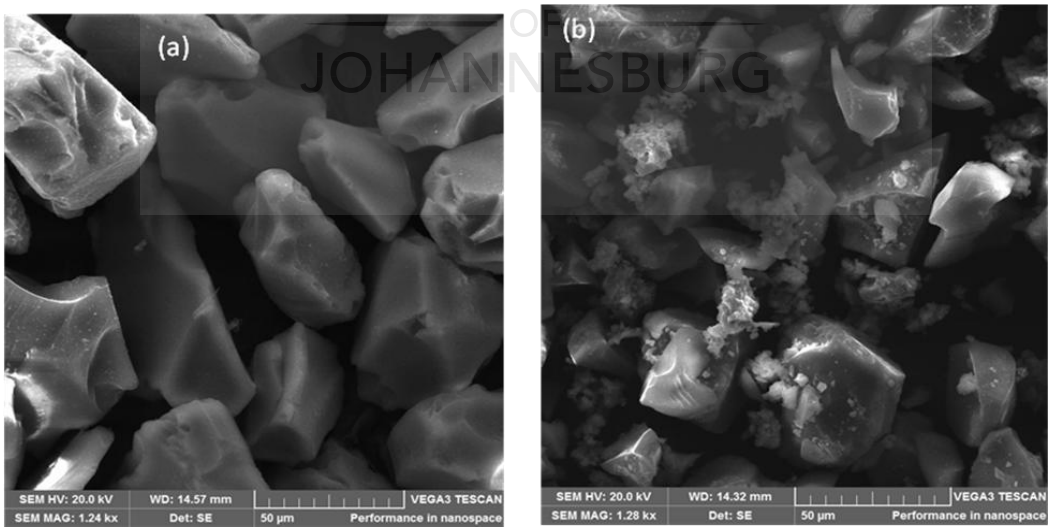

Fig 2. 20 SEM images of silica gel (a) and complex **C3** (b).

The complex **C3** was further characterized by Energy Dispersive X-ray spectroscopy (EDX) to determine the distribution of the metal particle size.

2.7.1.7 Ni elemental mapping- The EDX image (Fig 2.21) shows that the Ni metal is highly dispersed on the SiO_2 support in the complex **C3** which might be due to the nickel metal salt ($NiCl_2.6H_2O$) which was used in the synthesis of complex **C3**.

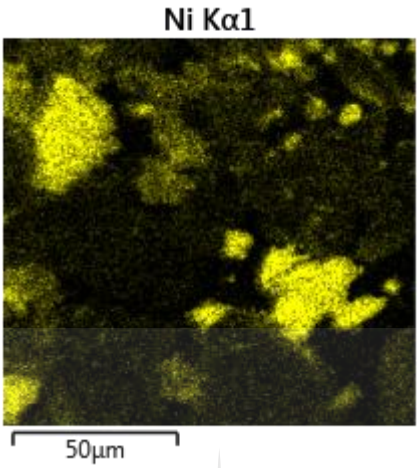

Fig 2. 21 Ni elemental mapping of complex **C3**

In order to get information on the surface composition of the complex **C3**, the energy dispersive X-ray microanalysis (EDX) was also performed.

2.7.1.8 Energy Dispersive X-ray spectroscopy - The EDX results (Fig 2.22) revealed the presence Si and O in the silica support (a) Si, O, C, Ni, P and Cl elements in complex **C3.** However, there are some traces of Iodine from the trimethoxysilane used in the synthesis of complex **C3.**

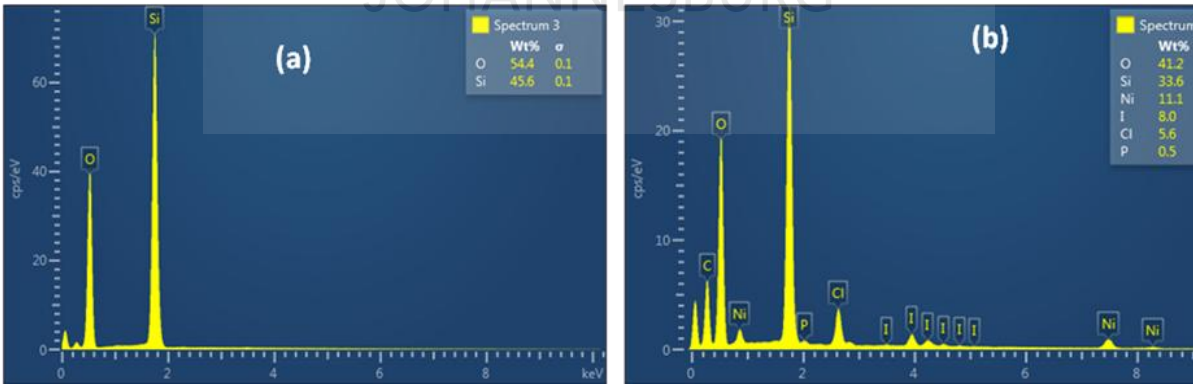

Fig 2. 22 EDX images showing silica support (a) and complex **C3** (b).

2.8 Conclusion

One ligand (**L1**), two homogenous half-sandwich Ni(II) complexes (**C1** and **C2**) were synthesized and characterized using spectroscopic techniques such as (^{1}H NMR, ^{13}C{^{1}H} NMR, ^{31}P{^{1}H} NMR, ^{29}Si{^{1}H} NMR, high resolution ESI mass spectrometry and elemental analysis. One heterogenous half-sandwich Ni(II) complex (**C3**) was also synthesized and characterized using both analytical and spectroscopic techniques such as ICP-MS, PXRD, BET, SEM and TEM. The complexes **C1-C3** were evaluated as catalyst precursors in the hydrogenation of furfural, the results are discussed in chapter four.

2.9 Experimental

2.9.1 Materials and chemicals

All reactions were performed under inert conditions using standard Schlenk techniques. Nickel chloride hexahydrate [$Ni(H_2O)_6Cl_2$], Bis(cyclopentadienyl) nickel(II), triphenylphosphine (PPh_3), 2(diphenylphosphino)ethylamine, furfural (FF), 3(Iodopropyl)trimethoxysilane, silica gel were all obtained from Sigma-Aldrich and used without purification. The solvents tetrahydrofuran (THF), ethanol (EtOH), methanol (MeOH), diethyl ether, and toluene were purchased from Sigma -Aldrich and dried before use. The metal precursor $Ni(PPh_3)_2Cl_2$ was prepared according to a literature procedure.[11] Nuclear magnetic resonance (NMR) was recorded on a Bruker Utrashield- 400/ 500 MHz spectrometer in chloroform. Characterization of the samples by powder X-Ray diffraction was performed by using P analytical X'PERT1000 Antan Paar Philips. Melting points were determined using Buchi melting point apparatus B-540. Mass spectrometry was obtained using an electro spray ionisation-mass spectrometer in the positive or negative mode. The surface area, pore volume and pore diameter of the samples were calculated using the multipoint Brunauer Emmett-Teller (BET) ASAP 2460. Transmission electron microscopy (TEM) study was carried out with a JEM-2100electron microscope. The catalysts were suspended in ethanol under sonication and applied on carbon-coated copper grids .Scanning Electron microscopy Energy Dispersive X-ray (SEM-EDX) images studies were carried out with TESCAN OXFORD microscope. Elemental analyses were carried out using a Thermo Scientific Flash 2000 series.

2.9.2 Synthesis of ligand L1

Ligand **L1** was prepared by modified synthetic procedure from the literature.[20] Sodium

hydride (0.0052 g, 0.218 mmol) was added to 2-(diphenylphosphino)ethylamine (0.051 g, 0.218 mmol) dissolved in diethyl ether (10 mL) and stirred at room temperature for 1 hour under argon. (3-Iodopropyl) trimethoxysilane (0.063 g, 0.218 mmol) was added to the reaction mixture and stirred for 48 hours at room temperature under argon. The solvent was removed using vacuum under reduced pressure to afford colourless oil. **Yield**: (0.113 g, 75%). Due to air and moisture sensitivity, the ligand **L1** could only be characterized by $^{31}P\{^{1}H\}$ NMR. **$^{31}P\{^{1}H\}$ NMR** (500MHz, $CDCl_3$)**:** δ= -21.95 ppm

2.9.3 Synthesis of $NiCl_2(PPh_3)_2$

The Ni(II) precursor was synthesized following a literature synthetic procedure.[11] Nickel chloride hexahydrate (0.0351 g, 0.271 mmol) dissolved in ethanol (20 mL) was added to triphenylphosphine (0.336 g, 0.542 mmol) dissolved in ethanol (30 mL) and the mixture was refluxed at 75 ^{o}C for 1 hour under argon. The purple product precipitated out and was filtered using gravity filtration, washed with ethanol (10 ml) and dried overnight under vacuum. **Yield**: (0.3329 g, 89%), Due to failure of $NiCl_2(PPh_3)_2$ to shim no conclusive ^{1}H NMR spectrum was obtained. Mp: 227-231 ^{o}C, **$^{31}P\{^{1}H\}$ NMR** (500MHz, $CDCl_3$): (δ, ppm) -5.21 ppm, **$^{31}C\{^{1}H\}$ NMR** (100 MHz, CDCl3): (δ, ppm) 137.43, 133.83, 128.88, 128.22. **Elemental analysis** (%): Calculated for $C_{36}H_{30}Cl_2NiP_2$: C, 66.10; H, 4.62; Cl, 10.84, Found: C, 66.52; H, 4.71. **High resolution ESI-MS** (positive): *m/z* = 619.0809 for $[M\text{-}Cl+H]^{+}$

2.9.4 Synthesis of complex C1[11]

The nickel precursor $[NiCl_2(PPh_3)_2]$ (0.908 g, 1.388 mmol) was dissolved in THF (60 mL) under argon. To this was added Bis(cyclopentadienyl) nickel(II) (0.262 g, 1.388 mmol) and the reaction was left to stir under reflux at 60 ^{o}C for 6 hours. The solvent was removed using vacuum under reduced pressure and the residue dissolved in hot benzene (5 mL) followed by recrystallizaion of the benzene filtrate in hexane (30 mL) at 0 ^{o}C to afford red purple crystals. **Yield**: (1.098 g, 82%), **Mp**: 168-170 ^{o}C, **^{1}H NMR** (500MHz, $CDCl_3$)**: (**δ, ppm) 7.81(m, 6H, H_{Ar}), 7.26(m, 9H, H_{Ar}), 5.10(s, 5H, H_{cp}). **$^{31}P\{^{1}H\}$ NMR** $CDCl_3$, 28.88 ppm. **$^{13}C\{^{1}H\}$ NMR** (100 MHz, $CDCl_3$): (δ, ppm) 134.19, 132.23, 130.62, 128.53, 94.66. **Elemental analysis** (%): Calculated for $C_{24}H_{23}ClNiP$: C, 66.03; H, 5.31, Found: C, 65.61; H, 4.59. **High resolution ESI-MS** (positive): *m/z* = 385.0657 for $[M\text{-}Cl+H]^{+}$.

2.9.5 Synthesis of compound (i)

The compound (i) was synthesized by a modified synthetic procedure.[11] Ligand **L1** (0.104 g, 0.256 mmol) dissolved in ethanol (30 mL) was added to nickel chloride hexahydrate (0.016 g, 0.127 mmol) dissolved in ethanol (20 mL) and the reaction mixture was refluxed at 75 ^{o}C for 3 hours under argon. The solvent was removed using rotary evaporation and the product was obtained as green oil. **Yield**: (0.081 g, 67%), Due to failure of compound (i) to shim no conclusive ^{1}H NMR spectrum was obtained. **^{31}P{^{1}H} NMR** (500MHz, $CDCl_3$): 45.68 pm. **^{13}C{^{1}H} NMR** (100MHz, $CDCl_3$): (δ, ppm) 134.53, 132.16, 128.92, 124.39, 58.71, 39.04, 37.16, 19.50, 18.21. **High resolution ESI-MS** (positive): *m/z* 939.6956 for $[M+H]^{+}$.

2.9.6 Synthesis of complexes C2 and C3

L1 (0.318 g: 0.812 mmol) was dissolved in ethanol (20 mL) and transferred to a round bottomed flask. To the stirring ligand **L1** added was nickel chloride hexahydrate (0.096 g, 0.404 mmol) dissolved in ethanol (30 mL) and the mixture was refluxed for 3 hours at 75 ^{o}C under argon. The solvent was removed using vacuum under reduced pressure to afford a green oil (compound (i)). Added to the flask was nickelocene (0.156 g, 0.812 mmol) dissolved in tetrahydrofuran (40 mL) and refluxed for 24 hours at 60 ^{o}C under argon .The solvent was removed under reduced pressure to afford a brown oily product (**C2**). **Yield**: (0.564 g, 69%). Due to failure of complex **C2** to shim no conclusive ^{1}H NMR spectrum was obtained. **^{31}P{^{1}H} NMR**, (500MHz, $CDCl_3$): 34.00 ppm, **^{29}Si{^{1}H} NMR**, (500MHz, $CDCl_3$). -43.03 ppm. **High resolution ESI-MS** (positive): *m/z* =593.1252 for $[M-H]^{-}$. **Elemental analysis** (%): Calculated for $C_{28}H_{44}ClNNiO_3PSi$: C, 69.96; H, 4.55; N, 2.63, Found: C, 71.07; H, 4.57; N, 2.45.

The complex **C2** was modified with silica gel to obtain complex **C3.**[15] **C2** (0.0175 g, 0.0285 mmol) was dissolved in dry toluene (40 mL) and stirred for 10 minutes. Added to the solution was silica gel (0.0224 g, 0.332 mmol) and the reaction mixture was refluxed at 100 ^{o}C under dry argon atmosphere for 72 hours. The solid phase was filtered using gravity filtration and washed with toluene: ethanol (1:1) and dried under vacuum at 30 ^{o}C for 24 hours to afford a brown powder. **Yield**: (0.0275 g, 71%).

2.10 References

1 A. P. Prakasham and P. Ghosh, *Inorganica Chim. Acta*, 2015, **431**, 61–100.

2 S. Ando, H. Matsunaga and T. Ishizuka, *J. Org. Chem.*, 2017, **82**, 1266–1272.

3 C. J. Weiss, P. Das, D. L. Miller, M. L. Helm and A. M. Appel, *ACS Catal.*, 2014, **4**, 2951–2958.

4 N. E. Leadbeater, *J. Org. Chem.*, 2001, **66**, 7539–7541.

5 T. Appleby and J. Derek Woollins, *Coord. Chem. Rev.*, 2002, **235**, 121–140.

6 J. A. Dias, E. Caliman, S. C. L. Dias, M. Paulo and A. T. C. . de Souza, *Catal. Today*, 2003, **85**, 39–48.

7 D. Shi, Q. Yang, C. Peterson, A.-F. Lamic-Humblot, J.-S. Girardon, A. Griboval-Constant, L. Stievano, M. T. Sougrati, V. Briois, P. A. J. Bagot, R. Wojcieszak, S. Paul and E. Marceau, *Catal. Today*, 2019, **334**, 162–172.

8 F. Hu, Y. Wang, S. Xu, Z. Zhang, Y. Chen, J. Fan, H. Yuan, L. Gao and G. Xiao, *Catal. Letters*, 2019, **149**, 2158–2168.

9 B. M. Reddy, G. K. Reddy, K. N. Rao, A. Khan and I. Ganesh, *J. Mol. Catal. A Chem.*, 2007, **265**, 276–282.

10 C. P. Jiménez-Gómez, C. Defilippi, J. A. Cecilia, R. Moreno-Tost, P. Maireles-Torres and C. Giordano, *Mol. Catal.*, 2020, **487**, 110889.

11 K. W. Barnett, *J. Chem. Educ.*, 1974, **51**, 422.

12 A. J. Bridgeman, *Dalt. Trans.*, 2008, **2**, 1989.

13 P. Valarmathi, S. Thirumaran, L. Sarmal and R. Kant, *Spectrochim. Acta - Part A Mol. Biomol. Spectrosc.*, 2014, **129**, 285–292.

14 S. K. Latypov, S. A. Kondrashova, F. M. Polyancev and O. G. Sinyashin, *Organometallics*, 2020, **39**, 1413–1422.

15 A. N. Kursunlu, E. Guler, H. Dumrul, O. Kocyigit and I. H. Gubbuk, *Appl. Surf. Sci.*, 2009, **255**, 8798–8803.

16 G. Leofanti, M. Padovan, G. Tozzola and B. Venturelli, *Catal. Today*, 1998, **41**, 207–219.

17 D. Shi, Q. Yang, C. Peterson, A.-F. Lamic-Humblot, J.-S. Girardon, A. Griboval-Constant, L. Stievano, M. T. Sougrati, V. Briois, P. A. J. Bagot, R. Wojcieszak, S. Paul and E. Marceau, *Catal. Today*, 2019, **334**, 162–172.

18 C. A. Akinnawo, N. Bingwa and R. Meijboom, *Microporous Mesoporous Mater.*, 2021, **311**, 110693.

19 G. Alloncle, N. Gilon, C.-P. Lienemann and S. Morin, *Comptes Rendus Chim.*, 2009, **12**, 637–646.

20 CYCLOPENTAEDENYFL NECKEL TRORGANO PHOSPHINE HALIDES, Gene E. Schro, Baton Rouge, La, assigner to Ethyl Corporation, New York, N.Y, a

corporation of Delaware Patented Sept 8, 1962

Chapter three

Synthesis and characterization of tridentate homogenous and supported Ni(II) complexes

3.1 Introduction

The use of schiff base ligands in coordination chemistry has been of great interest as a result of their tunable chemical properties.[1] Schiff base ligands are derived from a condensation reaction of a carbonyl compound (aldehyde or ketone) with a primary amine. The resultant imine plays a major role in binding with metal ions via nitrogen lone pairs. Organometallic chemistry has given more attention towards the need to search for the appropriate ligand as the ligand has the ability to effectively control the reactivity and stability of metal complexes used in catalysis.[2] The type of substituent group present plays a major role in the stability of the ligand. Schiff base ligands with aryl substituents tend to be more stable compared to those that contain alkyls, therefore schiff base ligands can be bidentate (N,O-), tridentate (N,O,O-, N,O,N-) and tetradentate (N,N,O,O-).[3]

Different metal centers can be accommodated by schiff base ligands which enables the formation of coordination metal complexes with different stereochemistry. Oxygen and nitrogen donor schiff bases have been extensively studied due to their ability to form labile complexes that are highly active.[4] The need to improve both catalyst activity and selectivity has led to the interest in studying in depth the design, preparation and characterization of metal complexes including schiff base complexes that have been reported for their high catalytic activity in both homogenous and heterogenous catalysis. [5,6,7] In addition, phosphine ligands are also an important class of ligands that has been reported to enhance the reactivity of metal complexes,[8] hence they are also explored in this study. Nickel(II) complexes can adopt different geometries, however the square planar geometry has been reported to be more stable.[9]

Non-noble metals are affordable[10,11] compared to noble metals[12,13] hence the use of nickel(II) complexes is reported in this work to overcome the high cost, Here in we report on the synthesis and characterization of one schiff base ligand, two homogenous and one heterogenous tridentate O^N^O nickel(II) complexes. The ligand and homogenous complexes have been characterized using nuclear magnetic resonance spectroscopy (NMR) ^{1}H NMR,^{13}C{^{1}H} NMR and ^{31}P{^{1}H} NMR), ^{29}Si{^{1}H} NMR ,Fourier-transform infrared spectroscopy, elemental analysis and high resolution electrospray ionisation-mass spectroscopy.

3.2 Synthesis and characterization of ligand L2

The schiff base ligand **L2** was synthesized following a reported synthetic procedure.[14] The schiff base ligand was prepared by refluxing 2-aminophenol with an equimolar amount of salicyaldehyde in ethanol (Scheme 3.1). The solvent was removed by rotary evaporation and dried overnight under vacuum and ligand **L2** was obtained in good yield (87 %) as an orange solid. The ligand **L2** is soluble in methanol, ethanol, dimethyl sulfoxide, chloroform, acetonitrile, diethyl ether and insoluble in hexane and water. The ligand **L2** has been characterized using ^{1}H NMR, ^{13}C{^{1}H} NMR, FT-IR, melting point, elemental analysis and high resolution mass spectrometry.

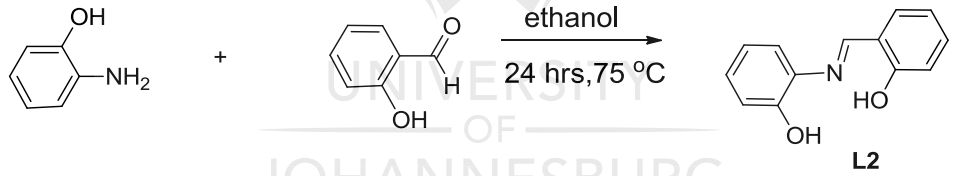

Scheme 3. 1 Synthesis of ligand **L2.**

3.2.1 ^{1}H NMR spectroscopy of ligand L2

The evidence of the condensation reaction is seen by the appearance of the imine singlet (HC=N) on the ^{1}H NMR spectrum at 8.68 ppm (Fig 3.1).This confirms that the ligand **L2** was successfully synthesized. The phenolic proton (OH) appeared as a broad peak at 12.28 ppm, all the aromatic protons for the ligand **L2** are observed in the region between 6.95 ppm and 7.44 ppm.

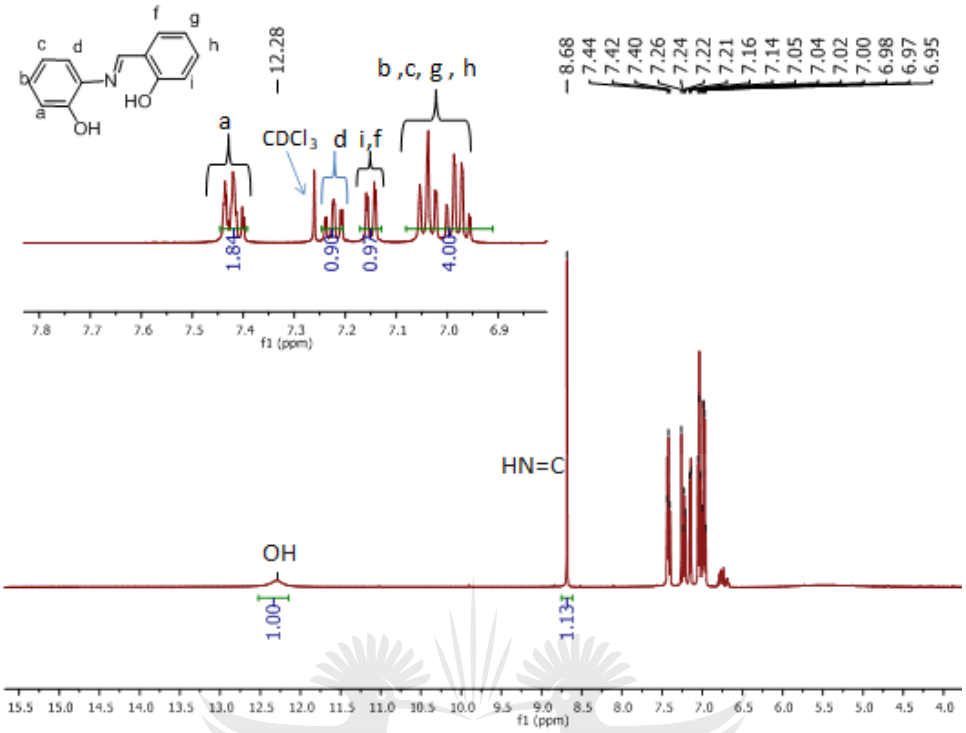

Fig 3. 1 ^{1}H NMR spectrum of ligand **L2** in $CDCl_3$ (500 MHz).

The ligand **L2** was further characterized using $^{13}C\{^{1}H\}$ NMR spectroscopy to confirm the identity of the ligand.

3.2.2 $^{13}C\{^{1}H\}$ NMR spectroscopy of Ligand L2

The $^{13}C\{^{1}H\}$ NMR spectrum of the ligand **L2 (**Fig 3.2) was recorded using TMS as internal reference in deteurated chlorofom. The $^{13}C\{^{1}H\}$ NMR spectrum shows the presence of the imine carbon (HC=N) appearing downfield at 160.66 ppm and the aromatic carbons appearing in the region 115- 149 ppm. The observed number of carbon signals is in agreement with the expected number of carbons of the expected ligand structure.

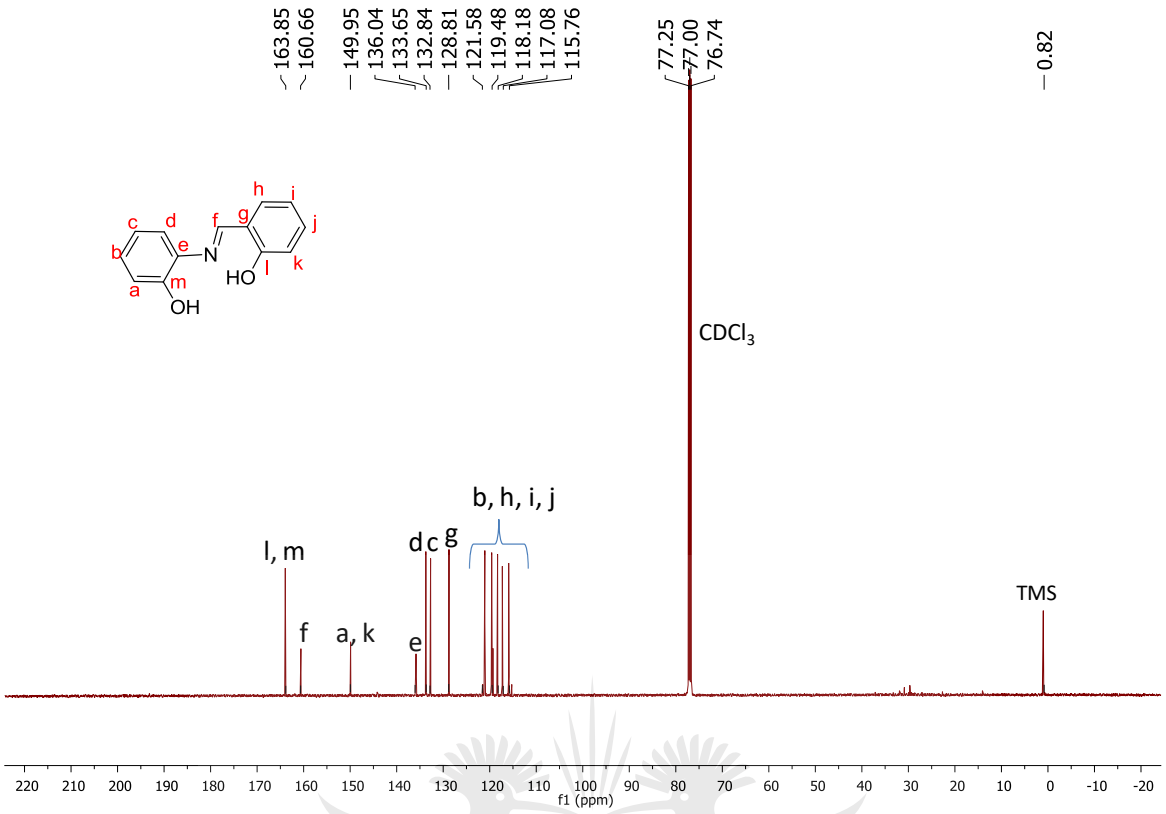

Fig 3. 2 ^{13}C {^{1}H} NMR spectrum of Ligand **L2** in $CDCl_3$ (500 MHz).

The ligand **L2** was also characterized by Infrared spectroscopy in order to identify functional groups of the ligand.

3.2.3 Infrared spectroscopy of ligand L2

The infrared spectrum of ligand **L2** (Fig 3.3) shows vibration characteristic of the imine at *ν*(C=N str.) 1625 cm^{-1} which shows evidence of the condensation reaction. The presence of other peaks such as *ν*(C=C) was observed at 1460 cm^{-1} wavenumber.

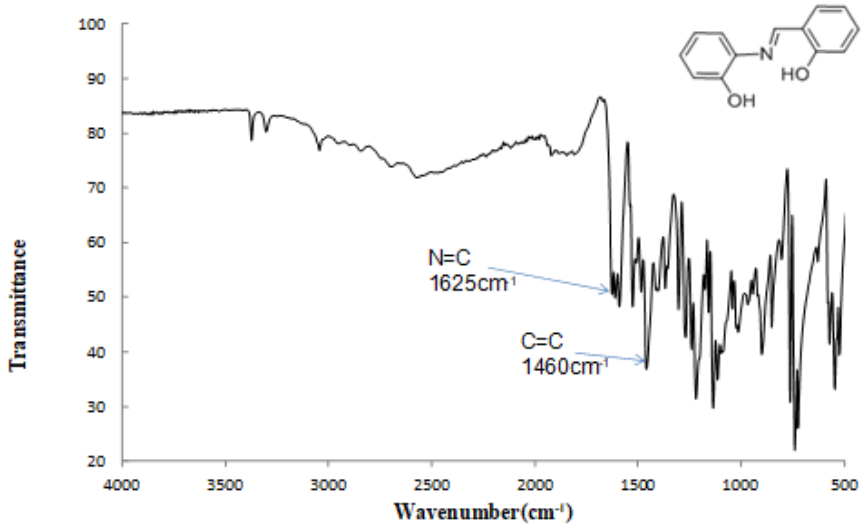

Fig 3. 3 Infrared spectrum of ligand **L2.**

In addition to NMR and IR characterization , HR-MS was also used to further characterize ligand **L2**.

3.2.4 High resolution mass spectroscopy of ligand L2

The high resolution mass spectrum of ligand **L2** (Fig 3.4) shows a peak for *m/z* = 214.0863 for $[M+H]^+$ which is corresponds to the molar mass of the ligand **L2.**

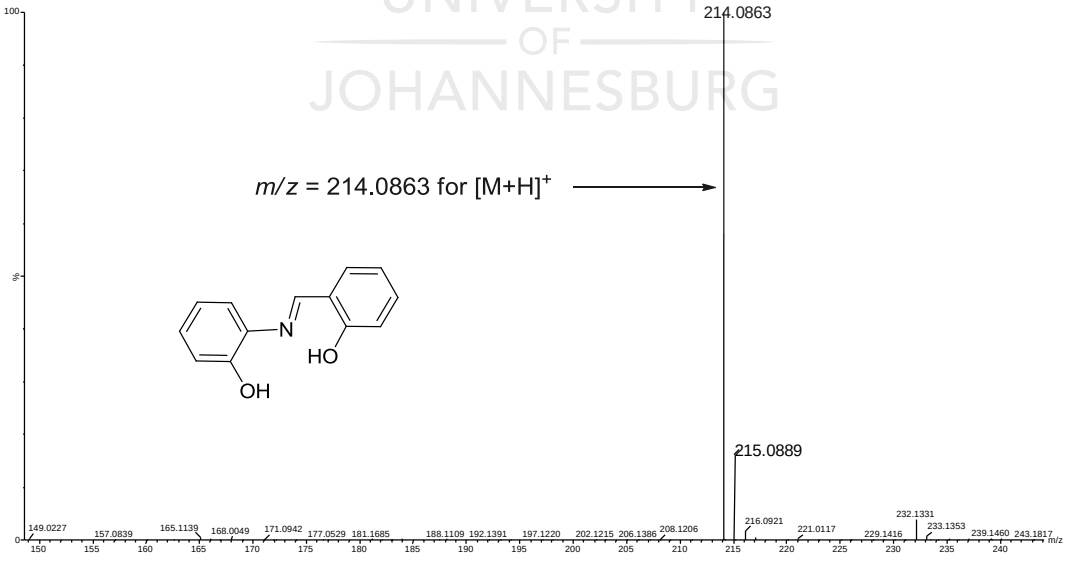

Fig 3. 4 Mass spectrum for ligand **L2**

The ligand **L2** was further characterized by elemental analysis to determine the quantity of elements present in the ligand and also the melting point of ligand **L2** was conducted to

ascertain the purity of the ligand.

3.2.5 Elemental analysis and melting point

The elemental analysis of the ligand **L2** was calculated and found to be within the acceptable limits of the calculated value and the melting point for ligand **L2** was in the range 187-189 ^{o}C which confirms the purity of the synthesized ligand.

3.3 Synthesis and characterization of complex C4

The complex **C4** was prepared using a literature synthetic procedure [15] (Scheme 3.2). One mole of the schiff base ligand **L2** was added to a methanolic solution containing nickel acetate tetrahydrate and triphenyl phosphine. The reaction mixture was refluxed for 2 hours at 65 ^{o}C under inert gas and a brown solid precipitated out. The precipitate was filtered using a Buchner funnel and dried overnight under vacuum. The complex **C4** was isolated as brown crystalline solid with good yield of 75 %. The complex **C4** is soluble in dichloromethane, ethanol, methanol, toluene, chloroform , dimethylsulfoxide and insoluble in hexane, diethyl ether and water. The complex **C4** has been characterized using ^{1}H NMR,^{13}C{^{1}H} NMR,^{31}P{^{1}H} NMR, FT-IR, high resolution mass spectroscopy, elemental analysis, thermal gravimetric analysis and X-ray crystallography.

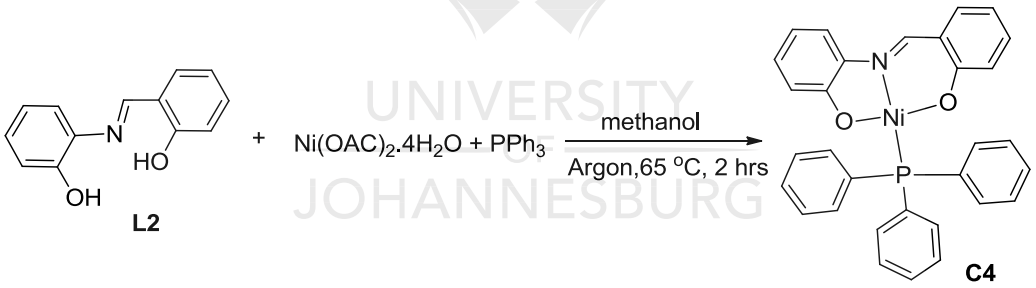

Scheme 3. 2 Synthesis of complex **C4.**

3.3.1 ^{1}H NMR spectroscopy of complex C4

The ^{1}H NMR spectrum of complex **C4** (Fig 3.5) shows a signal for the imine proton (8.49 ppm) shifted upfield compared to that of ligand **L2** (8.68 ppm) which confirms coordination of the nickel metal to the nitrogen atom. The imine hydrogen (HC=N) was splitted by phosphine and appeared as a doublet signal around 8.49 ppm, similar results have been reported in literature.[15,16] The aromatic protons of the schiff base ligand and triphenylphosphine appeared in the range 6.29-7.86 ppm. The disappearance of the hydroxyl proton (OH) at 12.28 ppm also confirms that the nickel metal is coordinated to both the oxygen and the imine nitrogen.

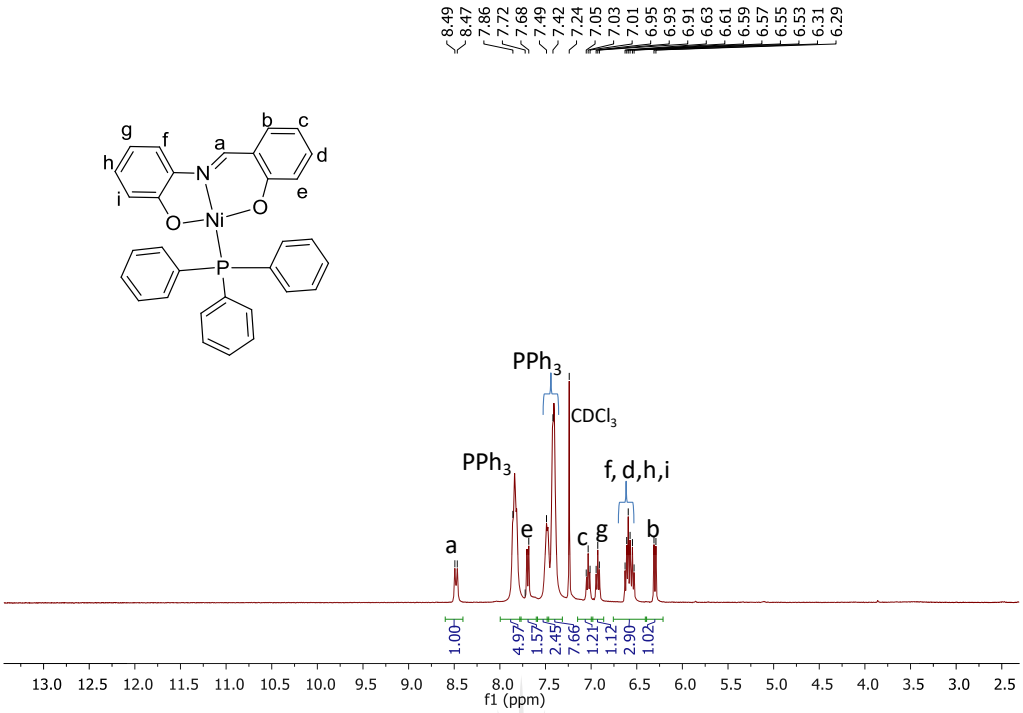

Fig 3. 5 ^{1}H NMR spectrum of complex **C4** in $CDCl_3$ (500 MHz).

The complex **C4** was further characterized using Attached Proton Test (APT) $^{13}C\{^{1}H\}$ NMR spectroscopy to differentiate the carbons unattached to protons and those that are attached to protons in the complex. This characterization was carried out after the number of carbon signals observed was lesser than the expected signals.

3.3.2 $^{13}C\{^{1}H\}$ NMR spectroscopy of complex C4

The $^{13}C\{^{1}H\}$ NMR spectrum of complex **C4** (Fig 3.6) was analysed in deuterated chloroform. The spectrum shows the imine carbon (HC=N) appearing downfield at 166.28 ppm and the aromatic carbons appeared in the region 114.04- 163.19 ppm. The number of carbon signals observed is in accordance with the expected carbons in the complex.

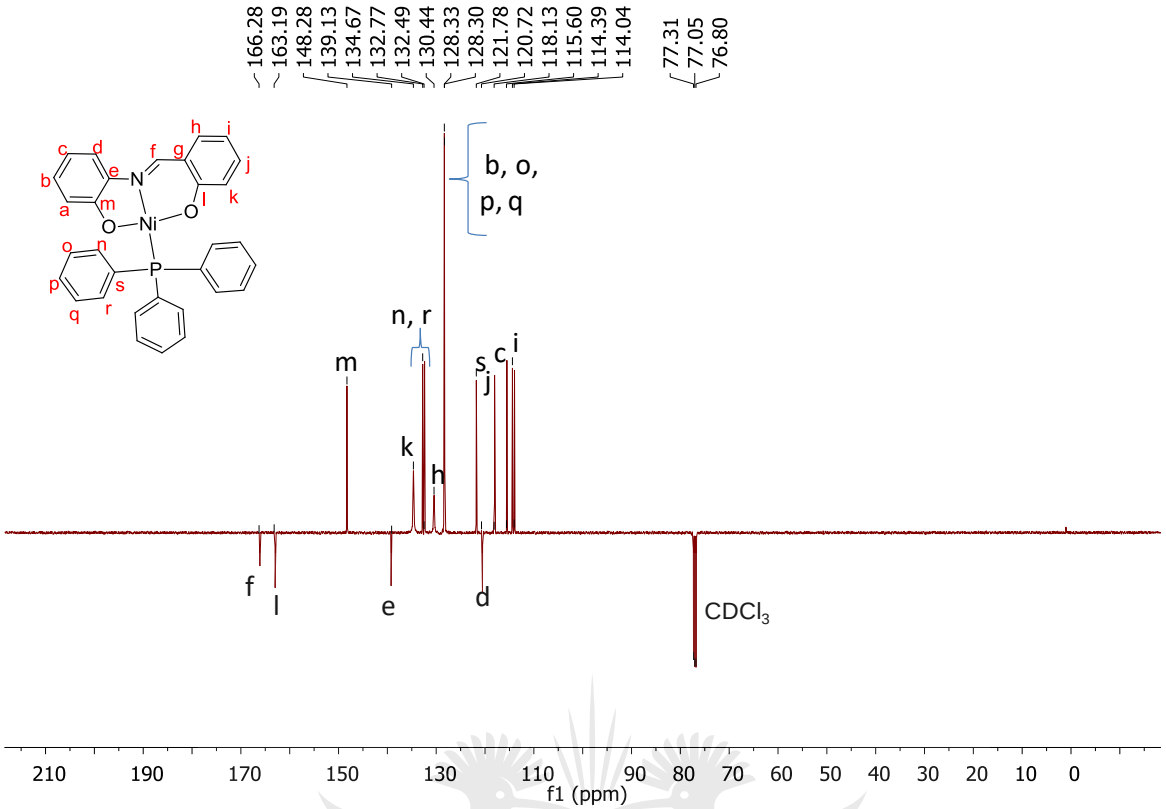

Fig 3. 6 $^{13}C\{^{1}H\}$ NMR of complex **C4** in $CDCl_3$ (500 MHz).

The phosphorus species in the complex **C4** were identified by conducting a $^{31}P\{^{1}H\}$ NMR experiment.

3.3.3 $^{31}P\{^{1}H\}$ NMR spectroscopy of complex C4

The $^{31}P\{^{1}H\}$ NMR spectrum of the complex **C4** (Fig 3.7) distinctly shows a single peak at 14.26 ppm which appeared downfield compared to the free triphenylphosphine (-6.28 ppm). This confirms the successful coordination of the phosphorus atom to the Ni centre. The downfield shift observed for complex **C4** is attributed to the movement of electron density from the phosphorus atom towards the nickel center thus results in deshielding of the phosphorus atom.

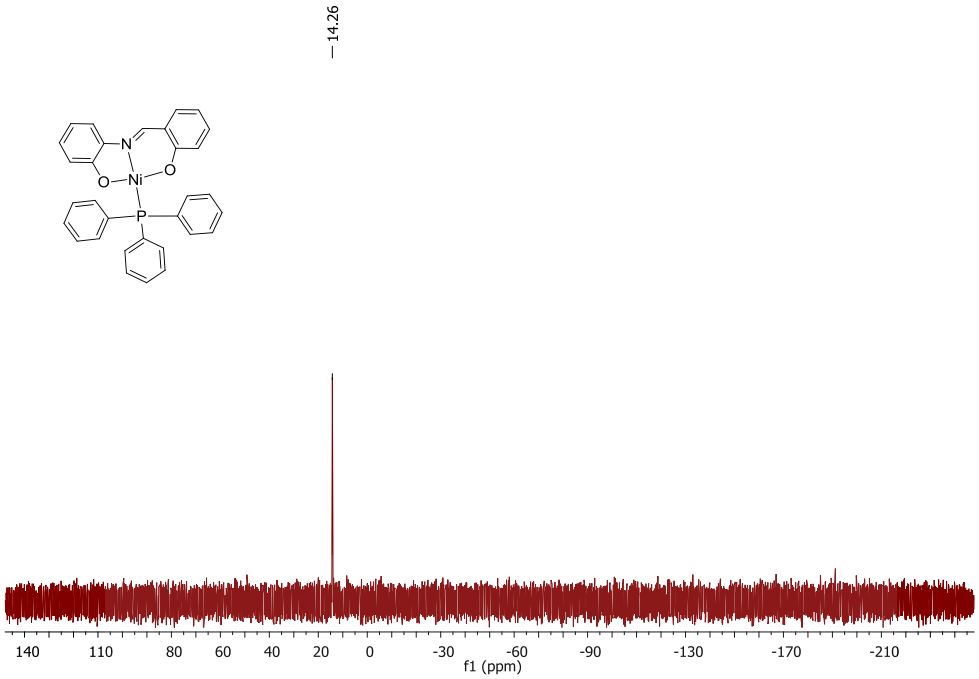

Fig 3.7 $^{31}P\{^{1}H\}$ NMR for complex **C4** in $CDCl_3$ (500 MHz)

The complex **C4** was also characterized by Infrared spectroscopy to identify the functional groups of the complex.

3.3.4 Infrared spectroscopy of complex C4

The infrared spectrum of complex **C4** (Fig 3.8) exhibited some characteristic bands at 1606 cm^{-1} and 1431 cm^{-1} for *ν*(C=N str.) and *ν*(C=C) respectively. The shift of *ν*(C=N str.) to lower wavenumber from 1625 cm^{-1} **L2** to 1606 cm^{-1} in complex **C4** shows that the schiff base ligand **L2** successfully coordinated to Ni(II) ion. Kianfar et al reported that the HN=C shifts to lower frequencies after coordination to the metal center which might be due to the electron withdrawing effects from the metal center resulting in weakening of the imine bond (synergic effect).[15] The bands around 2950-3200 cm^{-1} are related to the aromatic C-H vibration of triphenylphosphine complexes and this has been reported before.[17]

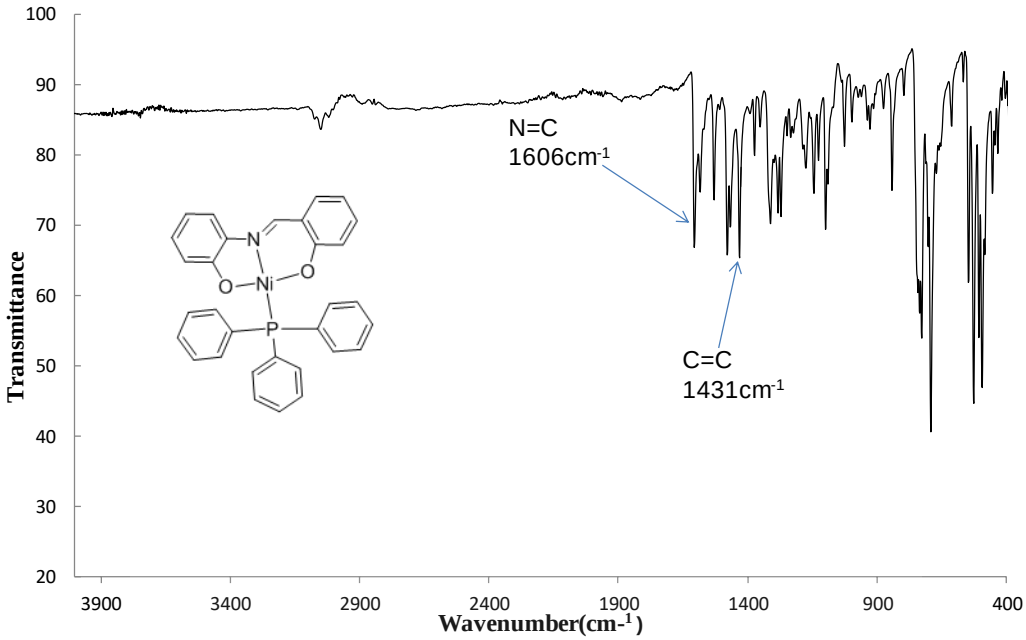

Fig 3. 8 IR spectrum of complex **C4**

In addition to NMR and IR characterization, high resolution mass spectroscopy was used to further characterize complex **C4.**

3.3.5 High resolution mass spectroscopy of complex C4

The high resolution mass spectrum of complex **C4** (Fig 3.9) shows a peak for *m/z* = 532.8445 for $[M+H]^+$ which corresponds to the molar mass of complex **C4** which confirms the successful synthesis of complex **C4**.

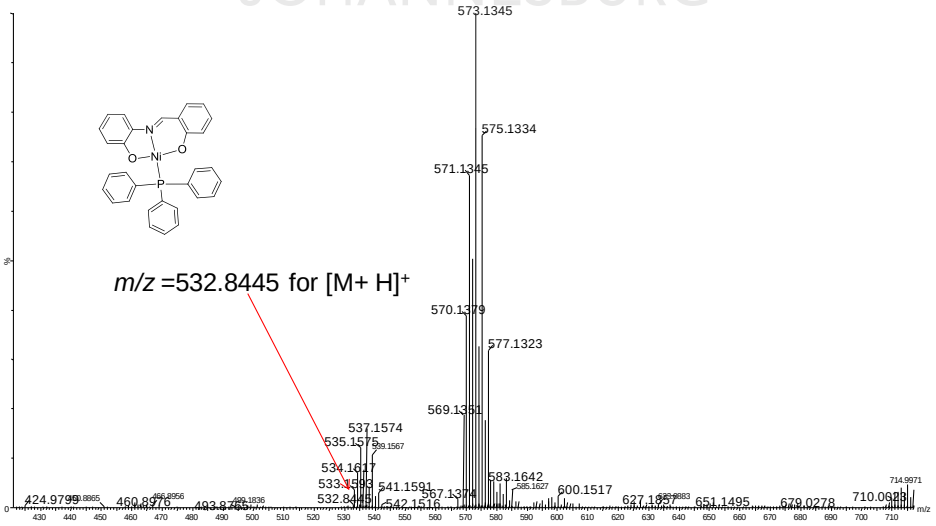

Fig 3. 9 Mass spectrum of complex **C4**

The complex **C4** was further characterized by elemental analysis to determine the quantity

of the elements present in the complex and also the thermal stability of the complex **C4** was determined by conducting thermal gravimetric analysis experiment.

3.3.6 Elemental analysis and Thermal Gravimetric analysis of complex C4

The elemental analysis of the complex **C4** was calculated and found to be within the acceptable limits of the calculated value. The TGA curve of the complex **C4** (Fig 3.10) shows two stages of decomposition within the temperature range 185-190 ^{o}C and 420- 460 ^{o}C. The complex **C4** does not show any loss in weight up to 185 ^{o}C, however when the temperature was increased there was weight loss between the temperature range 185-190 ^{o}C corresponding to the decomposition of the ligand part of the complex (wt % 1.019). The second decomposition temperature is observed in the temperature range 420-460 ^{o}C corresponding to the decomposition of the complex **C4** (wt% 8.681). This indicates that complex **C4** is thermally stable.

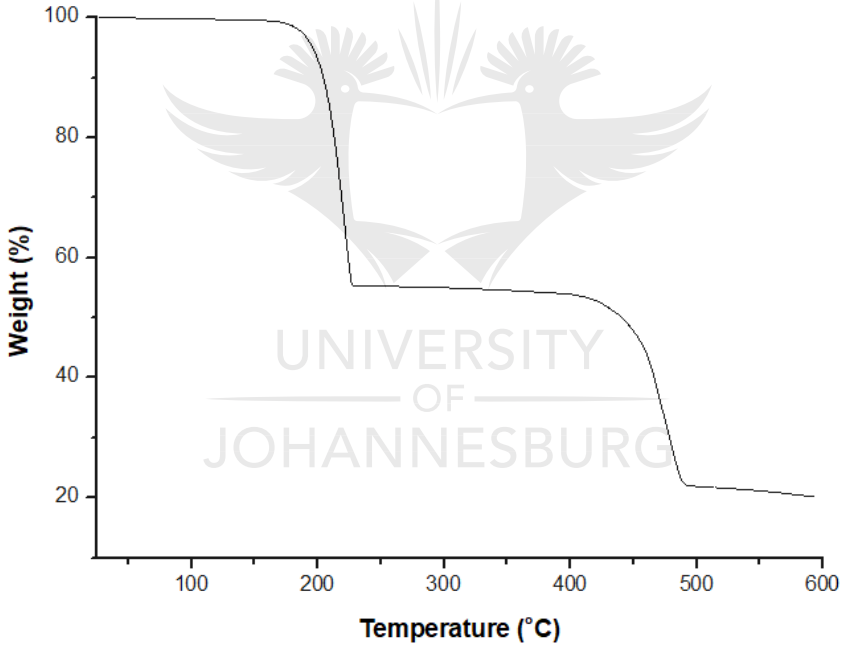

Fig 3. 10 Thermal gravimetric analysis spectrum of complex **C4**

The complex **C4** was also characterized using single crystal x-ray diffraction.

3.3.7 X-ray crystallography of complex C4

Brown crystals of complex **C4** (Fig 3.11) were crystallized from a mixture of dichloromethane and hexane at room temperature. The crystal data collected confirmed that complex **C4** is crystallized in the monoclinic space group P2 1/n. Complex **C4** showed a tridentate ONO coordination of the schiff base and a monodentate triphenylphosphine

ligand. The bond angles and bond lengths are in range with the literature values for Ni(II) square planar complexes hence the geometry of complex **C4** was confirmed to be square planar.[16,18]

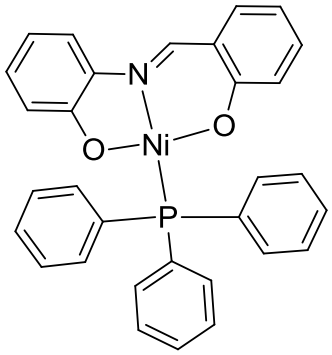

Fig 3.11 Molecular structure of complex **C4**

3.4 Synthesis and characterization of complexes C5 and C6

The complex **C5** was prepared using a one pot procedure (Scheme 3.3). Sodium hydride was added into a flask containing 2(diphenylphosphino)ethylamine dissolved in dry THF and stirred at room temperature for one hour. 3(Iodopropyl)trimethoxysilane was added to the solution and the reaction mixture continued to stir for 48 hours. The solvent was removed at reduced pressure to afford ligand **L1** as colourless oil. To this added were equimolar amounts of nickel acetate tetrahydrate and the schiff base ligand **L2** and the mixture was refluxed at 65 ^{o}C for 24 hours. The solvent was removed using rotary evaporation to afford complex **C5** as brown oil with fair yield (52 %). The complex **C5** is soluble in chloroform, dichloromethane, ethanol, methanol, acetonitrile, dimethyl sulfoxide and insoluble in diethyl ether, hexane and water. Due to failure of complex **C5** to shim no conclusive ^{1}H NMR spectrum was obtained. The complex **C5** was characterized using ^{31}P{^{1}H} NMR, ^{13}C{^{1}H} NMR, ^{29}Si{^{1}H} NMR, FT-IR, high resolution mass spectrometry, elemental analysis and thermal gravimetric analysis.

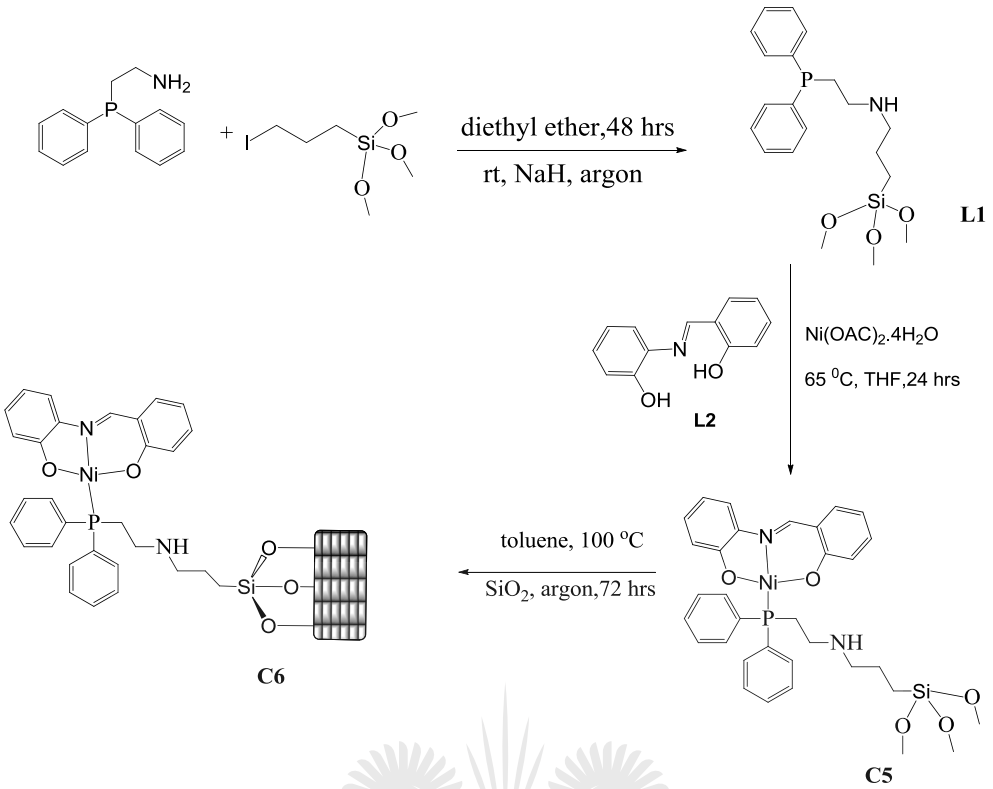

Scheme 3. 3 Synthesis of complexes **C5** and **C6.**

3.4.1 $^{31}P\{^{1}H\}$ NMR spectroscopy of complex C5

The $^{31}P\{^{1}H\}$ NMR spectrum of the complex **C5** (Fig 3.12) was analysed in deuterated chlorofom. The spectrum shows a broad peak which appeared around 50.34 ppm which shows a great shift downfield compared to the ligand **L1** (-21.95 ppm) which confirms that the phosphorus atom is coordinated with the nickel metal center. A very high deshielding of the observed phosphorus signal is attritubted to the phosphorus ligand being a σ-donor and π acceptor therefore there might be a drift of the electron density from the phosphorus atom to the nickel center resulting in the phosphorus atom being more deshielded. Koten and co-workers also observed broad peaks in their spectras of silane complexes and it was confirmed that broad peaks is one of the characteristics of complexes with silane moiety.[19]

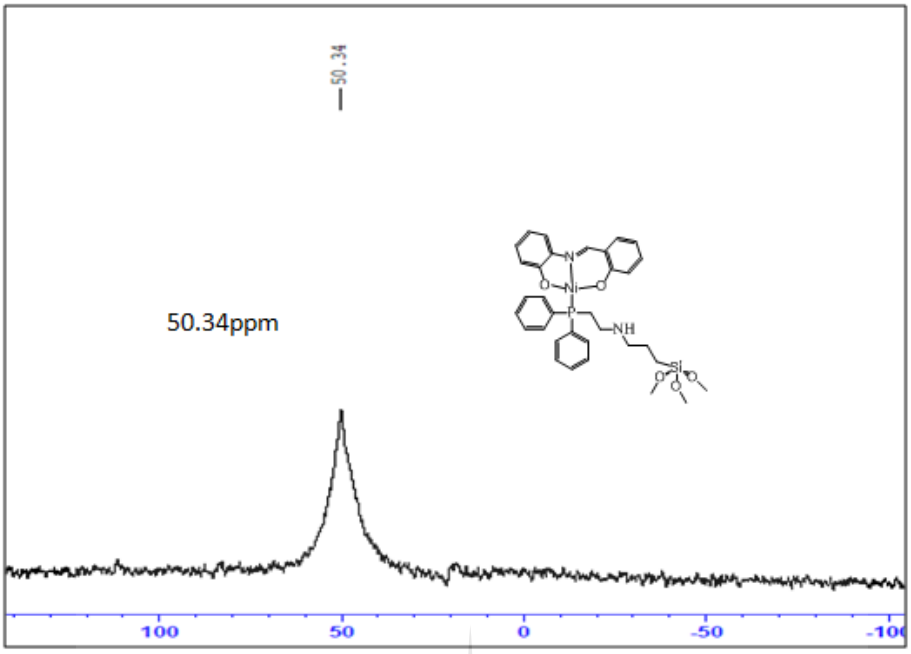

Fig 3. 12 $^{31}P\{^{1}H\}$ NMR spectrum of complex **C5**

The $^{13}C\{^{1}H\}$ NMR spectroscopy was used to further characterize complex **C5**

3.4.2 $^{13}C\{^{1}H\}$ NMR spectroscopy of complex C5

The $^{13}C\{^{1}H\}$ NMR spectrum of complex **C5** (Fig 3.13) was analysed in deuterated chloroform using TMS as internal reference. The spectrum shows the imine carbon appearing downfield at 162.45 ppm. The aromatic carbons appeared in the region 115.34-134.84 ppm. The number of carbon signals observed are in accordance with the proposed structure of the complex. This shows that the complex **C5** was successfully synthesized.

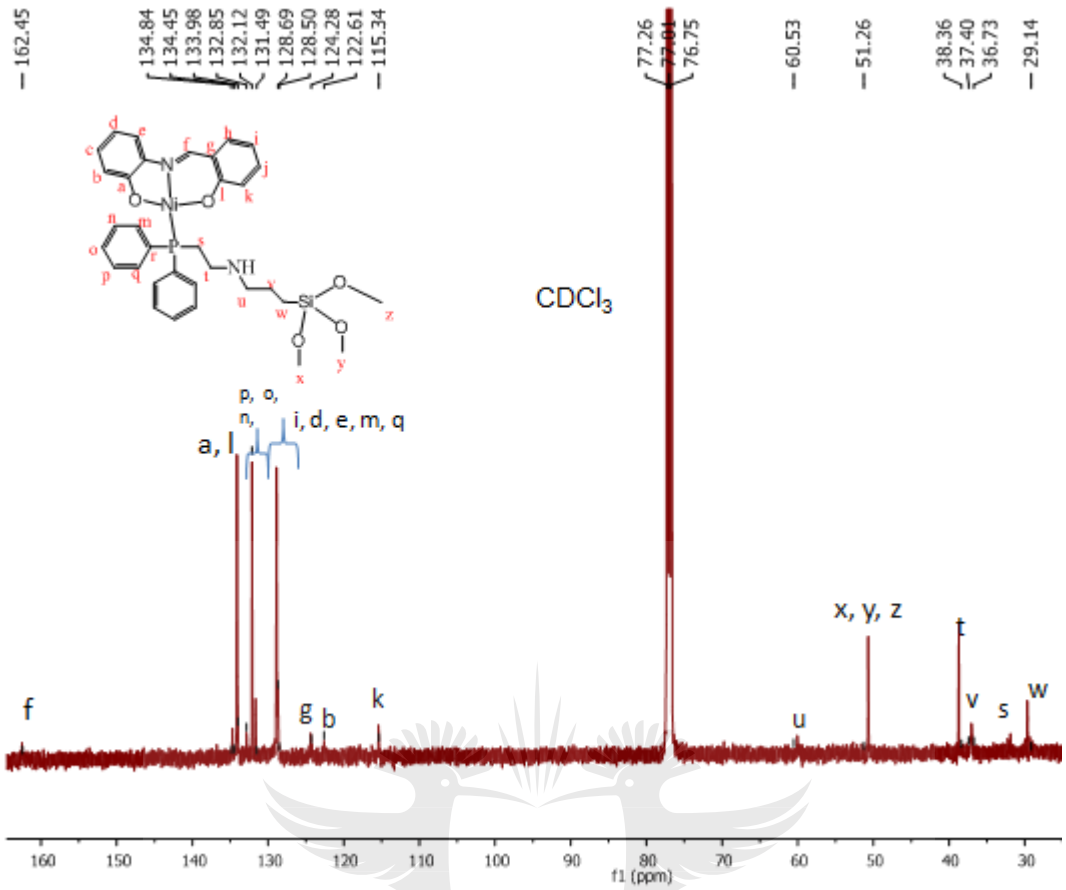

Fig 3. 13 $^{13}C\{^{1}H\}$ NMR spectrum of complex **C5**

The complex **C5** was also characterized by $^{29}Si\{^{1}H\}$ NMR to confirm the presence of silicon species.

3.4.3 $^{29}Si\{^{1}H\}$ NMR spectroscopy of complex C5

The $^{29}Si\{^{1}H\}$ NMR spectrum of complex **C5** (Fig 3.14) was analysed using $CDCl_3$. The spectrum shows a signal appearing at -21.35 ppm assigned to complex **C5** which is a downfield shift compared to **L1** (-43.80 ppm) which confirms that complex **C5** has silicon species now in a different chemical environment compared to that of the ligand **L1**. A second signal appeared as a broad peak appeared around -107.80 ppm which is assigned to the silicon of the NMR tubes used during analysis as it has been reported by El-Damrawi et al that NMR tubes are made of borosilicate glass.[20]

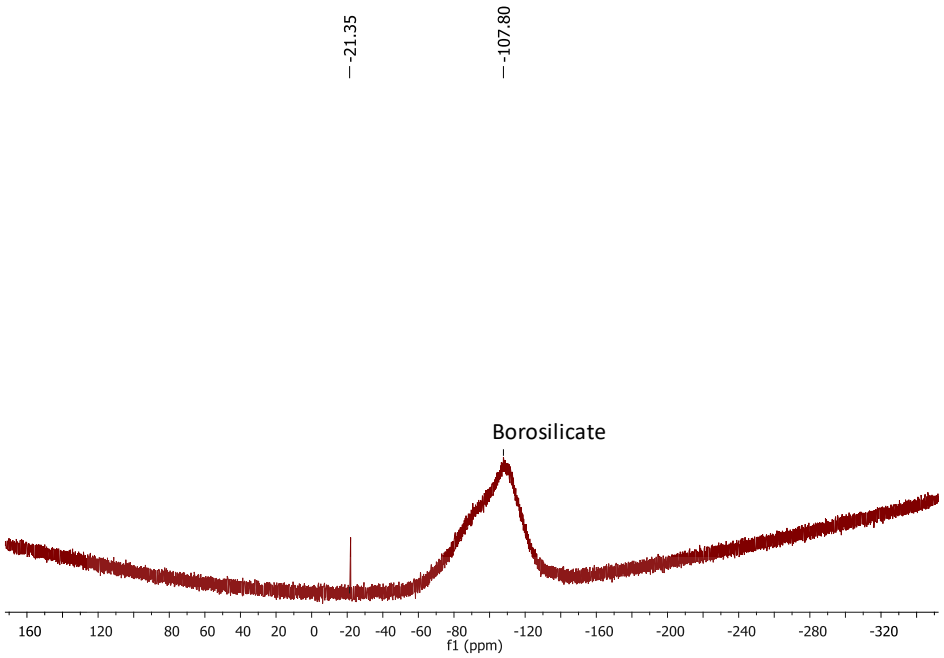

Fig 3. 14 ^{29}Si NMR spectrum of complex **C5**

The complex **C5** was also characterized by high resolution mass spectroscopy to determine the molar mass of the complex.

3.4.4 High resolution mass spectroscopy of complex C5

The high resolution mass spectrum of complex **C5** (Fig 3.15) showed a peak m/z = 694.7498 for $[M+Cl-H]^-$ which corresponds to the molar mass of the complex **C5**.

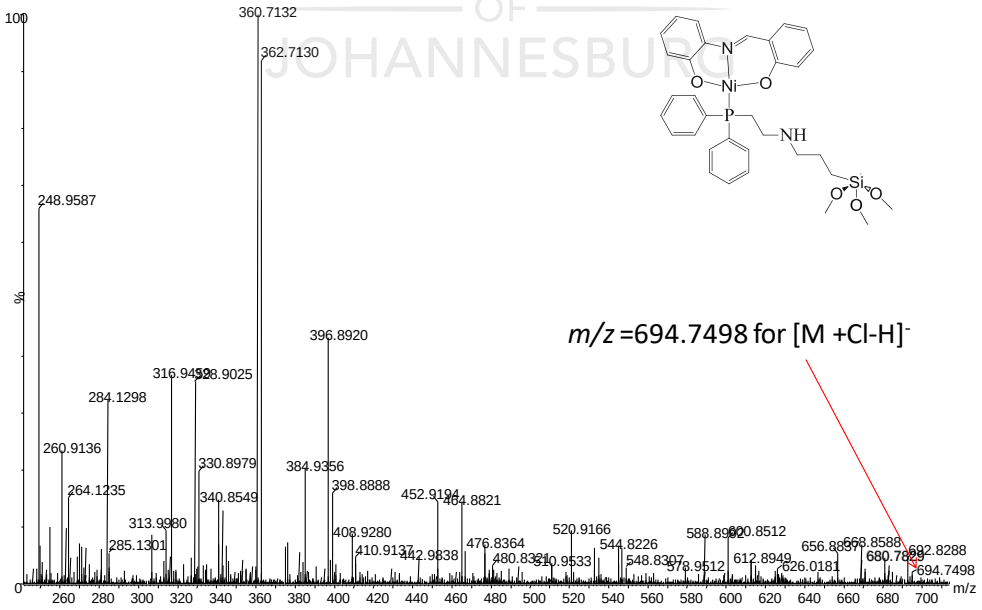

Fig 3. 15 Mass spectrum of complex **C5**

The complex **C5** was further characterized by Infrared spectroscopy to identify the

functional groups.

3.4.5 Infrared spectroscopy of complex C5

The Infrared spectrum of complex **C5** shown in Fig 3.16 shows the characteristic imine *v*(HC=N) peak appearing at 1573 cm^{-1}, relative to the free schiff base ligand **L2** (1625 cm^{-1}) the imine peak in the complex **C5** shifted to a lower frequency which might be attributed to the decrease in the HC=N bond as a result of the coordinate bond formed between the lone pair of the nitrogen and the Ni centre. The peaks corresponding to *v*(C=C) 1435 cm^{-1} and *v*(Si-OCH_3) 2870 cm^{-1} were also observed including *v*(C-H str.) frequencies which appeared around 2900-3000 cm^{-1}.The broad band between 3550 and 3400 cm^{-1} was attributed to the presence of the O-H stretching frequency of silanol groups which confirms that complex **C5** has a silane moiety.

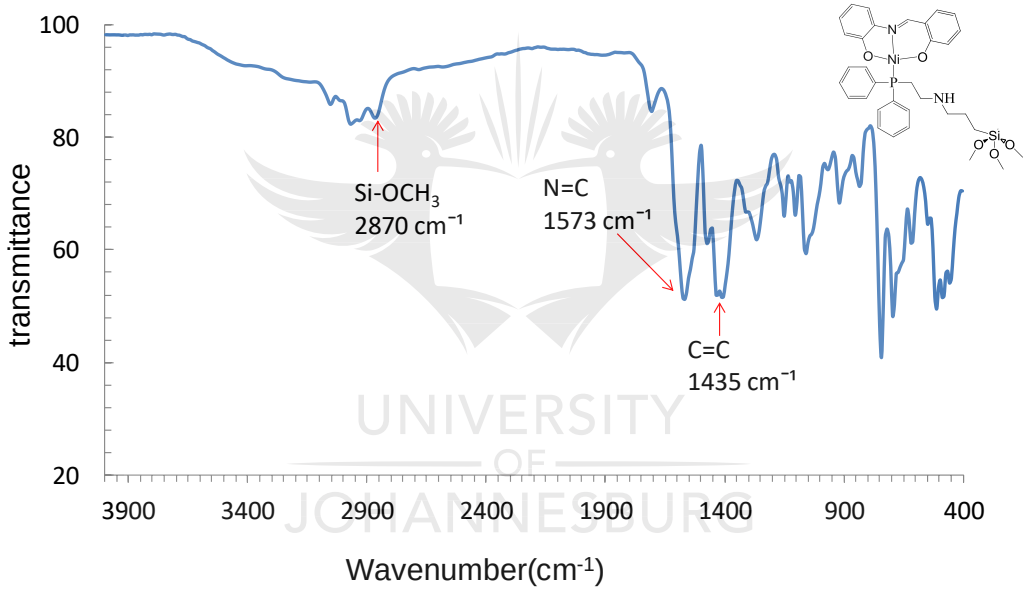

Fig 3. 16 Infrared spectrum of complex **C5.**

In addition to the NMR, IR and mass spectroscopy characterization the complex **C5** was also characterized by elemental and thermal gravimetric analysis.

3.4.6 Elemental analysis and Thermal Gravimetric Analysis of complex C5

The elemental analysis of the complex **C5** was calculated and found to be within the acceptable limits of the calculated value. The TGA spectrum of the complex **C5** (Fig 3.17) shows a gradual decrease in mass at the first stage which is around 75- 210 ^{o}C (wt % 6.887) which might be attributed to the loss of solvent used during synthesis. The following stage of 19.9% weight loss could be due to condensation of the silanols which resulted in loss of intramolecular water of the complex **C5** from 350- 425 ^{o}C.

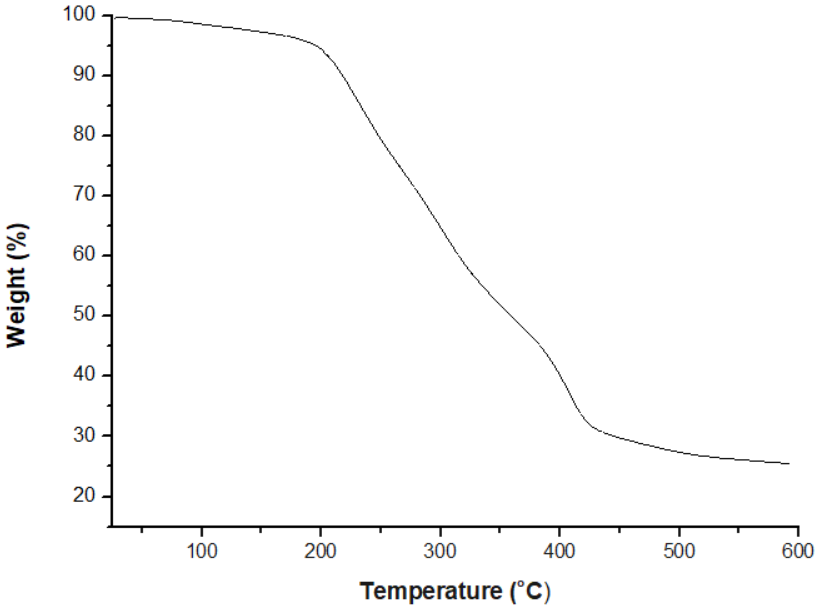

Fig 3. 17 Thermal gravimetric analysis of complex **C5**

3.5 Synthesis and characterization of complex C6

The complex **C6** was synthesized using a literature synthetic procedure.[21] The complex **C5** was dissolved in dry toluene, the silica gel was dispersed in the reaction mixture and refluxed at 100 ^{o}C under dry argon atmosphere for 72 hours. The solid phase was filtered using gravity filtration and washed with equimolar amounts of toluene: ethanol and dried in the oven at 30 ^{o}C for 24 hours to afford a yellow powder with good yield (87 %). The complex **C6** was characterized by BET, PXRD, ICP-MS, TGA, SEM and TEM.

3.5.1 Surface properties of complex C6

3.5.1.1 Nitrogen adsorption-desorption studies– The Brunauer-Emmett-Teller surface area, pore volume and pore size data of the SiO_2 support and the complex **C6** is shown in Table 3.1 and Fig 3.18. The importance of the catalyst surface area in determining the catalyst activity was reported by Venturelli and core workers in the literature.[22] The complex **C6** exhibited a high surface area of 185 m^2/g although it was lower compared to that of SiO_2 (442 m^2/g) which might be attributed to the presence of the nickel metal on the support and also the fact that SiO_2 support might have undergone transformation during synthesis.[23]

In addition, the catalyst pore structure (volume and size) were determined using BET because the pore structure can affect the activity of the catalyst. The pore volume decreased from 0.69 cm^3/g of SiO_2 to 0.27 cm^3/g (**C6**) which might be due to pores collapsing at elevated temperatures during synthesis. The physisorption isotherms (Fig 3.18a) are typical

of type IV based on the literature reported IUPAC classification,[24] this confirms that the complex **C6** is mesoporous. The pore diameter of complex **C6** (4.21 nm) shown in Fig 3.18b falls within the range for mesoporous materials (2 nm < size < 50 nm)[22] which also confirms that complex **C6** is mesoporous.

Table 3. 1 The surface properties of silica gel and silica supported complex **C6**

Entry	Catalyst	S_{BET} (m^2/g)	Vp (cm^3/g)	Dp (nm)
1	SiO_2	442	0.69	5.13
2	$C6/SiO_2$	185	0.27	4.21

S_{BET} (BET specific surface area), Vp (pore volume), Dp (pore diameter).

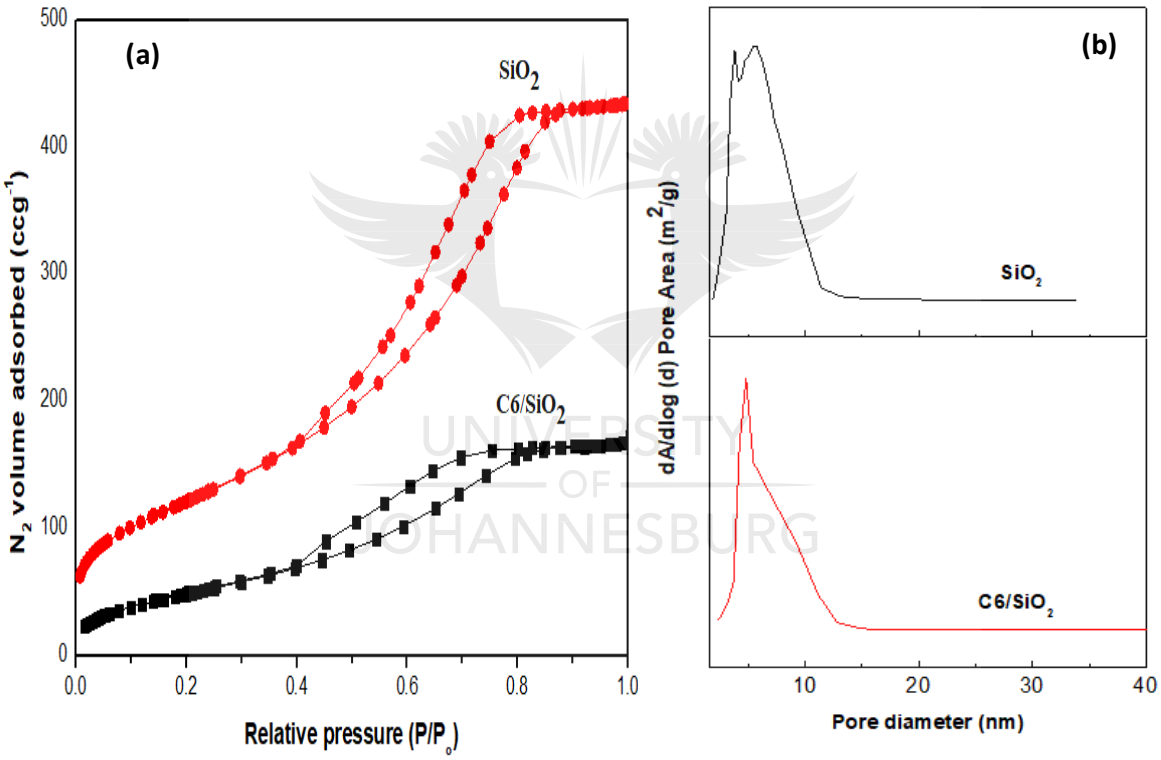

Fig 3. 18 (a) N_2 adsorption-desorption isotherms and (b) pore size distribution of the silica gel and complex **C6**

In order to further confirm that the schiff base complex **C6** was supported on silica IR spectroscopy characterization was conducted.

3.5.1.2 Fourier transform-infrared spectroscopy -The peaks observed in the IR spectrum (Fig 3.19) such as the Si-O-Si stretching frequency are assigned to the silanol groups at 802

cm^{-1} and the peak around 1553-1558 cm^{-1} is attributed to the presence of C=N bond of schiff bases. The peaks of SiO_2 and the characteristic peak of complex **C6** appeared in the spectrum of complex C6/SiO_2 which confirms that complex **C6** was immobilized on the silica surface. The shift and decrease of the intensity of the *ν*(Si-O) vibration band assigned to SiO_2 around 800 cm^{-1}also confirms that complex **C6** was successfully supported on silica.

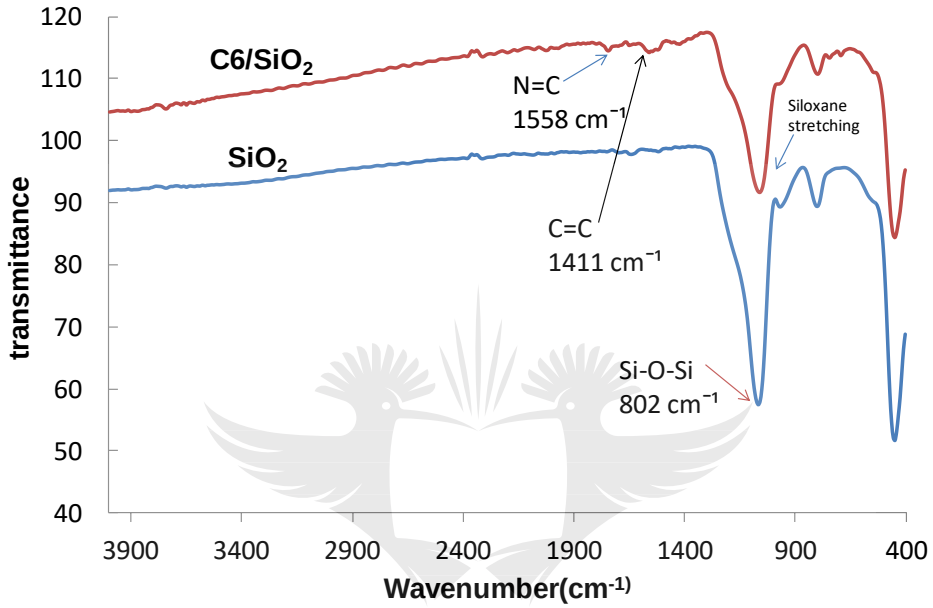

Fig 3. 19 FT-IR spectra of silica gel (bottom), supported schiff base complex **C6** (top).

The complex **C6** was also characterized by ICP-MS to determine the metal content.

3.5.1.3 Inductively Coupled Plasma- Mass Spectroscopy- The amount of metal present on a supported complex is of paramount importance as this helps in determining the catalyst productivity per gram of metal. The metal loading on complex **C6** was measured by ICP-MS and it was found that complex **C6** has 3.31 % Ni content.

The complex **C6** was further characterized by thermal gravimetric analysis to determine the thermal stability of the complex.

3.5.1.4 **Thermal gravimetric analysis of complex C6**

The thermal gravimetric analysis spectrum of complex **C6** (Fig 3.20) shows a gradual mass loss compared to the other version which is not mobilized on silica (complex **C5**) which indicated that immobilization of the complex on silica improved the thermal stability of the

complex. The TGA spectrum shows two steps of weight loss. One from 70- 110 ^{o}C which is attributed to the toluene used during synthesis and the following stage of 12.69 % from 260- 500 ^{o}C which might be due to decomposition of complex **C6**.

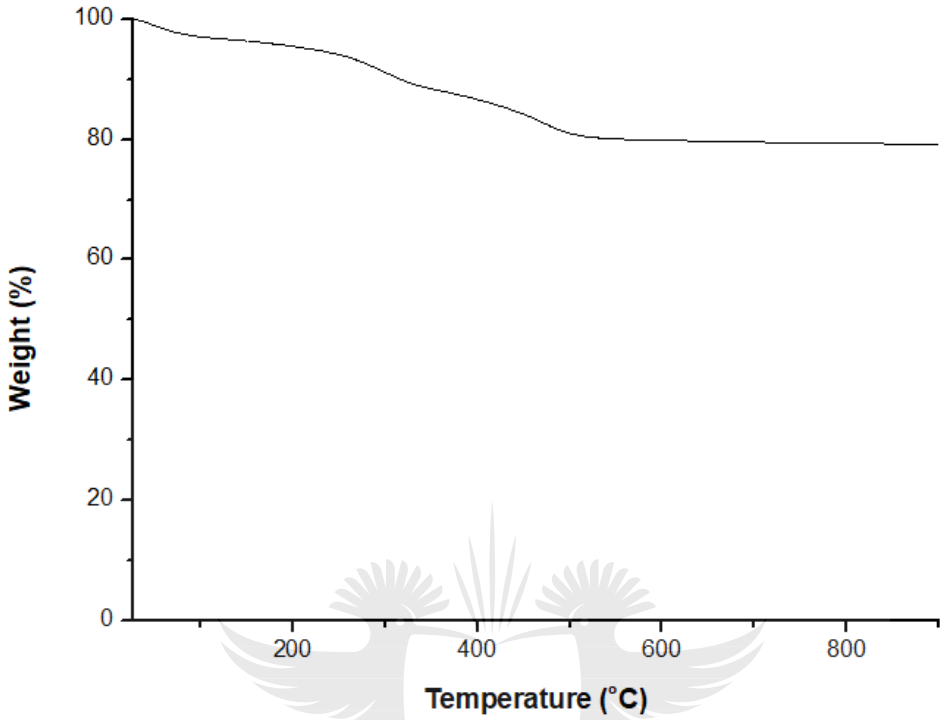

Fig 3.20 Thermal gravimetric analysis spectrum of complex **C6**

The SiO_2 support and the complex **C6** were further characterized by X-ray powder diffraction to determine their phase composition.

3.5.1.5 X-ray Powder Diffraction- The XRD patterns are as shown in Fig 3.21 .There were no new peaks observed for complex **C6** which might be due to low Ni metal loading which was confirmed from the ICP-MS results. Also, similar results have been reported in literature by Park et al when they obtained similar XRD patterns for the supported catalyst and support and they attributed this to the small size of the metal particles as well as the high dispersion of metal particles on the support[11,23] which was confirmed by Ni elemental mapping (Fig 3.24) The diffraction pattern of complex **C6** shows a broad peak around 2Θ = 22^{o} corresponding to silica gel which has been reported in literature and this confirms that the complex **C6** has been supported on SiO_2.[25] Lienemann and co-workers have also reported that the deposition of catalytic metals occurs in different ratios on a large surface area such as silica or alumina.[26]

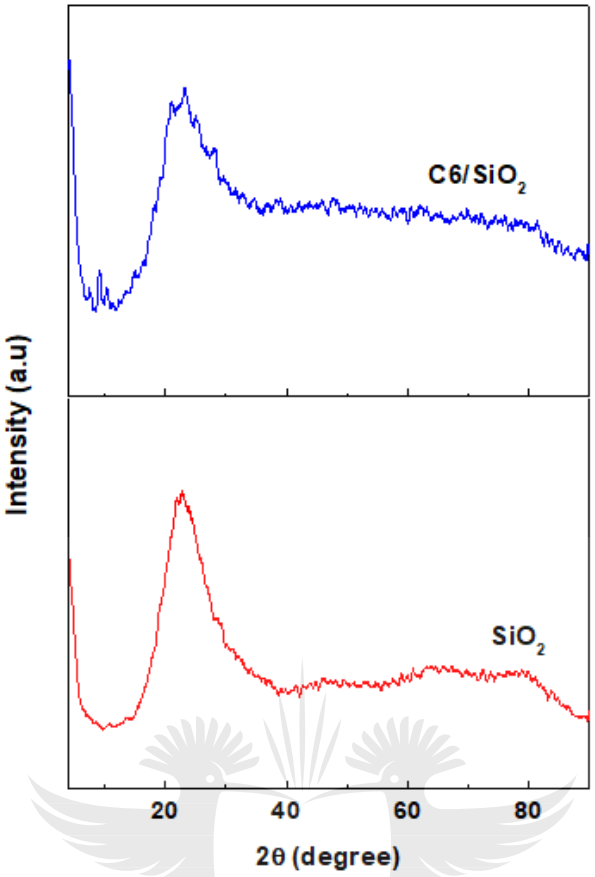

Fig 3. 21 XRD spectra of complex **C6** (top) and silica gel (bottom).

The SiO2 support and the complex **C6** were also characterized by TEM

3.5.1.6 Transmission Electron Microscopy- The TEM images of the silica support and complex **C6** (Fig 3.22) confirmed the presence of pores in both the SiO_2 support and the complex **C6** , however the pores are very small and not so well defined hence point scans could not be performed along the diameter of the particles.

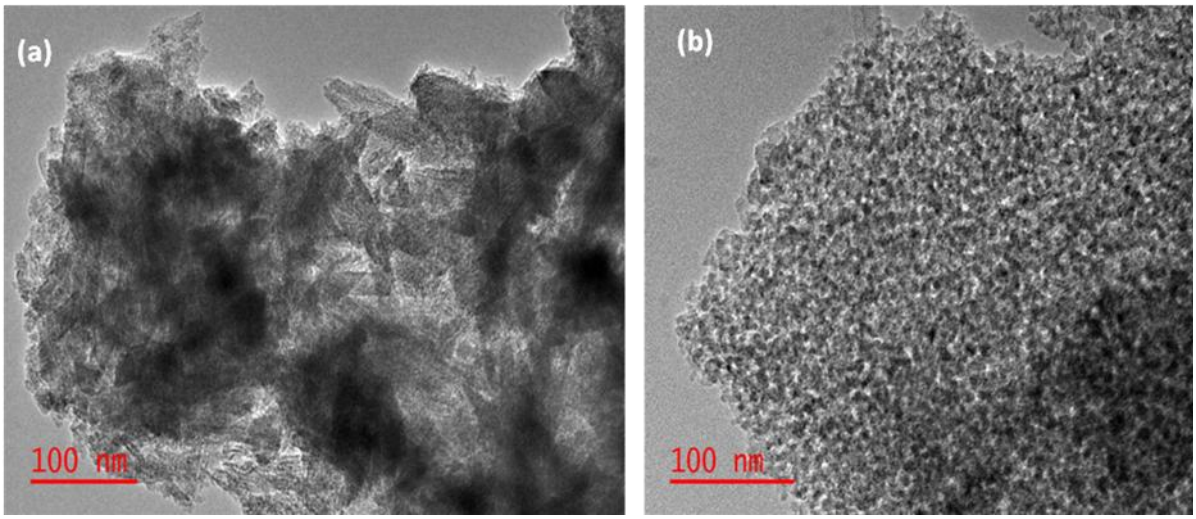

Fig 3. 22 TEM images of silica gel (a) and complex **C6** (b).

The surface morphology of the SiO_2 support and complex **C6** was investigated by performing SEM analysis.

3.5.1.7 Scanning Electron Microscopy- The SEM images (Fig. 3.23) showed that silica texture was significantly altered in complex **C6** which results in complex **C6** having lower pore diameter (4.21 nm) compared to that of SiO_2 (5.13 nm) which was confirmed by the BET results.

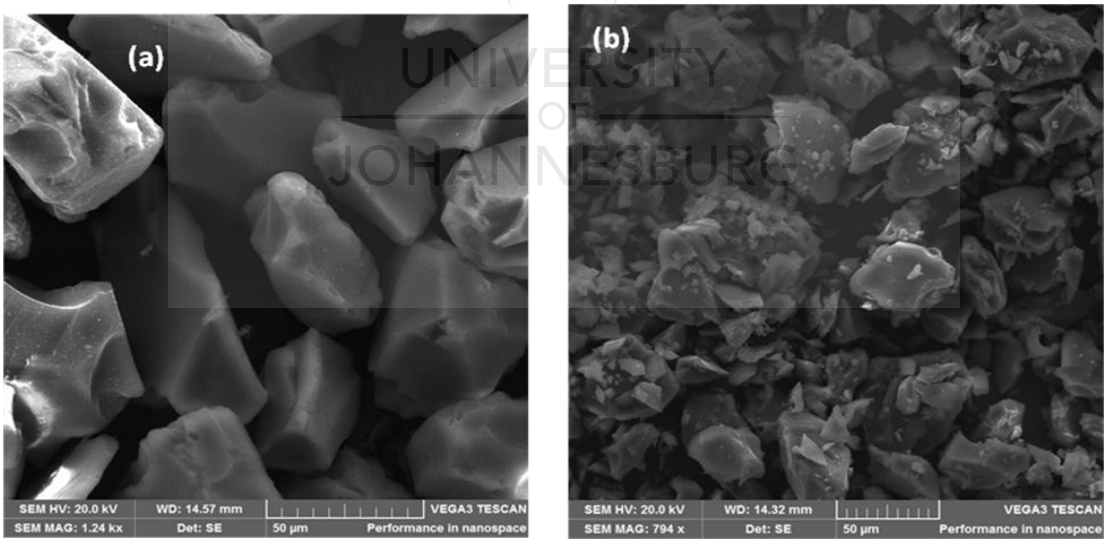

Fig 3. 23 SEM images of silica gel (a) and complex **C6** (b).

The metal particle size distribution of the complex **C6** was investigated by Energy Dispersive X-ray spectroscopy.

3.5.1.8 Ni elemental mapping- The EDX image (Fig 3.24) shows that the Ni metal is

highly dispersed on the SiO_2 support which might be attributed to the nickel precursor which was used in the synthesis of complex **C6** ($Ni(OAC)_2.4H_2O$).

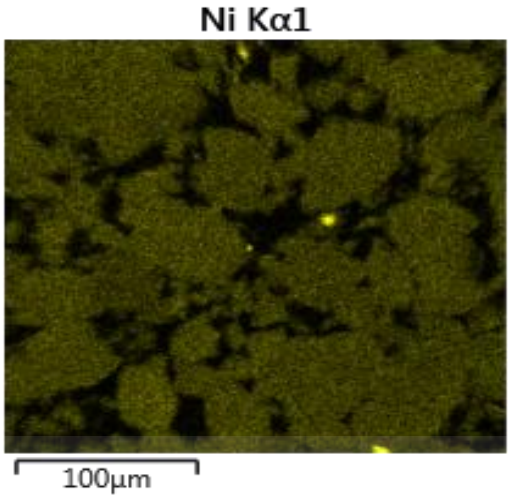

Fig 3. 24 EDX images showing Ni mapping on the complex **C6**

The surface composition of both the SiO_2 support and complex **C6** was confirmed by energy dispersive X-ray microanalysis (EDX).

3.5.1.9 Energy Dispersive X-ray microanalysis- The EDX images (Fig 3.25) as expected revealed the presence Si and O in the SiO_2 support (a) and Si, O, C, Ni and P in complex **C6** (b)**.** This confirms that complex **C6** was successfully synthesized.

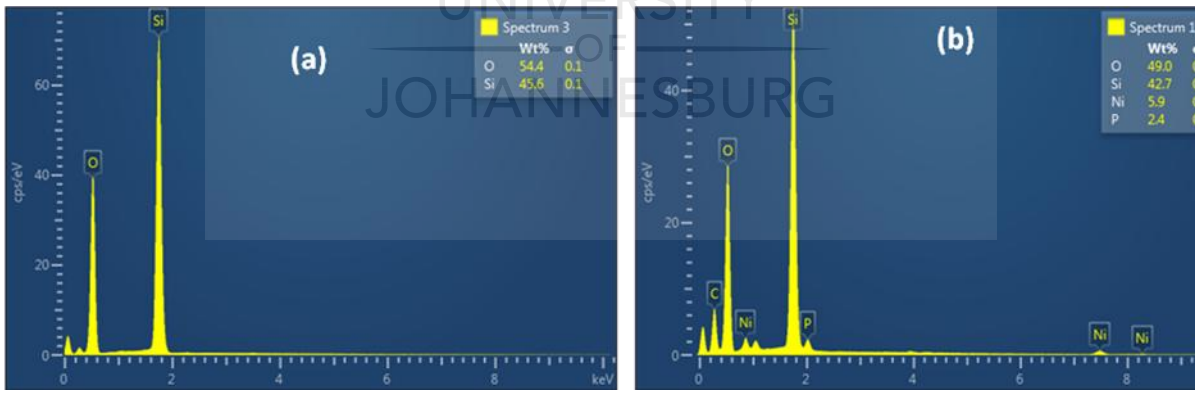

Fig 3. 25 EDX images of silica gel (a) and complex **C6** (b).

3.6 Conclusion

One ligand (**L2**), two homogenous O^N^O tridentate Ni(II) complexes (**C4** and **C5**) were synthesized and characterized using spectroscopic techniques such as ^{1}H NMR, $^{13}C\{^{1}H\}$

NMR, $^{31}P\{^{1}H\}$ NMR, $^{29}Si\{^{1}H\}$ NMR, high resolution ESI mass spectrometry, FT-IR spectroscopy and elemental analysis. One heterogenous complex (**C6**) was also synthesized and characterized using both analytical and spectroscopic techniques such as ICP-MS, BET, PXRD, TEM and SEM-EDX. The complexes **C4-C6** were evaluated as catalyst precursors in the hydrogenation of furfural, the results are discussed in chapter four.

3.7 Experimental

3.7.1 Materials and chemicals

All reactions were performed under inert conditions using standard Schlenk techniques. Nickel acetate tetrahydrate [$Ni(OAC)_2.4H_2O$], triphenylphosphine (PPh_3), 2(diphenylphosphino)ethylamine, 2-aminophenol, salicyaldehyde, furfural (FF), 3(Iodopropyl)trimethoxysilane, silica gel were all obtained from Sigma-Aldrich and used without purification. The solvents tetrahydrofuran (THF), ethanol (EtOH), methanol (MeOH), diethyl ether, and toluene were purchased from Sigma -Aldrich and dried before use. Nuclear magnetic resonance (NMR) was recorded on a Bruker Utrashield- 400/ 500 MHz spectrometer in chloroform. Characterization of the samples by powder X-Ray diffraction was performed by using P analytical X'PERT1000 Antan Paar Philips. Melting points were determined using Buchi melting point apparatus B-540. Mass spectrometry was obtained using an electro spray ionisation-mass spectrometer in the positive or negative mode. The functional groups of the ligand and complexes were confirmed using Infrared spectroscopy which was recorded using Thermo-Nicolet FTIR spectrophotometer. The surface area, pore volume and pore diameter of the samples were calculated using the multipoint Brunauer Emmett-Teller (BET) ASAP 2460. Transmission electron microscopy (TEM) study was carried out with a JEM-2100electron microscope. The catalysts were suspended in ethanol under sonication and applied on carbon-coated copper grids .Scanning Electron microscopy Energy Dispersive X-ray (SEM-EDX) images studies were carried out with TESCAN OXFORD microscope. Elemental analyses were carried out using a Thermo Scientific Flash 2000 series.

3.7.2 Synthesis of ligand L2[14]

Ligand, **L2** was prepared in a condensation reaction between 2-aminophenol (0.101 g, 0.926 mmol) and salicyaldehyde (0.129 g, 0.926 mmol) in ethanol (50 mL). The solution was refluxed for 24 hours during which the colour of the solution was changed from brown

to orange. The solvent was removed by rotary evaporation to afford an orange crystalline solid. **Yield**: (0.168 g, 87%). **Mp**: 187-189 ^{o}C. **^{1}H NMR** (400 MHz, $CDCl_3$)**:** (δ, ppm) 12.28(s, 1H, H_{OH}), 8.68(s, 1H, N=C$\underline{H}_{imine}$), 7.43(t, 2H, H_{Ar}), 7.25(m, 1H, H_{Ar}) 7.16(d, 1H, H_{Ar}), 7.13(m, 4H, H_{Ar}). **^{13}C{^{1}H} NMR** (100 MHz, $CDCl_3$): (δ, ppm) 163.85, 160.66(N=$\underline{C}$H), 149.95, 136.04, 133.65, 132.84, 128.81, 121.58, 119.48, 118.18, 117.08, 115.76. **FT-IR** (*v*max: cm^{-1}) at *v* =1625 cm^{-1}(C=N str.), **Elemental analysis** (%): Calculated for $C_{13}H_{11}NO_2$: C, 73.23; H, 5.20; N, 6.57, Found: C, 73.63; H, 4.76; N, 5.65, **High resolution ESI-MS** (positive): *m/z* =214.0863 for $[M+H]^+$.

3.7.3 Synthesis of complex C4 [15]

Nickel acetate (0.0868 g, 0.349 mmol) and triphenylphosphine (0.0915 g, 0.349 mmol) dissolved in methanol (40 mL) was stirred for 15 minutes. To this added was Ligand **L2** (0.0746 g, 0.349 mmol) and the mixture was refluxed at 80 ^{o}C for 2 hours under argon. A brown precipitate formed which was filtered using a Buchner funnel and dried under vacuum to afford the product as a brown crystalline solid. **Yield**: (0.281 g, 75%),. **^{1}H NMR** (400 MHz, $CDCl_3$)**:** (δ, ppm) 8.49(d, 1H, N=C$\underline{H}_{imine}$), 7.85(t, 5H, H_{Ar}), 7.70(d, 1H, H_{Ar}), 7.42(m,10H, H_{Ar}) 7.05(t, 1H, H_{Ar}), 7.03(t, 1H, H_{Ar}), 6.68(m, 3H, H_{Ar}), 6.2(d,1H, H_{Ar}), **^{13}C{^{1}H} NMR** (100 MHz, $CDCl_3$): (δ, ppm) 166.28, 163.19, 148.28, 139.13, 134.67, 132.77, 130.44, 128.33, 128.30, 121..78, 120.72, 118.13, 115.60, 114.39, 114.04. **^{31}P{^{1}H} NMR**: δ = 14.97ppm. **Elemental analysis** (%): Calculated for $C_{31}H_{24}NNiO_2P$: C, 57.57; H, 8.05; N, 2.24, Found: C, 58.69; H, 7.29; N, 1.66, **FT-IR** (V_{max}: cm^{-1}): at *v*=1606cm^{-1} (HC=N). **X-ray crystallography,** monoclinic space group P2 1/n, square planar geometry.

3.7.4 Synthesis of complexes C5 and C6

2(diphenylphosphino)ethylamine (0.122 g, 0.533 mmol) was dissolved in dry THF (50 mL) under argon. To this added was NaH (0.016g, 0.533mmol) and stirred at room temperature for 1 hour. 3(Iodopropyl)trimethoxysilane (0.155g, 0.533 mmol) was added to the reaction mixture and the solution was stirred at room temperature for 48 hours. To this added was nickel acetate tetrahydrate (0.137 g, 0.533 mmol) and ligand **L2** (0.213 g, 0.997 mmol) and the reaction mixture was stirred under reflux for 24 hours. The solvent was removed using rotary evaporation and dried under vacuum to afford brown oil (**C5**) **Yield**: (0.332 g, 52%). **^{31}P NMR** (500 MHz, $CDCl_3$): **^{31}P{^{1}H} NMR**: 50.34ppm, **^{29}Si NMR**: δ= -21.35ppm. **FT-IR** (V_{max}: cm^{-1}): at *v*=1573cm^{-1} (HC=N str.), **High resolution ESI-MS** (negative): *m/z* = 694.7498 for $[M+Cl-H]^-$, **Elemental analysis** (%): Calculated for

$C_{33}H_{39}N_2NiO_5PSi$: C, 60.79; H, 6.56; N, 4.05, Found: C, 59.96; H, 5.02; N, 3.79.

The complex **C5** was modified with silica gel to obtain complex **C6**.[21] Into a round bottom flask containing 40 mL of dry toluene (0.0175 g, 0.0257 mmol) of **C5** was added and the mixture was stirred for 10 minutes. To this added was 0.0224g (0.332 mmol) of silica gel and the reaction mixture was refluxed at 100 ^oC under argon atmosphere for 72 hours[21]. The solid phase was filtered using gravity filtration and washed with toluene: ethanol (1:1) and dried under vacuum at 30 ^oC for 24 hours to afford a yellow powder. **Yield**: (0.0351 g, 87%). **FT-IR** (V_{max}: cm-1) at *v* =1558cm-1 (HC=N str.)

3.8 References

1 A. Majumder, G. M. Rosair, A. Mallick, N. Chattopadhyay and S. Mitra, *Polyhedron*, 2006, **25**, 1753–1762.

2 L.-C. Liang, *Coord. Chem. Rev.*, 2006, **250**, 1152–1177.

3 Q. Shi, L. Xu, J. Ji, Y. Li, R. Wang, Z. Zhou, R. Cao, M. Hong and A. S. C. Chan, *Inorg. Chem. Commun.*, 2004, **7**, 1254–1257.

4 Z.-L. You, H.-L. Zhu and W.-S. Liu, *Zeitschrift für Anorg. und Allg. Chemie*, 2004, **630**, 1617–1622.

5 K. C. Gupta and A. K. Sutar, *Coord. Chem. Rev.*, 2008, **252**, 1420–1450.

6 A. A. Abdel Aziz, A. N. M. Salem, M. A. Sayed and M. M. Aboaly, *J. Mol. Struct.*, 2012, **1010**, 130–138.

7 A. M. Abu-Dief and I. M. A. Mohamed, *Beni-Suef Univ. J. Basic Appl. Sci.*, 2015, **4**, 119–133.

8 S. Chakraborty, P. Bhattacharya, H. Dai and H. Guan, *Acc. Chem. Res.*, 2015, **48**, 1995–2003.

9 X. Liu, C. Manzur, N. Novoa, S. Celedón, D. Carrillo and J.-R. Hamon, *Coord. Chem. Rev.*, 2018, **357**, 144–172.

10 A. P. Prakasham and P. Ghosh, *Inorganica Chim. Acta*, 2015, **431**, 61–100.

11 Y. Park, T. Kang, Y. Cho, P. Kim, J. Park and J. Yi, in *Studies in Surface Science and Catalysis*, 2003, vol. 146, pp. 637–640.

12 P. S. Moyo, L. C. Matsinha and B. C. E. Makhubela, *J. Organomet. Chem.*, 2020, **922**, 121362.

13 C. Wang, Z. Liu, L. Wang, X. Dong, J. Zhang, G. Wang, S. Han, X. Meng, A. Zheng and F. S. Xiao, *ACS Catal.*, 2018, **8**, 474–481.

14 A. O. Sobola and G. M. Watkins, *J. Chem. Pharm. Res.*, 2013, **5**, 147–154.

15 A. H. Kianfar, H. Farrokhpour, P. Dehghani and H. R. Khavasi, *Spectrochim. Acta Part A Mol. Biomol. Spectrosc.*, 2015, **150**, 220–229.

16 A. H. Kianfar and M. Ebrahimi, *Spectrochim. Acta Part A Mol. Biomol. Spectrosc.*, 2013, **115**, 725–729.

17 A. H. Kianfar, H. Farrokhpour, P. Dehghani and H. R. Khavasi, *Spectrochim. Acta Part A Mol. Biomol. Spectrosc.*, 2015, **150**, 220–229.

18 M. M. Tamizh and R. Karvembu, *INOCHE*, 2012, **25**, 30–34.

19 L. A. Van De Kuil and D. M. Grove, 1994, 1675–1683.

20 G. El-Damrawi, W. Müller-Warmuth, H. Doweidar and I. A. Gohar, *J. Non. Cryst. Solids*, 1992, **146**, 137–144.

21 A. N. Kursunlu, E. Guler, H. Dumrul, O. Kocyigit and I. H. Gubbuk, *Appl. Surf. Sci.*, 2009, **255**, 8798–8803.

22 G. Leofanti, M. Padovan, G. Tozzola and B. Venturelli, *Catal. Today*, 1998, **41**, 207–219.

23 D. Shi, Q. Yang, C. Peterson, A.-F. Lamic-Humblot, J.-S. Girardon, A. Griboval-Constant, L. Stievano, M. T. Sougrati, V. Briois, P. A. J. Bagot, R. Wojcieszak, S. Paul and E. Marceau, *Catal. Today*, 2019, **334**, 162–172.

24 C. A. Akinnawo, N. Bingwa and R. Meijboom, *Microporous Mesoporous Mater.*, 2021, **311**, 110693.

25 J. A. Dias, E. Caliman, S. C. L. Dias, M. Paulo and A. T. C. . de Souza, *Catal. Today*, 2003, **85**, 39–48.

26 G. Alloncle, N. Gilon, C.-P. Lienemann and S. Morin, *Comptes Rendus Chim.*, 2009, **12**, 637–646.

Chapter four

Catalytic evaluation of Ni(II) complexes in the hydrogenation of furfural

4.1 Introduction

The attention of researchers has shifted to the selective hydrogenation of furfural (FF) to produce furfuryl alcohol (FA).[1,2] The industrial importance of FA has increased as it has the potential to be valorized into various valuable chemicals and fuels, also FA is an environmentally friendly solvent that has different applications which includes corrosion resistant coating and as an additive for the pharmaceutical or fuel industries.[3] More so, the conditions employed in hydrogenation of FF such as the type of catalyst and solvent used has a great influence on the different types of products formed.[1]

Noble metal catalysts such as Pd and Pt have been used in FF hydrogenation, however the high cost of these is a challenge which tends to limit their application.[4,5,6] Copper chromite is the most commonly used catalyst for the conversion of FF to afford FA in industry,[7] However the major drawback of using copper chromite is the toxicity of chromite ions (Cr_2O_3) to the environment.[1,8] Therefore, the design of an active and environmentally friendly catalysts for the hydrogenation of FF is an issue of interest.

Non-noble metal catalysts such as nickel can be modified by immobilizing them on a support in order to improve both catalytic activity and product selectivity.[9] Mesoporous supports such as silica are usually employed due to its desirable properties such as large surface area for adsorption, high thermal stability and the ability of its surface functions to be modified.[10] Homogenous nickel based catalysts have not been employed in the hydrogenation of FF to FA and to the best of our knowledge no information is available in the open literature. In unpublished reports Os(II) and Pt(II) complexes have been explored as pre-catalysts for the hydrogenation of FF to FA and other products. However, in view of the high cost of the metals used we focused our research on the application of inexpensive nickel complexes as pre-catalysts for the direct and transfer hydrogenation of FF to afford FA selectively (Scheme 4.1)

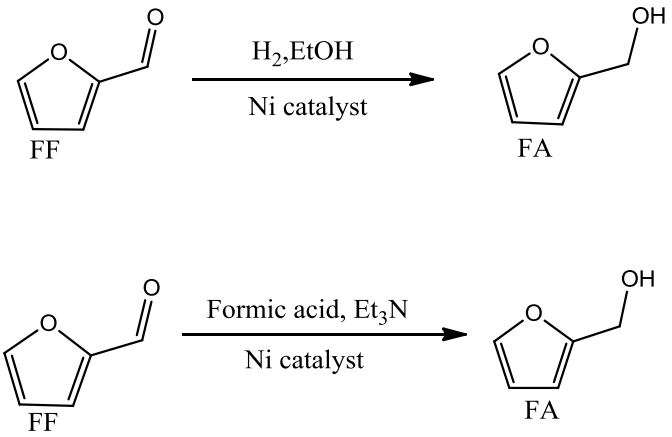

Scheme 4. 1 Direct and catalytic transfer hydrogenation of FF

4.2 Direct hydrogenation of furfural

The catalytic activities of the complexes **C1-C6** (**Fig 4.1**) were evaluated as pre-catalysts for the hydrogenation of FF (Scheme 4.1). In order to establish the best catalytic conditions for all the catalyst precursors various reaction parameters were investigated.

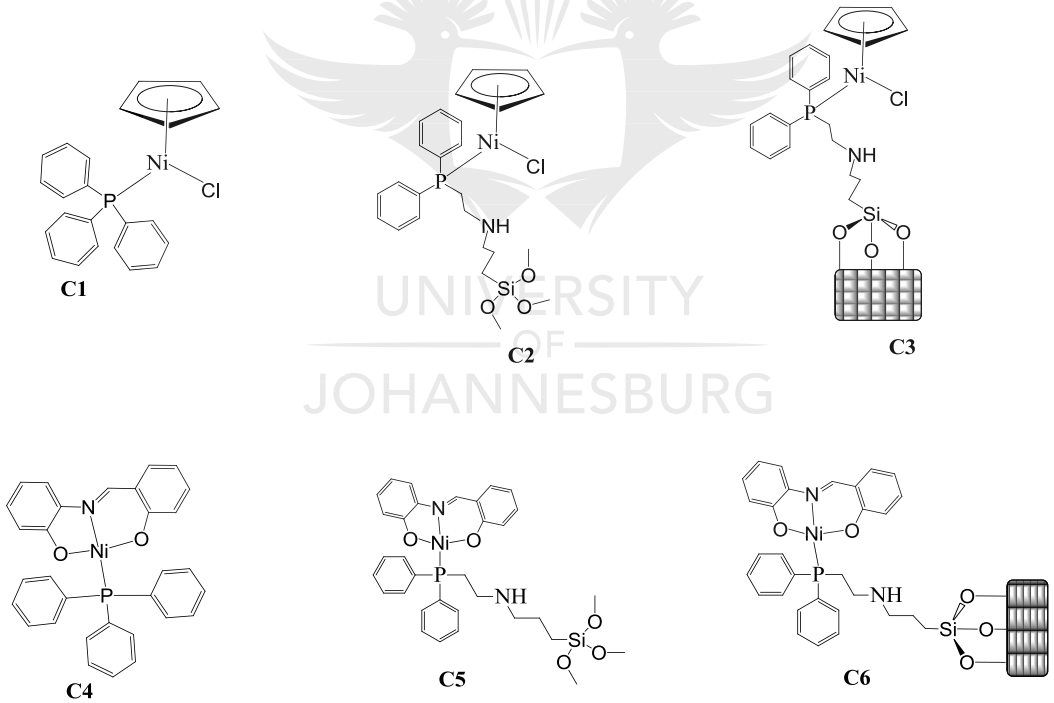

Fig 4. 1 Ni(II) complexes (**C1-C6**)

The catalytic studies to obtain optimum conditions for the hydrogenation of FF were performed with the homogenous complexes **C1** and **C4.** The complexes **C2**, **C3**, **C5** and **C6** were screened in the hydrogenation of FF using the obtained optimum conditions.

4.2.1 Effect of temperature

The FF conversion was slightly affected by the reaction temperature as pre-catalysts **C1** and **C4** were screened at various temperatures (100 ^{o}C-160 ^{o}C). Pre-catalyst **C1** showed the highest FF conversion at 140 ^{o}C with a turnover number (TON) of 389 and precatalyst **C4** showed highest FF conversion at 160 ^{o}C with a TON of 463 (Fig 4.2). The conversion of FF decreased when temperature was increased to 160 ^{o}C for pre-catalyst **C1** which might have been due to catalyst decomposition at high temperatures compared to precatalyst **C4** which was stable. Both precatalyst **C1** and **C4** were 100 % selective to FA.

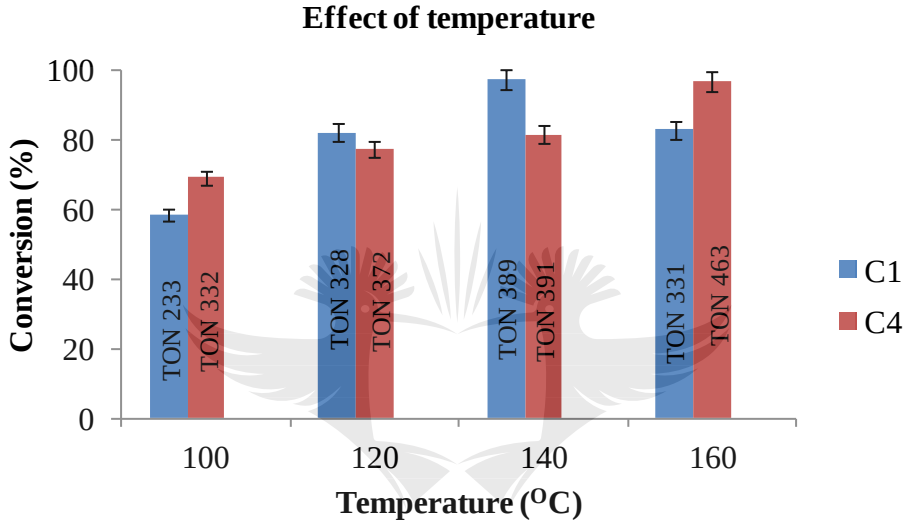

Conditions: ethanol (5 mL), substrate (FF, 2.4 mmol), molecular hydrogen (45 bar, 40 bar) for catalyst precursors **C1** and **C4** respectively, catalyst precursors (**C1** and **C4**; 0.06 mmol), time (24 hours). Conversion and selectivity was determined by ^{1}H NMR spectroscopy.

Fig 4. 2 Effect of temperature in the hydrogenation of FF

4.2.2 Effect of hydrogen pressure

Hydrogenation studies of FF using pre-catalysts **C1** and **C4** were investigated at various hydrogen pressure (15-60 bar). Increasing the hydrogen pressure from 15 bar to 45 bar slightly increased the FF conversion for both pre-catalysts (Fig 4.3), this could be attributed to the pushing effect of excess hydrogen on the reaction balance resulting in an increase in the FF conversion and similar results have been reported by Liu et al,[8] However there was no significant increase in FF conversion when the hydrogen pressure was increased from 45 bar to 60 bar therefore 45 bar was the optimum pressure used. A TON of 391 was obtained at 45 bar using pre-catalyst **C4** which was considerably higher than that observed at 30 bar. A slight increase in TON by a value of 10 was not significant enough to select 60 bar as the

best pressure.

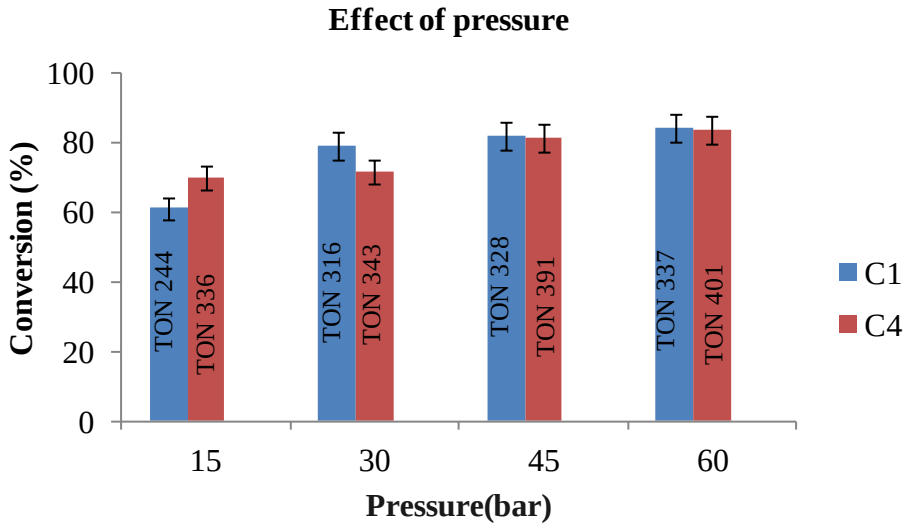

Conditions: ethanol (5 mL), substrate (FF, 2.4 mmol), temperature (140 ^{o}C, 160 ^{o}C) for catalyst precursor **C1** and **C4** respectively, catalyst precursors (**C1** and **C4**; 0.06 mmol), time (24 hours). Conversion and selectivity was determined by ^{1}H NMR spectroscopy.

Fig 4. 3 Effect of pressure in the hydrogenation of FF

Once the optimum temperature and pressure were obtained, solvents were also screened.

4.2.3 Effect of solvent

The effect of the solvent in the conversion of FF to FA was investigated using different solvents (Table 4.1). Both pre-catalysts **C1** and **C4** gave high FF conversion when ethanol was used as the solvent (97 % and 96 % respectively). There was no observed FF conversion when water or toluene were used as solvent which might be due to poor solubility of pre-catalysts **C1** and **C4** in both water and toluene. Isopropanol gave 75 % and 74 % FF conversion for pre-catalysts **C1** and **C4** which was lower than that of ethanol which might be attributed to the differences in alcohol dehydrogenation activity. This is similar to what has been reported in literature by Puthiaraj et al when the Pd precursors were employed in FF hydrogenation.[11] Both ethanol and isopropanol were active in the FF hydrogenation, this indicated that the conversion of FF to FA using pre-catalysts **C1** and **C4** is favourable in the presence of organic polar solvents.

Table 4. 1 Results obtained from hydrogenation of FF using different solvents

Entry	Complex	Solvent	Conv.(%)	TON	TOF	Sel.(%)
1	**C1/C4**	water	0	-	-	-
2	**C1/C4**	toluene	**0**	-	-	-
3	**C1**	ethanol	97.31	468	19	100
4	**C4**	ethanol	96.51	386	18	100
5	**C1**	Isopropanol	75.24	301	13	100
6	**C4**	Isopropanol	74.2	297	12	100

Conditions: substrate (FF, 2.4 mmol), molecular hydrogen (45 bar, 40 bar) for catalyst precursors **C1** and **C4** respectively, catalyst precursors (**C1** and **C4**; 0.06 mmol), time (24 hours). Conversion and selectivity was determined by ^{1}H NMR spectroscopy.

Once the optimum temperature, pressure and best solvent were obtained catalyst loading was also investigated.

4.2.4 Effect of catalyst loading

The reaction was performed using various catalyst loadings from 0.05 mol% (0.5 mg) to 0.2 mol% (3 mg) for 24 hours (Fig 4.4). The FF conversion increased with the increase in catalyst loading. Pre-catalyst **C1** showed 97 % FF conversion with TON of 389 and precatalyst **C4** showed 96 % FF conversion with a TON of 414 at 0.2 mol% (3 mg) catalyst loading with 100 % selectivity to FA. It has been reported before that increasing the catalyst loading results in more active sites which increases catalytic activity[8] and this is similar to what was observed when pre-catalysts **C1** and **C4** were employed.

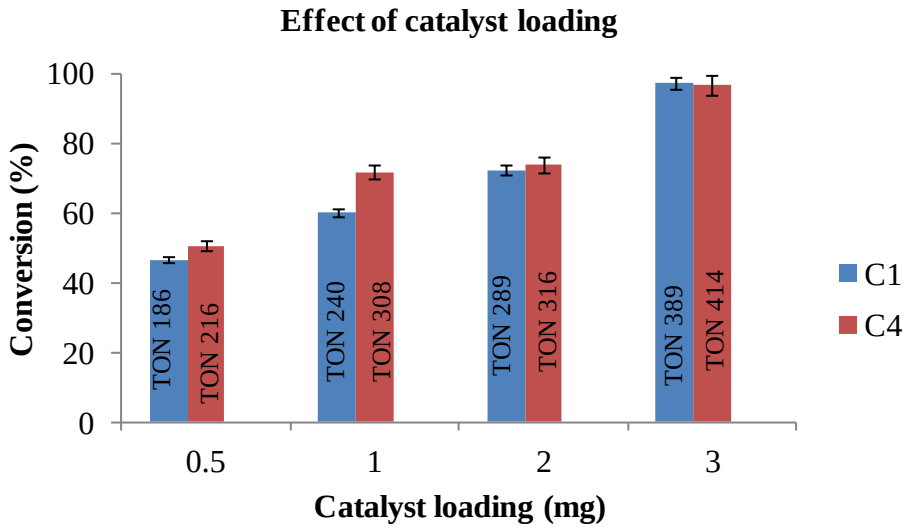

Conditions: ethanol (5 mL), substrate (FF, 2.4 mmol), molecular hydrogen (45 bar, 40 bar) for catalyst precursors **C1** and **C4** respectively, time (24 hours). Conversion and selectivity was determined by ^{1}H NMR spectroscopy.

Fig 4. 4 Effect of catalyst loading in the hydrogenation of FF

A time study was performed under the optimum temperature, pressure, solvent and catalyst loading.

4.2.5 Conversion as a function of time

The effect of reaction time on the FF conversion was investigated at 140 ^{o}C, 45 bar hydrogen pressure for pre-catalyst **C1** and 160 ^{o}C, 40 bar hydrogen pressure for **C4** (Fig 4.5). The reactions were stopped at various time intervals (4 -24 hours). The FF conversion increased gradually with prolonged reaction time, the highest turnover frequency (TOF) was recorded when the reaction was stopped in the first four hours (60 h^{-1} for pre-catalyst **C1** and 59 h^{-1} for **C4)**. However, the TON increased from 239 to 389 for pre-catalyst **C1** as the time was increased from 4 hours to 24 hours and from 252 to 414 for pre-catalyst **C4** hence 24 hours was the optimum reaction time.

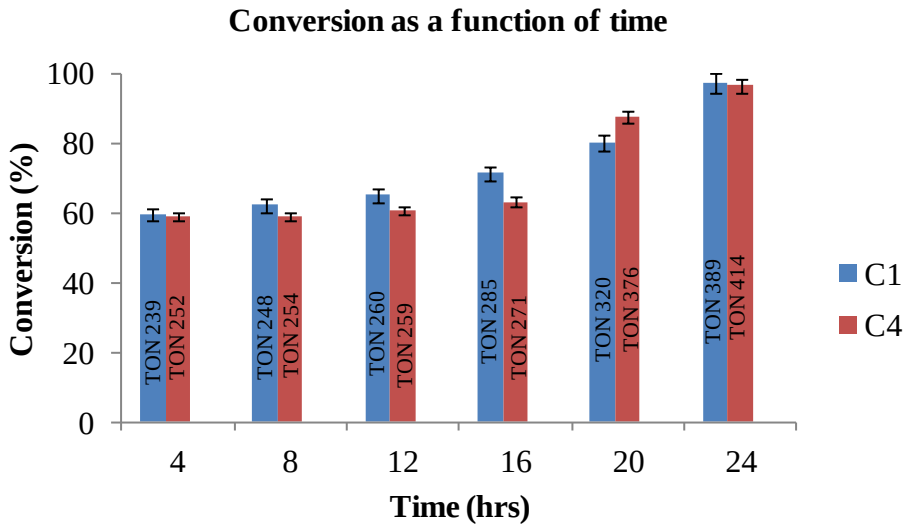

Conditions: ethanol (5 mL), substrate (FF, 2.4 mmol), molecular hydrogen (45 bar,40 bar) for catalyst precursor **C1** and **C4** respectively, catalyst precursors (**C1** and **C4**; 0.06 mmol), time (24 hours). Conversion and selectivity was determined by ^{1}H NMR spectroscopy.

Fig 4. 5 Effect of time in the hydrogenation of FF

Once the optimum reaction conditions were established using pre-catalysts **C1** and **C4**, it was important to screen various nickel precursors in order to see if the ligand had an influence in **C1** and **C4**.

4.2.6 Hydrogenation of FF using different metal precursors

The catalytic reactions were performed with different metal salts (Table 4.2) under optimum conditions and all these salts showed some activity in the conversion of FF to FA. Of interest to note was that $NiCl_2.6H_2O$ and $Ni(OAC)_2.4H_2O$ (Entry 1 and 2) showed poor results on FF conversion compared to synthesized metal precursors (Entry 3 and 4) which showed better performance. Synthesized metal precursors showed improvement in the conversion of FF to FA which might be due to the presence of ligands such as phosphines which improved the catalytic activity of the metal precursors. Steyl and co-workers reported that tertiary phosphine ligands can impact electronic and steric effects to the active metal centre,[12] which usually positively impacts the catalytic activity of the catalyst and all metal precursors displayed 100 % selectivity to FA. The silica gel used as a support was also screened in FF hydrogenation in order to evaluate the effect of the support in the reaction and it was of interest to note that SiO_2 was active in FF hydrogenation although the conversion was low (36 %) with a TON of 174.

Table 4. 2 Results obtained from screening metal precursors in the hydrogenation of FF using optimum conditions obtained from complex **C1** and **C4.**

Entry	Name	Conv.(%)	TON	TOF
1	$NiCl_2.6H_2O$	26.07	52	2
2	$Ni(OAC)_2.4H_2O$	38.49	77	3
3	$NiCl_2(PPh_3)_2$	71.51	74	3
4	$2[PPh_2ClNHSiO_3]Ni$	67.48	270	11
5	SiO_2	36.28	174	7

Conditions: ethanol (5 mL), substrate (FF, 2.4 mmol), molecular hydrogen (45 bar, 40 bar), catalyst precursors (0.06 mmol), time (24 hours). Conversion and selectivity was determined by ^1H NMR spectroscopy.

The optimum conditions were then employed to see the efficacy of the synthesized catalyst precursors **C1-C6.**

4.2.7 Hydrogenation of FF using complexes (C1-C6) as pre-catalysts

The reactions were performed with the complexes **C1-C6** as catalyst precursors (Fig 4.1). All the catalysts were active in the hydrogenation of FF in the presence of molecular hydrogen and gave 100 % selectivity to FA (Fig 4.6).

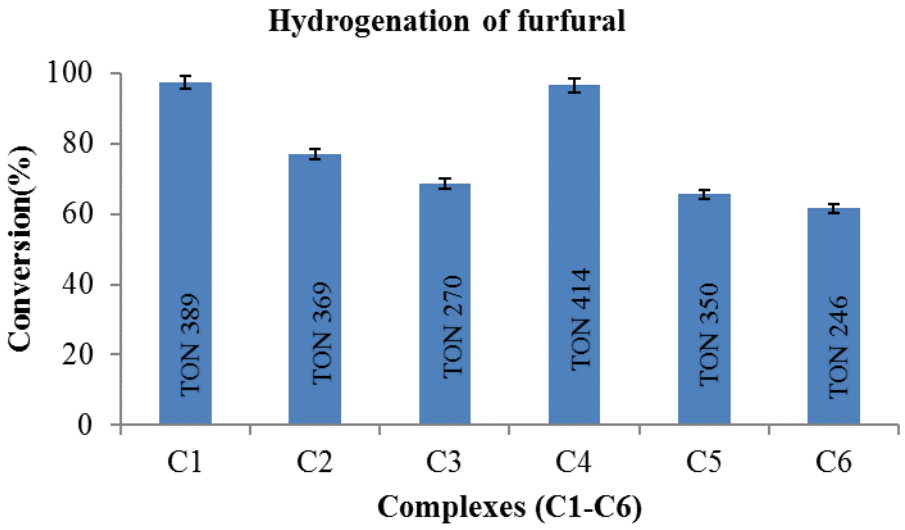

Conditions: ethanol (5 mL), substrate (FF, 2.4 mmol), molecular hydrogen (45 bar, 40 bar), catalyst precursors (**C1-C6**; 0.06 mmol), time (24 hours). Conversion and selectivity was determined by ^{1}H NMR spectroscopy.

Fig 4. 6 Hydrogenation of FF using complexes **C1-C6** as pre-catalysts

The homogenous complexes containing triphenylphosphine ligand, **C1** and **C4** gave the highest FF conversion (97 % and 95 % respectively) whilst homogenous complexes **C2** and **C5** which contain diphenyl-phosphine and siloxane ligands had a lower FF conversion (68 % and 65 % respectively). This shows that the phosphine is a good σ-donor and π acceptor (Fig 4.7) which has been reported and hence the electronic properties of the phosphine ligands are effective in enhancing the catalytic activity of the pre-catalysts. Similar results have been reported by Kubiak et al on a diphosphine complex $[Rh(P_2N_2)_2]^+$ which the authors explored in the catalytic activity of carbon dioxide hydrogenation and they reported that the electron donating ability of phosphine ligands is the key factor to increase the catalytic activity.[12]

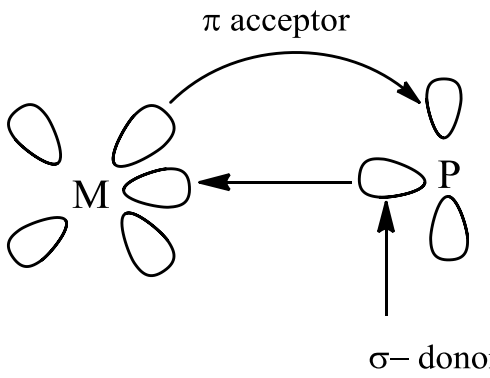

Fig 4. 7 Molecular orbital diagram illustrating metal centre (M)- phosphine (P) interaction.

The pre-catalysts containing siloxane ligand **C2**, **C3, C5** and **C6** showed some activity in the conversion of FF to FA, however the FF conversion was lower than what was expected. This could be attributed to the longer hydrocarbon chain between the Ni active center and the surface Si-O groups which results in reduced influence of the electron donor abilities of the surface on the catalytic centre. Also, the steric bulkiness of these pre-catalysts might have also contributed to the low catalytic activity. A similar trend was reported by Sakthivel et al in olefin epoxidation using molybdenum siloxane complexes.[13]

The silica supported pre-catalyst **C3** had higher FF conversion (69 %) compared to pre-catalyst **C6** (61 %). This is in good agreement with the results obtained by BET analysis where pre-catalyst **C3** exhibited higher surface area (258 m^2/g) as well as higher nickel loading (7.42 %).

A mercury poisoning experiment was done in order to check if our catalytic systems were entirely homogenous.

4.2.8 Homogeneity test

The distinction between homogeneous and heterogeneous has been done using mercury poisoning tests.[14] This method is based on the assumption that mercury poisons the nanoparticles which act as catalytically active centres and is inert to molecular metal complexes as such the absence of a significant effect of mercury on a metal catalyzed reaction is considered a homogenous mechanism. This implies that the inhibition of a catalytic reaction in the presence of mercury is evidence of nanoparticles or clusters in the catalytic mechanism. There was a great decrease in FF conversion in the presence of mercury when pre-catalyst **C1** was used which shows that the catalytic system might have been a mixture of both homogenous and heterogenous as black particles were observed in the catalysis product. Pre-catalysts **C2**, **C4** and **C5** showed a slight decrease in FF conversion in the presence of mercury (Fig 4.8). The obtained results showed that there might be some activity due to Ni(0) which contributed to the overall catalytic activity.

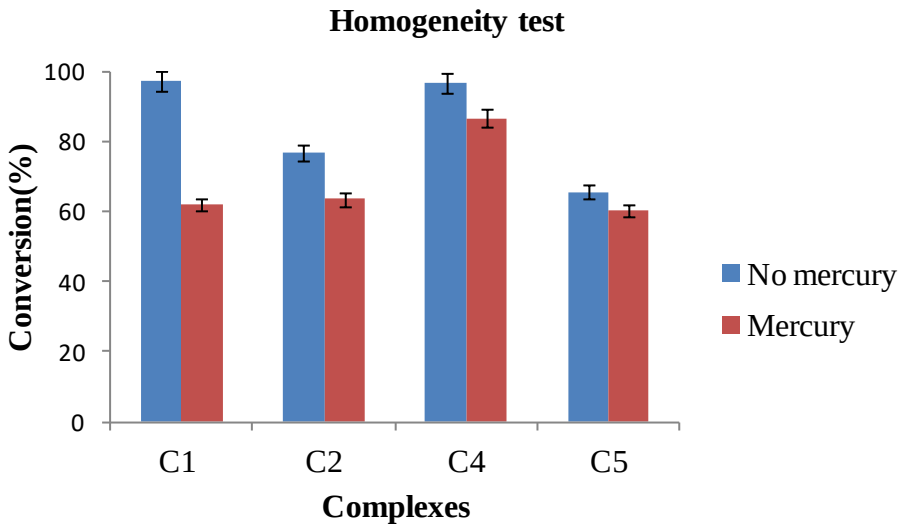

Conditions: ethanol (5 mL), substrate (FF, 2.4 mmol), molecular hydrogen 45 bar for pre-catalysts **C1**,**C2** and 40 bar for pre-catalysts **C4**, **C5**, catalyst precursors (**C1**, **C2**, **C3** and **C4**; 0.06 mmol), mercury (0.06 mmol), time (24 hours). Conversion and selectivity was determined by ^{1}H NMR spectroscopy.

Fig 4. 8 Homogeneity test during the hydrogenation of FF to FA using pre-catalysts (**C1, C2, C4, C5**)

The possibility to recycle the catalysts was also investigated, this is very important because most industrial processes make use of catalysts that are recyclable in order to make the process less expensive.

4.2.9 Recyclability studies of homogenous pre-catalyst C1

The stability of the pre-catalyst **C1** was examined by conducting recyclability studies under optimized conditions. After stopping the reaction, the catalysis mixture was dissolved in ethanol and dried in a schlenk tube under vacuum at 110 ^{o}C. Ethanol was added in the reactor vessel and dried under vacuum. The reactor vessel was recharged with furfural (2.4 mmol), hydrogen gas (45 bar), temperature (140 ^{o}C) and ethanol (5 mL). The reaction mixture was heated at 140 ^{o}C for 24 hours and the procedure was repeated until the fourth cycle (Fig 4.9). The pre-catalyst **C1** displayed excellent recyclability (Fig 4.8) and could be recycled efficiently three times without significant loss in activity. However in the fourth cycle there was a decrease in FF conversion which could be due to the partial decomposition of the active species during the reaction. The selectivity was 100 % towards FA.

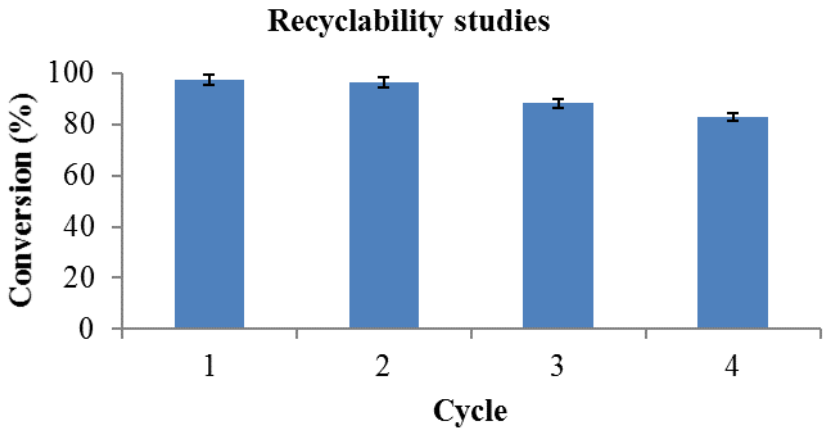

Conditions: ethanol (5 mL), substrate (FF, 2.4 mmol), molecular hydrogen 45 bar, **C1** (0.06 mmol), time (24 hours). Conversion and selectivity was determined by ^{1}H NMR spectroscopy.

Fig 4. 9 Recyclability of pre-catalyst **C1**

4.2.10 Recyclability studies of supported pre-catalysts C3 and C6

Recyclability test was performed using supported pre-catalysts **C3** (Fig 4.10) and pre-catalyst **C6**. Upon completion of the reaction, DMF was added as the internal standard and a sample was taken from the mixture for analysis. The crude mixture was filtered using gravity filtration followed by washing with ethanol five times making sure that all the furfural and was washed away. The pre-catalyst **C3** was dried using an oven at 30 ^{o}C overnight and re-used for the next cycle. The same procedure was repeated four times. Both pre-catalysts **C3** and **C6** were still active even on the fourth cycle, however the FF conversion decreased gradually from the first cycle (69 %) to the fourth (32 %) for pre-catalyst **C3** and 61 % to 40 % for pre-catalyst **C6** (Fig 4.11). The decrease in catalyst activity could be attributed to catalyst loss at each cycle. Moreover, the swelling or leaching of the active species which are some of the draw backs associated with metal centres in mesoporous silicates that have been reported in literature could also have contributed to the decrease in catalyst activity.[13] The pre-catalyst **C6** can be recycled better than pre-catalyst **C3**, it can be seen from the results that C6 is stable between cycle 1 and 2 followed by a gradual decrease in cycle 3 and 4.

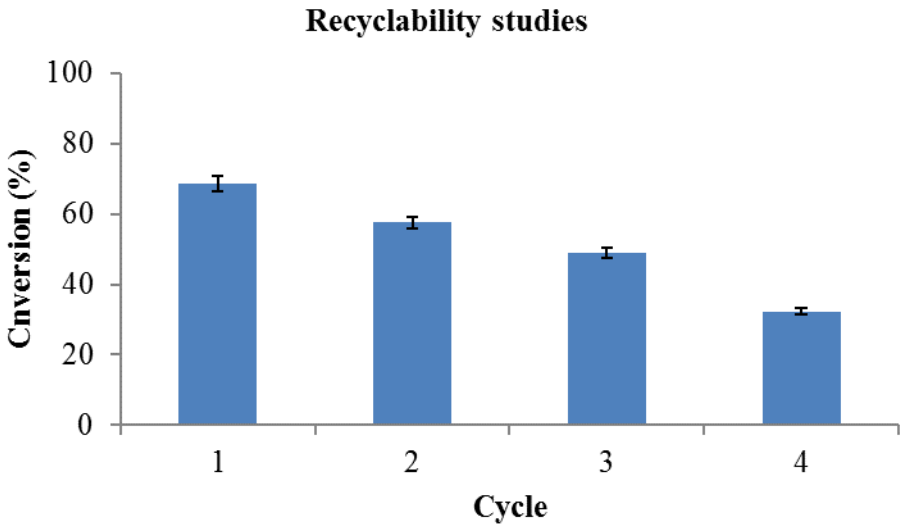

Conditions: ethanol (5 mL), substrate (FF, 2.4 mmol), molecular hydrogen 45 bar, **C3** (0.06 mmol), time (24 hours). Conversion and selectivity was determined by ^{1}H NMR spectroscopy.

Fig 4. 10 Recyclability of pre-catalyst **C3**

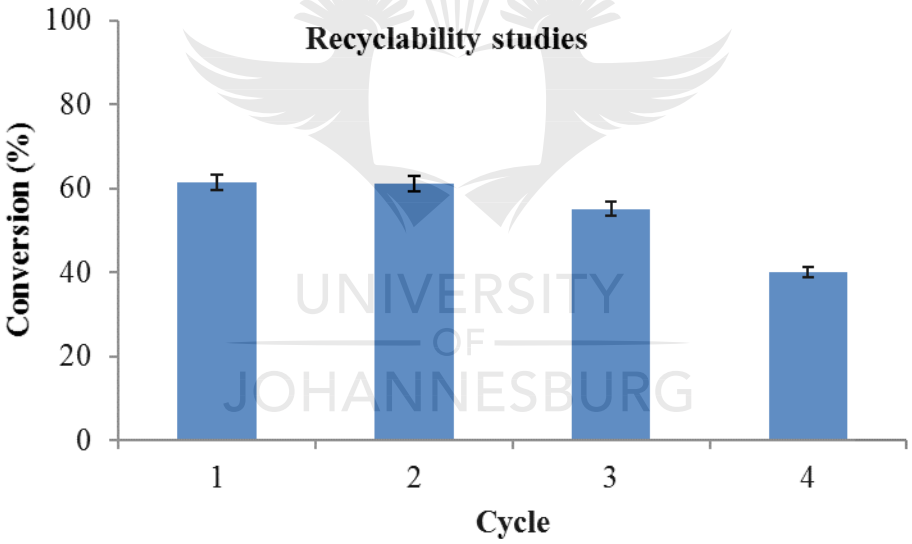

Conditions: ethanol (5 mL), substrate (FF, 2.4 mmol), molecular hydrogen 40 bar, **C6** (0.06 mmol), time (24 hours). Conversion and selectivity was determined by ^{1}H NMR spectroscopy.

Fig 4. 11 Recyclability of pre-catalyst **C6**.

4.3 Catalytic transfer hydrogenation of furfural

Catalytic transfer hydrogenation is considered less expensive compared to direct hydrogenation.[15] Transfer hydrogenation helps in reducing production costs by using organic molecules as hydrogen donors instead of molecular hydrogen. This makes transfer hydrogenation safer due to the fact that there is no use of molecular hydrogen which needs

safe handling.

The catalytic activity of pre-catalysts **C1** and **C4** was also evaluated in the hydrogenation of FF using formic acid as the hydrogen source. The hydrogenation of FF was performed by reacting catalyst (0.05 mmol), FF (10 mmol), Et_3N (10 mmol) and formic acid (20 mmol) in an autoclave reactor at 140 ^oC for 4 hours.

4.3.1 Effect of temperature

The reaction was performed using 0.05 mol% of complex **C1** and **C4** as pre-catalysts at different temperatures ranging from 120-140 ^oC (Fig 4.12). Both pre-catalysts showed an increase in furfural conversion as the temperature increased up to 140 ^oC. An increase in temperature to 150 ^oC gave less furfural conversion which might be due to both catalysts being unstable at high temperatures when formic acid is used as the hydrogen source. In direct hydrogenation of furfural to furfuryl alcohol, the optimum temperature for pre-catalyst **C1** was also 140 ^oC. This could be attributed to the fact that temperatures above 140 ^oC will now be getting closer to the melting point of pre-catalyst **C1** which was obtained in the range 168-170 ^oC. At 140 ^oC pre-catalyst **C1** and **C4** showed high FF conversion of 93 % and 90 % respectively, the selectivity for both pre-catalysts was 100 % towards FA. As a result, 140 ^oC was selected as the best temperature.

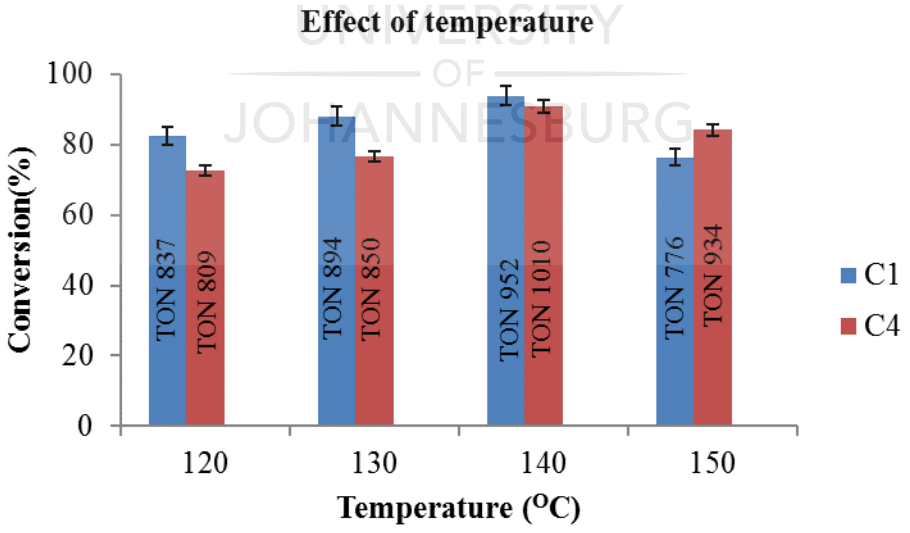

Conditions: FF (10 mmol), Et_3N (10 mmol), formic acid (20 mmol), catalyst precursors (**C1** and **C4**; 0.05 mol%), time (4 hours). Conversion determined by ^1H NMR spectroscopy.

Fig 4. 12 Effect of temperature in the catalytic transfer hydrogenation of FF.

Once the optimum temperature was obtained, the effect of base was also investigated.

4.3.2 Effect of base

Based on the previous experimental results obtained in the direct hydrogenation of FF, pre-catalyst **C1** and **C4** were chosen as the best performing catalysts and these were evaluated as pre-catalysts for the catalytic transfer hydrogenation of FF.

The reactions were performed using 1 equivalent of each of the bases at 140 ^{o}C, among the screened organic bases (Et_3N, DBU and pyridine) and inorganic base (KOH) only Et_3N and DBU showed activity in the hydrogenation of FF (Fig 4.13).

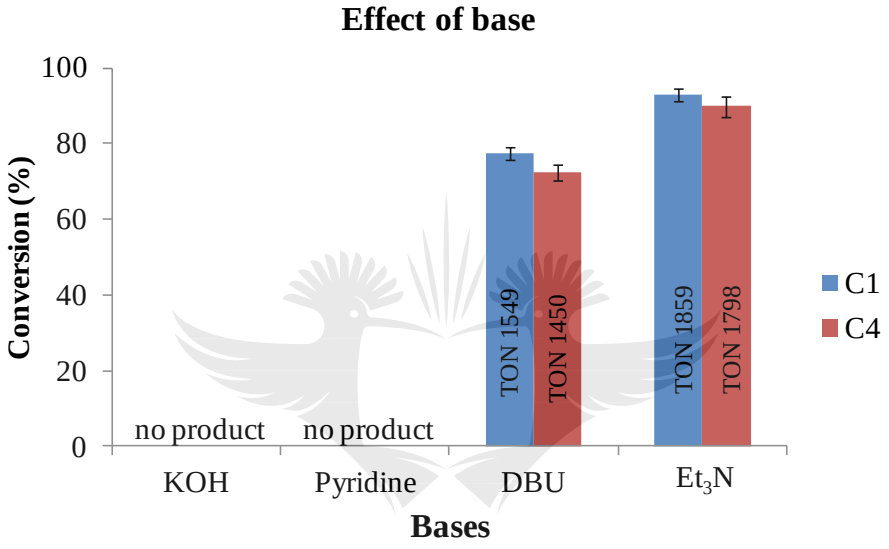

Conditions: FF (10 mmol), formic acid (20 mmol), catalyst precursors (**C1** and **C4**; 0.05 mol %), time (4 hours). Conversion determined by ^{1}H NMR spectroscopy.

Fig 4. 13 Effect of base in the catalytic transfer hydrogenation of FF

With 1 molar equivalent of Et_3N, 93 % FF conversion was obtained with a TON of 1859 when pre-catalyst **C1** was used and pre-catalyst **C4** gave 90 % FF conversion with a TON of 1798. On the other hand, with 1 molar equivalent of DBU, gave the highest conversion of FF (93 % and 90 %) for precatalyst **C1** and **C4** respectively. However, no product was obtained for both pre-catalysts when the reaction was performed in the presence of one equivalent of an organic base pyridine and inorganic base KOH. This might have been due to the potential of KOH and pyridine acting as coordinating bases resulting in inhibition of the catalytic reaction. This can be due to the available nitrogen lone pair in pyridine which might have coordinated and also in KOH the oxygen atom in OH is known as a strong electron donor due to its available lone pair of electrons, the K^{+} cations might have coordinated with other groups. These type of interactions have been reported in literature by

Fernandez and co-workers when they employed PVA-KOH in structural modifications and ionic transport used for hydrogels in Zn/Air batteries.[16] Precatalysts **C1** and **C4** both were 100 % selective to FA and the results show that both pre-catalysts **C1** and **C4** performed better with Et3N , therefore Et_3N was used for all subsequent reactions.

4.3.3 Effect of base concentration

To study the effect of base concentration on the catalytic reactions, several amounts of Et_3N were screened. The concentration of base (Et_3N) was varied from 0 to 10mmol and no FF conversion was observed in the absence of a base (0 mmol) therefore a base is required to decompose formic acid into H_2 and CO_2 in order to obtain the hydrogen gas required for the reaction.[17] With 0.3 molar equivalent (3.3 mmol) of Et_3N, 86 % FF conversion was obtained using pre-catalyst **C1** (Fig 4.14) whilst no FF conversion was obtained when pre-catalyst **C4** was employed which might be due to insufficient base to produce H_2 gas required to initiate the catalytic reaction. An increase of the base to 5.0 mmol for pre-catalyst **C1**, the FF conversion remained as high as 86 % whilst with pre-catalyst **C4** the FF conversion increased to 78 % indicating the importance of sufficient base in the catalytic process. Further increase of the base to 1 molar equivalent (10 mmol) the FF conversion increased to 93 % with a TON of 1737 and 90 % with a TON of 1729 for pre-catalysts **C1** and **C4** respectively, therefore 10 mmol of Et_3N was chosen as the optimum base concentration.

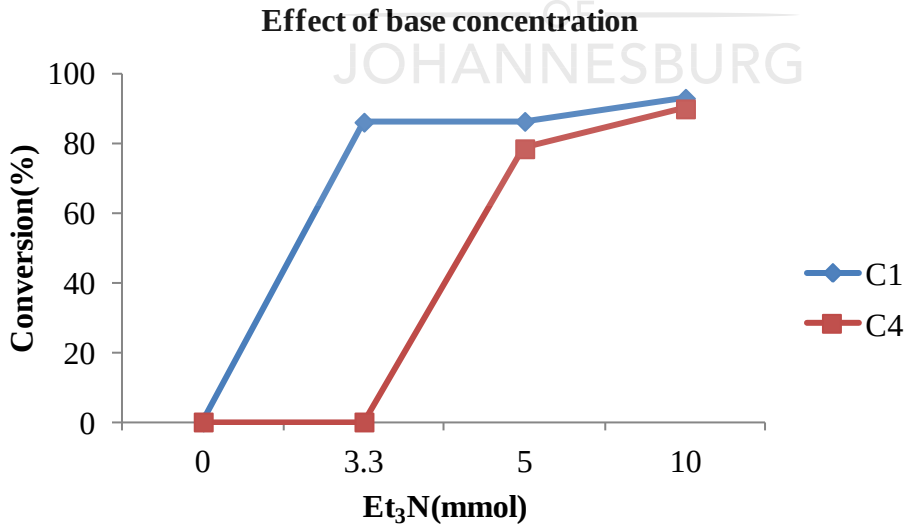

Conditions: FF (10 mmol), formic acid (20 mmol), catalyst precursors (**C1** and **C4**; 0.05 mol%), time (4 hours). Conversion determined by ^{1}H NMR spectroscopy.

Fig 4. 14 Effect of base concentration in the catalytic transfer hydrogenation of FF.

Once the optimum temperature and base were obtained, the effect of catalyst loading was also investigated.

4.3.4 Effect of catalyst loading

The reaction was performed using various catalyst loadings ranging from 0.05 mol% to 2 mol% (Fig 4.15) and formic acid for 4 hours at 140 ^{o}C. The results obtained showed that as catalyst loading increases there was a slight increase in FF conversion. However, the highest turnover number (TON) was obtained at 0.05 mol% catalyst loading. Pre-catalyst **C1** gave a TON of 1859 and **C4** gave a TON of 1797, both pre-catalysts showed 100 % selectivity to FA. Compared to direct hydrogenation which required higher catalyst loading, transfer hydrogenation showed good FF conversion even at lower catalyst loading. This is a good indication, because it makes the catalytic reaction with less catalyst loading in the absence of molecular hydrogen. Therefore, 0.05 mol% was the optimum catalyst loading.

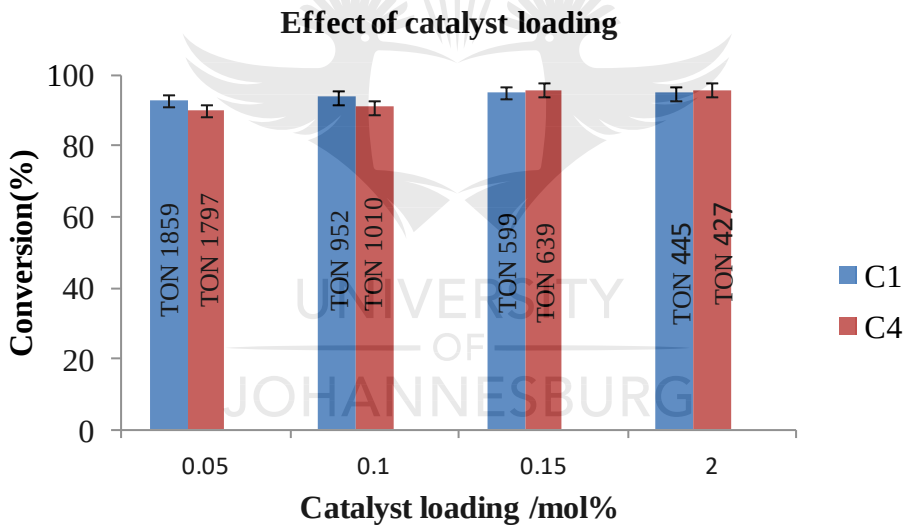

Conditions: FF (10 mmol), Et_3N (10 mmol), formic acid (20 mmol), catalyst precursors (**C1** and **C4**; 0.05 mol%), time (4 hours). Conversion determined by ^{1}H NMR spectroscopy.

Fig 4. 15 Effect of catalyst loading in the catalytic transfer hydrogenation of FF.

4.3.5 *Conversion as a function of time*

The reactions were performed between 4 hours and 12 hours (Fig 4.16). After 4 hours both pre-catalysts **C1** and **C4** do not show any significant increase in FF conversion. The highest turnover frequency (TOF) for the pre-catalyst **C1** was 465 h^{-1} at 4 hours and 450 h^{-1} for pre-catalyst **C4** in entry 1 and 2 (Table 4.3).

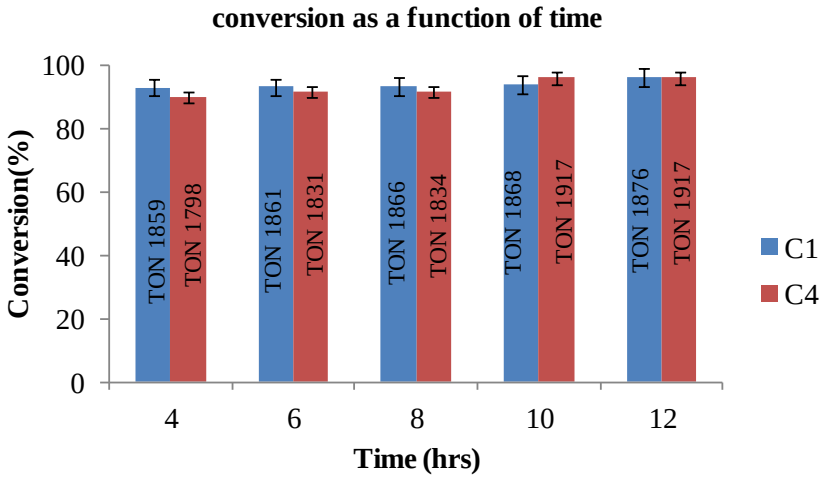

Conditions: FF (10 mmol), Et_3N (10 mmol), formic acid (20 mmol), catalyst precursors (**C1** and **C4**; 0.05 mol %), time (4 hours). Conversion determined by ^1H NMR spectroscopy.

Fig 4. 16 Conversion as a function of time in the catalytic transfer hydrogenation of FF

Table 4. 3 Results of TON and TOF versus time obtained from catalytic transfer hydrogenation of FF

Entry	**Complex**	**Time/h**	**TON**	**TOF/h-^{1}**
1	**C1**	4	1859	465
2	**C4**	4	1798	450
3	**C1**	6	1861	310
4	**C4**	6	1831	305
5	**C1**	8	1866	233
6	**C4**	8	1834	229
7	**C1**	10	1868	187
8	**C4**	10	1917	192
9	**C1**	12	1876	156
10	**C4**	12	1917	159

Conditions: substrate FF (10 mmol), Et_3N (10 mmol), formic acid (20 mmol), catalyst precursors (**C1** and **C4**; 0.05 mol%), 140 ^oC. Conversion determined by ^1H NMR spectroscopy (500 MHz).

The TOF decreased from 4 hours to 12 hours, therefore 4 hours was selected as the best time and both pre-catalysts showed 100 % selectivity to FA. After 4 hours, the same conversion is produced even when the reaction is continued beyond 4 hours.

The ^{1}H NMR spectrum of a sample from the reaction mixture is shown in Fig 4.17. The reaction mixture was also spiked with DMF as internal standard.

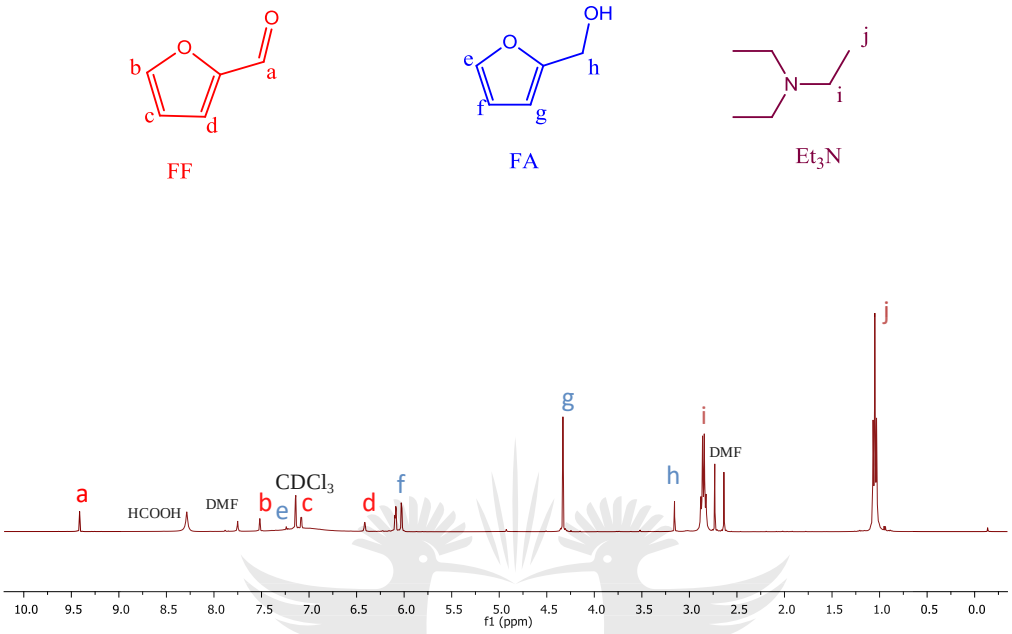

Conditions: substrate FF (10 mmol), Et_3N (10 mmol), formic acid (20 mmol), catalyst precursor (**C1**; 0.05 mol%, 140 ^{o}C. Conversion determined by ^{1}H NMR spectroscopy (500 MHz).

Fig 4. 17 ^{1}H NMR spectrum of the transfer hydrogenation of FF to FA using pre-catalyst **C1** in $CDCl_3$, DMF internal standard (500 MHz).

The ^{1}H NMR spectrum on Fig 4.17 shows that the pre-catalysts **C1** is active in the transfer hydrogenation of FF to FA using formic acid as the hydrogen donor in the presence of Et_3N base. The spectrum also shows unreacted FF after the reaction indicating that the pre-catalyst **C1** does not completely convert FF, However it is a good catalyst because it is able to convert FF to FA selectively which is a good characteristic for industrial application as this catalyst can direct the reaction to yield a particular product compared to catalysts that yield different products which will require separation making the reaction process expensive and time consuming.

4.4 Homogeneity test

The homogeneity of the pre-catalysts **C1** and **C4** in catalytic transfer of FF was determined using the mercury poisoning experiment.[14] The precatalysts **C1** was operationally homogenous when formic acid was used as the hydrogen source as no significant change was observed in the FF conversion upon addition of mercury to the reaction (Fig 4.18).

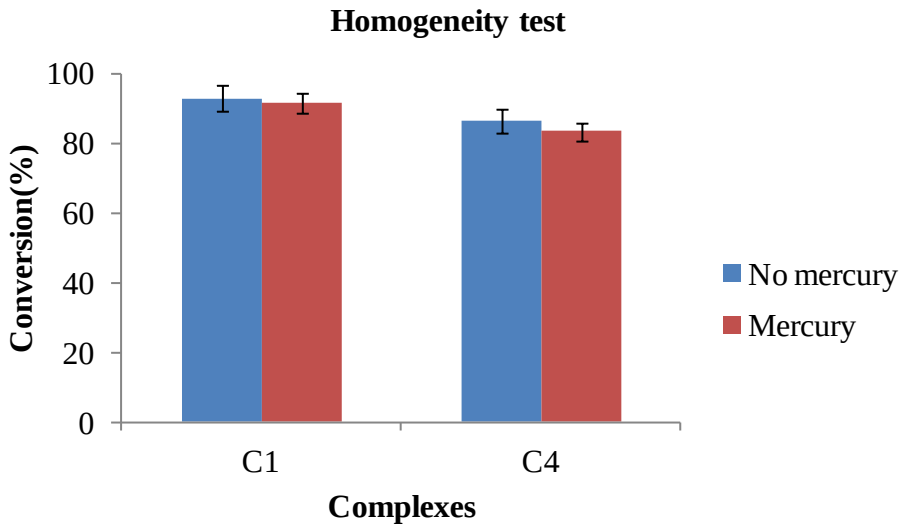

Conditions: FF (10 mmol), Et_3N (10 mmol), formic acid (20 mmol), catalyst precursors (**C1** and **C4**; 0.05mol %), mercury (0.005 mmol), time (4 hours). Conversion determined by ^1H NMR spectroscopy.

Fig 4. 18 Homogeneity test in the catalytic transfer hydrogenation of FF using pre-catalysts **C1** and **C4.**

The obtained results show a slight decrease in the conversion of FF to FA when pre-catalyst **C4** was employed in the presence of mercury, this indicates minute activity from Ni(0).

The catalyst recycling is important from an economic and environmental point of view, therefore recyclability studies were conducted using pre-catalyst **C1**.

4.5 Recyclability Studies

The stability of the precatalyst **C1** was examined by conducting recyclability studies under optimized conditions. After stopping the reaction, the catalysis mixture was dissolved in ethanol and dried in a schlenk tube under vacuum at 110 ^oC. Ethanol was added in the reactor vessel and dried under vacuum. The reactor vessel was recharged with furfural (10 mmol), Et_3N (10 mmol) and formic acid (20 mmol). The reaction mixture was heated at 140 ^oC for 4 hours and the procedure was repeated until the fourth cycle (Fig 4.19). The FF conversion decreased gradually within the first three cycles then decreased drastically in the fourth cycle. The selectivity remained 100 % towards FA.

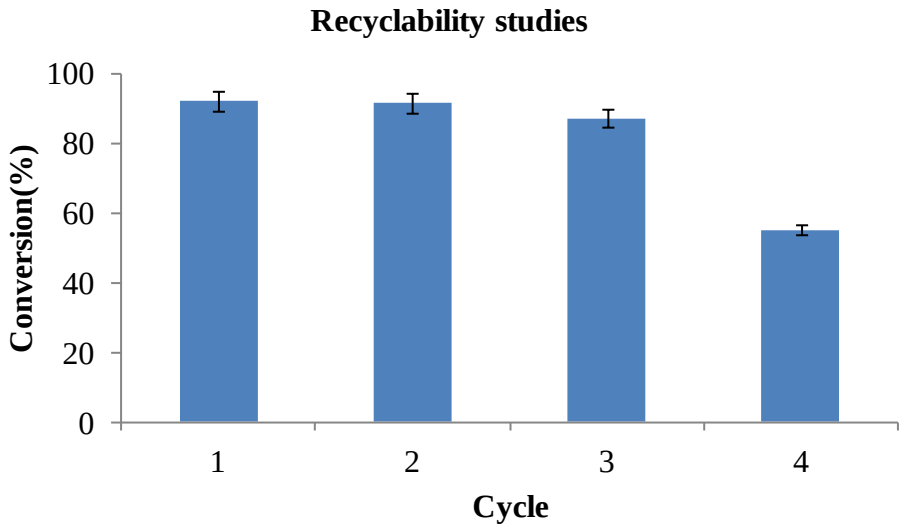

Conditions: FF (10 mmol), Et_3N (10 mmol), formic acid (20 mmol), catalyst precursor (**C1**; 0.05 mol %), time (4 hours). Conversion determined by ^1H NMR spectroscopy.

Fig 4. 19 Recyclability of precatalyst **C1**

4.6 Catalytic transfer hydrogenation of other substrates

This investigation was done to investigate the specificity of these catalyst whether the catalyst are selective towards the aldehyde or the ring.

4.6.1 Transfer hydrogenation of cinnamaldehyde and 2-thiophenecarboxaldehyde

The reactions were performed under optimum conditions obtained in the hydrogenation of FF using pre-catalysts **C1** and **C4**. Both pre-catalysts showed some activity in the transfer hydrogenation of cinnamaldehyde and 2-thiophenecarboxaldehyde (Table 4.4). The cinnamaldehyde conversion was 85 % and 80 % with TONs of 1709 and 1590 when pre-catalyst **C1** and **C4** were employed respectively and both pre-catalysts were 100 % selective to cinnamyl alcohol (CA). When the substrate was changed to 2-thiophenecarboxaldehyde, the conversion was 69 % and 60 % with TONs of 1371 and 1204 for pre-catalysts **C1** and **C4** respectively both pre-catalysts were 100 % selective to 2-thiophenemethanol**.** Using the results obtained in both direct and transfer hydrogenation of FF, cinnamaldehyde and 2-thiophenecarboxaldehyde it was observed that the pre-catalysts **C1** and **C4** show some activity towards alpha-$_\beta$ unsaturated substrates and both pre-catalysts are selective towards the aldehyde instead of the ring although the conversion does not come to completion. A selective catalyst is also a good catalyst that can be employed in the industry for large scale production of the desired product.

Table 4. 4 Transfer hydrogenation of cinnamaldehyde and 2-thiophenecarboxaldehyde

Entry	**Complex**	**Substrate**	**Conv.(%)**	**TON**	**TOF**	**Selectivity**
1	**C1**	cinnamaldehyde	85.46	1709	427	Cinnamyl alcohol
2	**C4**	cinnamaldehyde	79.52	1590	398	Cinnamyl alcohol
3	**C1**	2-thiophenecarboxaldehyde	68.59	1371	343	2-thiophene methanol
4	**C4**	2-thiophenecarboxaldehyde	60.22	1204	301	2-thiophene methanol

Conditions: substrates cinnamaldehyde, 2-thiophenecarboxaldehyde (10 mmol), Et_3N (10 mmol), formic acid (20 mmol), catalyst precursors (**C1** and **C4**; 0.05 mol%), 140 ^{o}C, 4 hours. Conversion determined by ^{1}H NMR spectroscopy (500 MHz).

The ^{1}H NMR spectrum of a sample from the hydrogenation of cinnamaldehyde reaction mixture is shown in Fig 4.20 the reaction mixture was also spiked with DMF as internal standard.

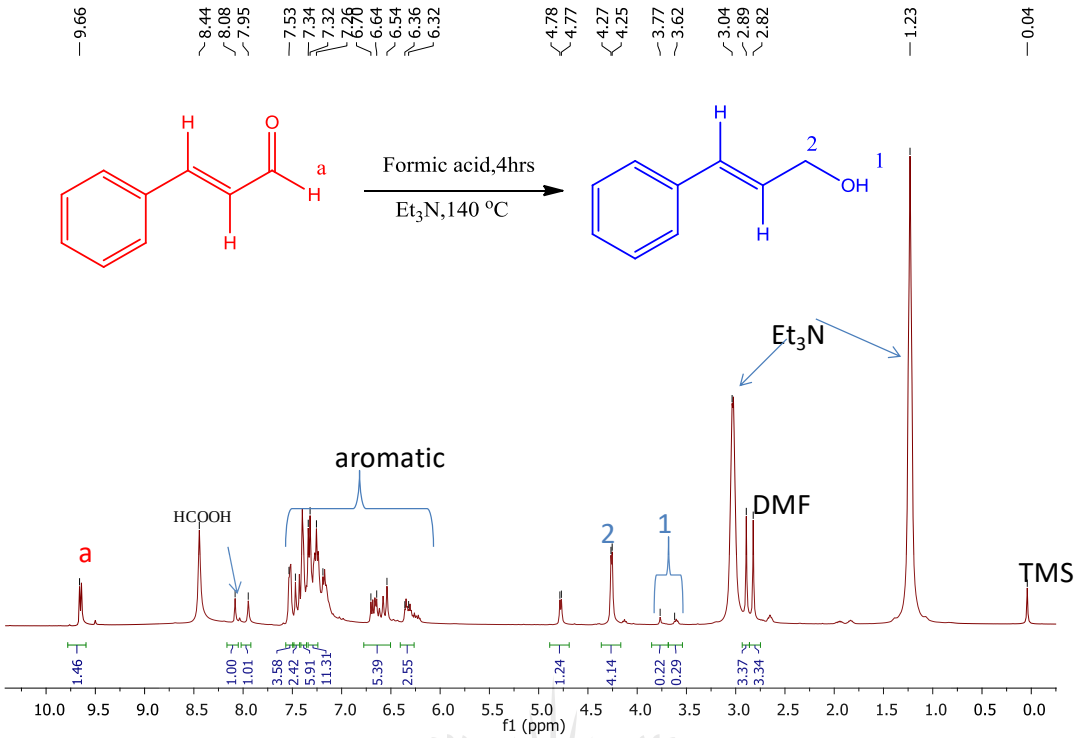

Conditions: substrate cinnamaldehyde (10 mmol), Et_3N (10 mmol), formic acid (20 mmol), catalyst precursor (**C1**; 0.05 mol%, 140 °C, 4 hours. Conversion determined by ^1H NMR spectroscopy (500 MHz).

Fig 4. 20 ^1H NMR spectrum of the transfer hydrogenation of cinnamaldehyde to cinnamyl alcohol using pre-catalyst **C1** in $CDCl_3$, DMF internal standard (500 MHz).

The ^1H NMR spectrum (Fig 4.20) shows that the pre-catalyst **C1** is active in hydrogenation of cinnamaldehyde using formic acid as the hydrogen donor in the presence of Et_3N. There is unreacted cinnamaldehyde indicating that pre-catalyst **C1** does not completely convert the cinnamaldehyde. The conversion was 85 % with a TON of 1709 and the selectivity was 100 % to cinnamyl alcohol, therefore pre-catalyst **C1** is a good catalyst even with a different substrate it was observed that the catalyst was selective.

The ^1H NMR spectrum of a sample from the hydrogenation of 2-thiophenecarboxaldehyde reaction mixture is shown in Fig 4.21. The reaction mixture was also spiked with DMF as internal standard.

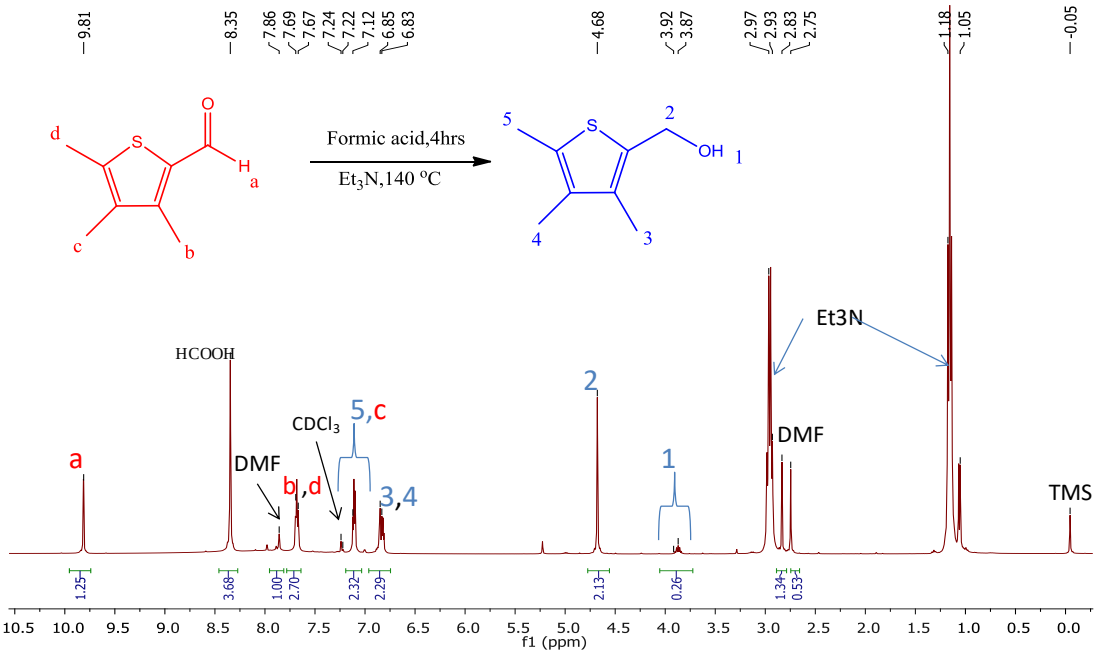

Conditions: substrate 2-thiophenecarboxaldehyde (10 mmol), Et_3N (10 mmol), formic acid (20 mmol), catalyst precursor (**C1**; 0.05 mol%), 140 °C, 4 hours. Conversion determined by ^1H NMR spectroscopy (500 MHz).

Fig 4. 21 ^1H NMR spectrum of the transfer hydrogenation of 2-thiophenecarboxaldehyde to 2-thiophenemethanol using pre-catalyst **C1** in $CDCl_3$, DMF internal standard (500 MHz).

The ^1H NMR spectrum (Fig 4.21) shows that the pre-catalyst **C1** is active in hydrogenation of 2-thiophenecarboxaldehyde using formic acid as the hydrogen donor in the presence of Et_3N. The spectrum shows unreacted 2-thiophenecarboxaldehyde indicating that pre-catalyst **C1** does not completely convert the 2-thiophenecarboxaldehyde, However the conversion was as high as 69 % in 4 hours with a TON of 1371 and the selectivity was 100 % to 2-thiophenemethanol. This indicates that pre-catalyst **C1** is selective.

4.7 In situ NMR studies of the catalytic process

We attempted to establish a mechanism for the catalytic process by conducting *In situ* NMR studies. The catalytic process was monitored by performing a small scale reaction with MeOH-d_4 solvent in the absence of substrate. Pre-catalyst **C1**, formic acid and Et3N were loaded into a J Young NMR tube and heated in an oil bath at 75 °C. The reaction progress was monitored by using ^1H NMR, However no metal hydride species were observed. Several attempts were carried out and none of them was successful, this could have been due to the instant formation of the metal hydride species after adding the reactants into the J Young tube and the metal hydride species formed might be unstable to be observed in the ^1H NMR spectrum.

Another small scale reaction was performed in the presence of substrate FF by loading FF, pre-catalyst **C1**, Et_3N and formic acid into the J Young NMR tube and heated in a magnet while monitoring the reaction by using ^1H NMR, again no metal hydride species were observed.

We also performed another small scale reaction in the presence of $CDCl_3$. The reaction was performed by loading pre-catalyst **C1** and molecular hydrogen into a high pressure tube and heated in a magnet at 65 ^oC. The reaction progress was monitored by using ^1H NMR, however, no metal hydride species was observed.

4.8 Conclusion

We have shown that six Ni(II) complexes are active pre-catalysts for the hydrogenation of FF using molecular hydrogen in ethanol solvent and pre-catalysts **C1** and **C4** showed excellent catalytic activity. All the pre-catalysts showed good selectivity towards formation of furfuryl alcohol. Mercury poisoning tests showed that pre-catalyst **C1** exhibited a drop in activity as a result of nanoparticles present indicating that the catalytic reaction was a result of both homogenous and nanoparticles activity and pre-catalyst **C4** exhibited a slight drop in activity due to nanoparticles indicating that the catalytic reaction was mostly homogenous. The reaction was entirely homogenous when pre-catalysts **C2** and **C5** were employed. Recyclability experiments were performed using pre-catalyst **C1**, **C3** and **C6** and the results show good recyclability when pre-catalysts **C1** and **C6** were employed. The pre-catalysts **C1** and **C4** showed greater activity for the hydrogenation of FF using formic acid as a hydrogen donor with good selectivity to furfuryl alcohol and reactions are complete in 4 hours. The pre-catalysts **C1** and **C4** showed activity towards alpha-β unsaturated substrates and were selective to saturation of the carbonyl functionality over alkene groups.

4.9 Experimental section

4.9.1 Materials and instrumentation

Furfural (FF), dimethylformamide (DMF), ethanol (EtOH), methanol (MeOH), chloroform, furfuryl alcohol (FA), triethylamine (Et_3N), pyridine, potassium hydroxide (KOH), toluene, isopropanol and formic acid were all purchased from Sigma-Aldrich and used as received. Nuclear magnetic resonance (NMR) spectra were recorded on a Bruker Ultrashield-500 MHz spectrometer (^1H: 500 MHz) in chloroform, methanol using TMS as an internal standard. All hydrogenation reactions were performed in PPV-CTRO1-CE high pressure

reactor vessels fitted into a high pressure autoclave reactor with built –in stirring, heating and cooling.

4.10 General hydrogenation

4.10.1 Direct hydrogenation using molecular hydrogen

Direct hydrogenation of FF was carried out in a 60 ml stainless autoclave reactor equipped with a mechanical stirrer, and electric temperature controller and a pressure gauge. An autoclave reactor was charged with FF (2.4 mmol), catalyst (0.06 mmol) and solvent (5 mL). The reactor was purged twice with hydrogen gas and pressured to desired pressure using molecular hydrogen. The temperature was set at desired temperature and stirring was done at stirring speed of 800 rpm. After the reaction time, the mixture was cooled to room temperature and then slowly depressurized. A sample of the reaction mixture was taken and analyzed by ^{1}H NMR spectroscopy to determine the conversion and product selectivity.

4.10.2 Transfer hydrogenation using formic acid as hydrogen donor

Catalyst (0.005 mmol), formic acid (20 mmol), Et_3N (10 mmol) and FF (10 mmol) were added to an autoclave reactor (50 mL). The reaction mixture was purged three times with nitrogen gas and then heated to 140 ^{o}C and the mixture was stirred at 800 rpm for 4 hours. After the reaction time the mixture was cooled to room temperature and the gas generated in the course of the reaction was released. A sample of the reaction mixture was taken and analyzed by ^{1}H NMR spectroscopy to determine the conversion and product selectivity.

4.11 References

1 K. E. Salnikova, V. G. Matveeva, Y. V. Larichev, A. V Bykov, G. N. Demidenko, I. P. Shkileva and M. G. Sulman, *Catal. Today*, 2019, **329**, 142–148.

2 J. Parikh, S. Srivastava and G. C. Jadeja, *Ind. Eng. Chem. Res.*, 2019, **58**, 16138–16152.

3 S. A. Khromova, M. V Bykova, O. A. Bulavchenko, D. Y. Ermakov, A. A. Saraev, V. V. Kaichev, R. H. Venderbosch and V. A. Yakovlev, *Top. Catal.*, 2016, **59**, 1413–1423.

4 S. Bhogeswararao and D. Srinivas, *J. Catal.*, 2015, **327**, 65–77.

5 M. J. Taylor, L. J. Durndell, M. A. Isaacs, C. M. A. Parlett, K. Wilson, A. F. Lee and G. Kyriakou, *Appl. Catal. B Environ.*, 2016, **180**, 580–585.

6 A. B. Merlo, V. Vetere, J. F. Ruggera and M. L. Casella, *Catal. Commun.*, 2009, **10**, 1665–1669.

7 J. Li, J. L. Liu, H. J. Zhou and Y. Fu, *ChemSusChem*, 2016, **9**, 1339–1347.

8 L. Liu, H. Lou and M. Chen, *Int. J. Hydrogen Energy*, 2016, **41**, 14721–14731.

9 K. L. MacIntosh and S. K. Beaumont, *Top. Catal.*, 2020, **23**, 122–151.

10 C. K. P. Neeli, Y. Chung and W. Ahn, *ChemCatChem*, 2017, **9**, 4570–4579.

11 P. Puthiaraj, K. Kim and W.-S. Ahn, *Catal. Today*, 2019, **324**, 49–58.

12 A. Roodt, S. Otto and G. Steyl, *Coord. Chem. Rev.*, 2003, **245**, 121–137.

13 A. Sakthivel, J. Zhao, M. Hanzlik, A. S. T. Chiang, W. A. Herrmann and F. E. Kühn, *Adv. Synth. Catal.*, 2005, **347**, 473–483.

14 R. H. Crabtree, *Chem. Rev.*, 2012, **112**, 1536–1554.

15 M. M. Villaverde, T. F. Garetto and A. J. Marchi, *Catal. Commun.*, 2015, **58**, 6–10.

16 F. Santos, J. P. Tafur, J. Abad and A. J. Fernández Romero, *J. Electroanal. Chem.*, 2019, **850**, 113380.

17 Z. Fu, Z. Wang, W. Lin, W. Song and S. Li, *Appl. Catal. A Gen.*, 2017, **547**, 248–255.

Chapter Five

Overall summary and Future outlook

5.1 Synthesis of Ni(II) complexes for the hydrogenation of furfural to furfuryl alcohol

5.1.1 Overall Summary

Two ligands and six Ni(II) complexes were synthesized and characterized using both analytical and spectroscopic techniques. These complexes were found to be active pre-catalysts for the direct hydrogenation of furfural to furfuryl alcohol using molecular hydrogen in ethanol. Complexes **C1** and **C4** displayed high catalytic activity in furfural conversion, other complexes **C2**, **C3**, **C5** and **C6** containing siloxane ligand displayed lower catalytic activity in the furfural conversion which might be due to the longer hydrocarbon chain between the Ni active center and the Si-O surface which reduces the influence of the electron donor ability of the Si-O group to the catalytic center.[1] The silica supported complexes **C3** and **C6** displayed lower FF conversion despite the presence of the acidic support which might be due to the steric bulkiness of the pre-catalyst. Mercury poisoning tests showed that pre-catalyst **C1** exhibited a drop in activity as a result of nanoparticles present indicating that the catalytic reaction was a result of both homogenous and nanoparticles activity and pre-catalyst **C4** exhibited a slight drop in activity due to nanoparticles indicating that the catalytic reaction was mostly homogenous. The reaction was entirely homogenous when pre-catalysts **C2** and **C5** were employed.

Recyclability experiments were performed using pre-catalyst **C1**, **C3** and **C6** and the results show good recyclability when pre-catalysts **C1** and **C6** were employed. The catalysts are found to be active even after three catalytic runs, however the catalytic activity decreases which might be due to chemisorption of organic molecules on the surface preventing the access of the furfural substrate.

The complexes **C1** and **C4** showed good performance and they were further evaluated as pre-catalysts in the transfer hydrogenation of FF using formic acid as the hydrogen donor. The highest turnover frequency was 465 h^{-1} and 450 h^{-1} after 4 hours for **C1** and **C4** respectively. Pre-catalyst **C1** showed good recyclability and could be recycled four times with a significant drop in FF conversion in the fourth cycle. The observed decrease in

activity could be due to partial decomposition of the active species resulting from the prolonged exposure to heat from one cycle to the other.

5.1.2 Future Outlook

The use of homogenous Ni(II) complexes for the hydrogenation of furfural to furfuryl alcohol has not been reported in the open literature, hence homogenous Ni(II) complexes can be employed on a large scale owing to their ability to selectively convert furfural to furfuryl alcohol. Researchers seek suitable catalysts that are less expensive for industrial application, since nickel has displayed some activity this can be a motivation to design other catalysts using first row transition metals and explore them in the conversion of furfural to other valuable products.

The use of different ligands in designing nickel complexes[2,3] may also be another avenue to explore giving more attention to the geometry of the complexes as some nickel complexes are paramagnetic which gives difficulties in characterization of such complexes specially using NMR spectroscopy. Moreover, computational studies could be performed to study the electronic structure, ligand field spectroscopy and magnetism of Ni(II) complexes. In addition, the length of the hydrocarbon chain may also be another avenue to explore in design and synthesis of siloxane complexes to increase the electron donor abilities between the metal center and Si-O surface.[1]

In-situ NMR studies to be conducted to bring about better understanding of the mechanism pathway involved in conversion of furfural to furfuryl alcohol using Ni(II) complexes.

5.2 References

1 A. Sakthivel, J. Zhao, M. Hanzlik, A. S. T. Chiang, W. A. Herrmann and F. E. Kühn, *Adv. Synth. Catal.*, 2005, **347**, 473–483.

2 N. E. Leadbeater, *J. Org. Chem.*, 2001, **66**, 7539–7541.

3 M. Kalita, K. J. Tamuli, P. Barman, B. Sarma, R. Baruah and H. P. Deka Boruah, *Polyhedron*, 2015, **97**, 140–147.

APPENDIX

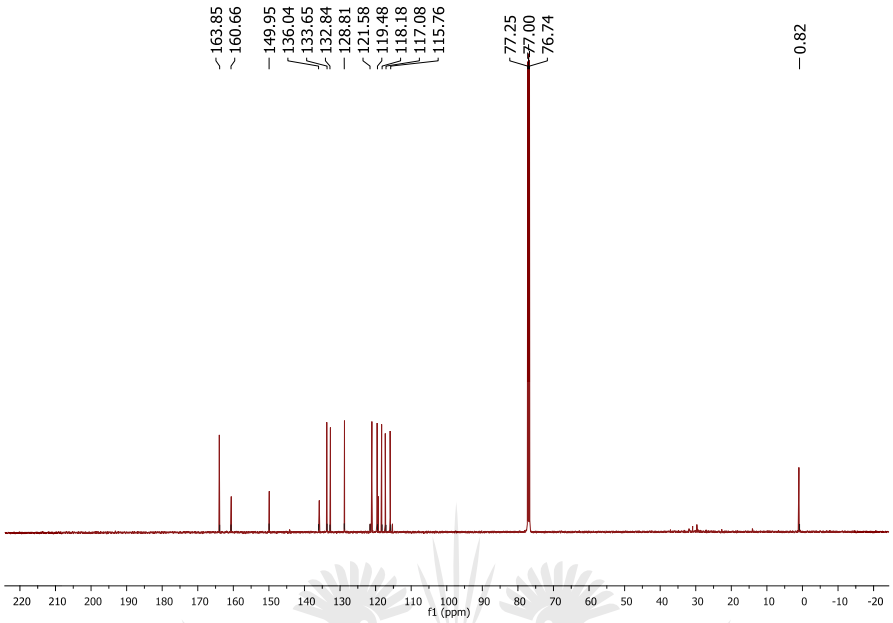

Figure A1 $^{13}C\{^{1}H\}$ NMR spectrum of ligand**, L2** in $CDCl_3$**.**

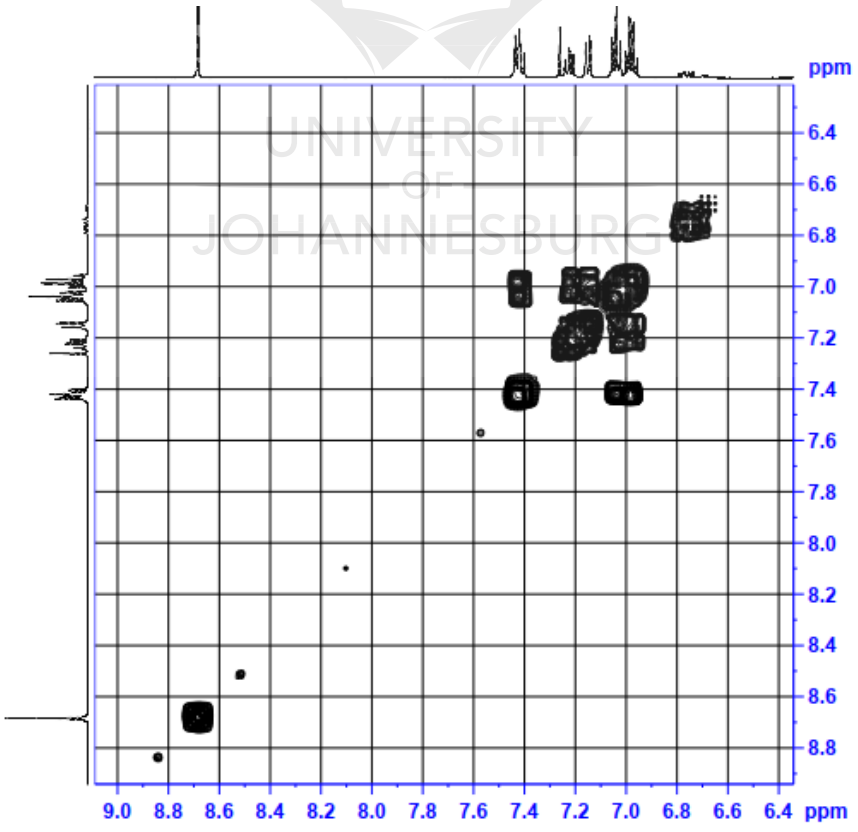

Figure A2 Cosy NMR spectrum of ligand**, L2** in $CDCl_3$.

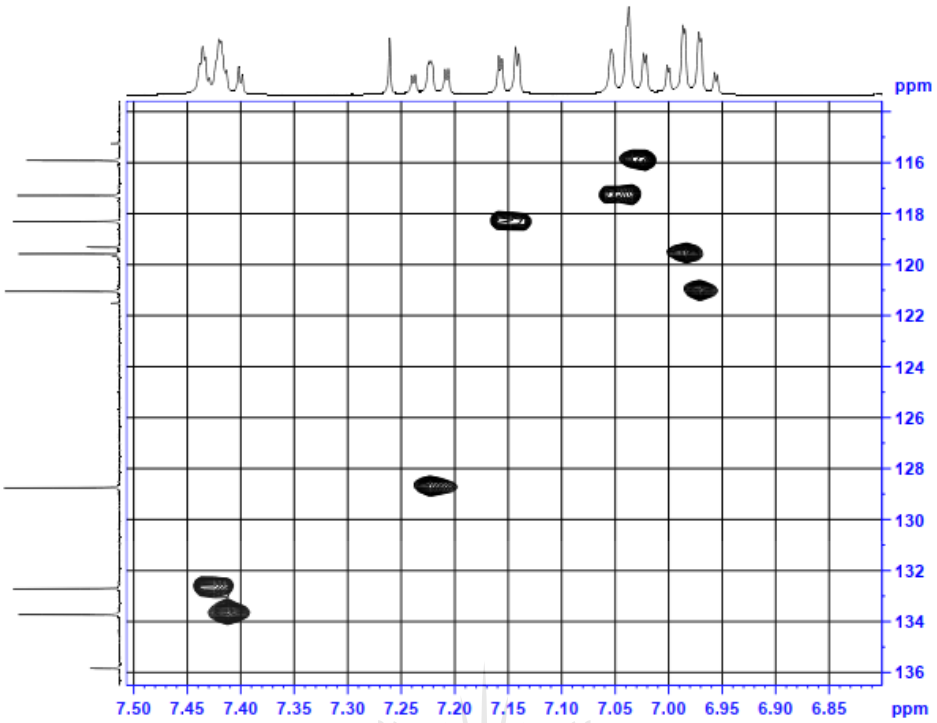

Figure A3 HSQC NMR spectrum of ligand**, L2** in $CDCl_3$.

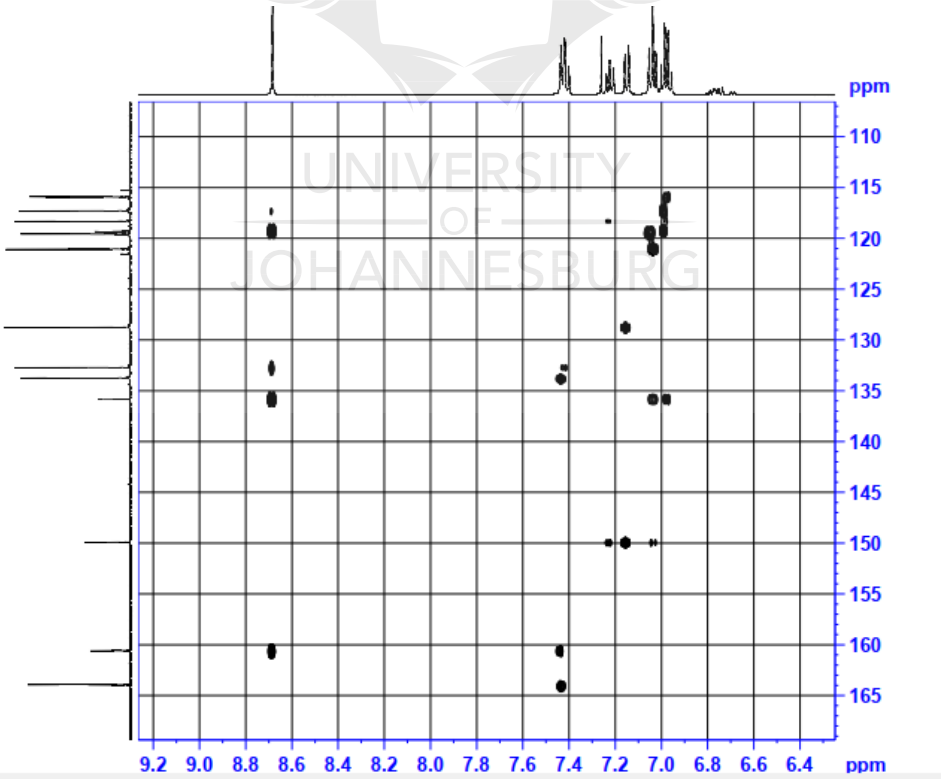

Figure A4 HMBC NMR spectrum of ligand**, L2** in $CDCl_3$.

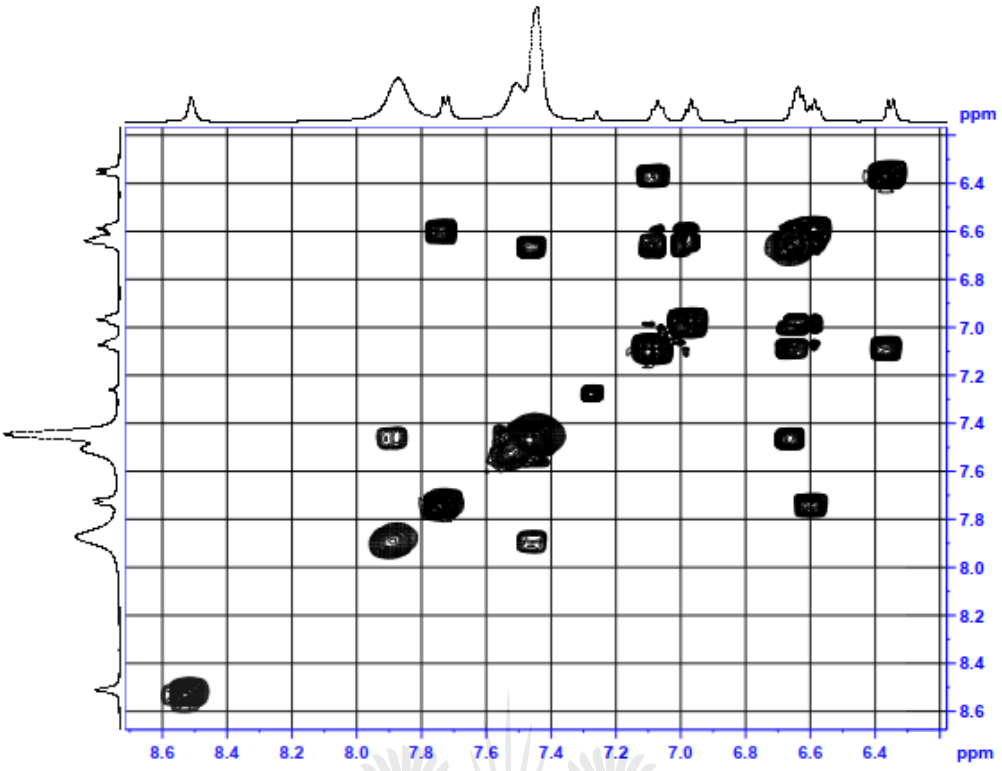

Figure A5 Cosy NMR spectrum of complex **C4** in $CDCl_3$.

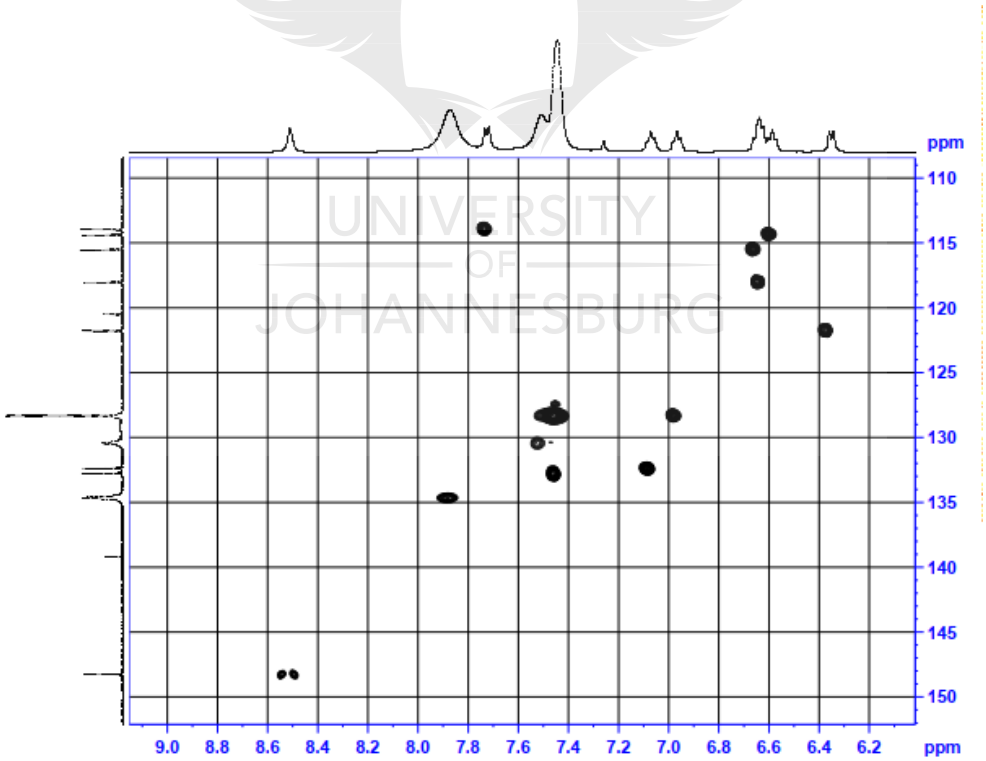

Figure A6 HSQC NMR spectrum of complex **C4** in $CDCl_3$.

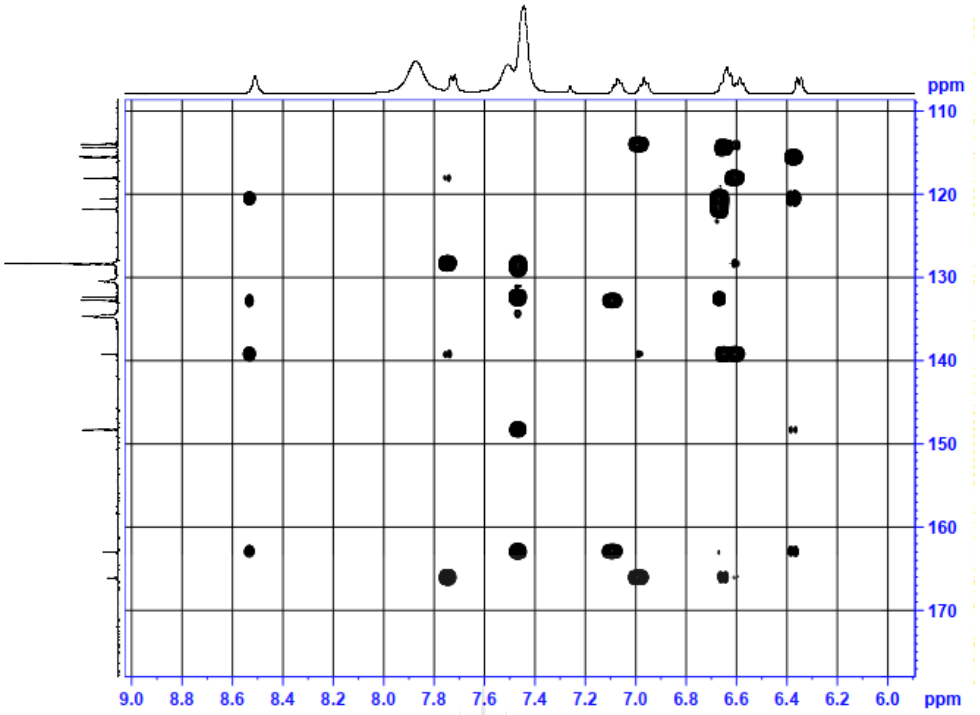

Figure A7 HMBC NMR spectrum of complex **C4** in $CDCl_3$.

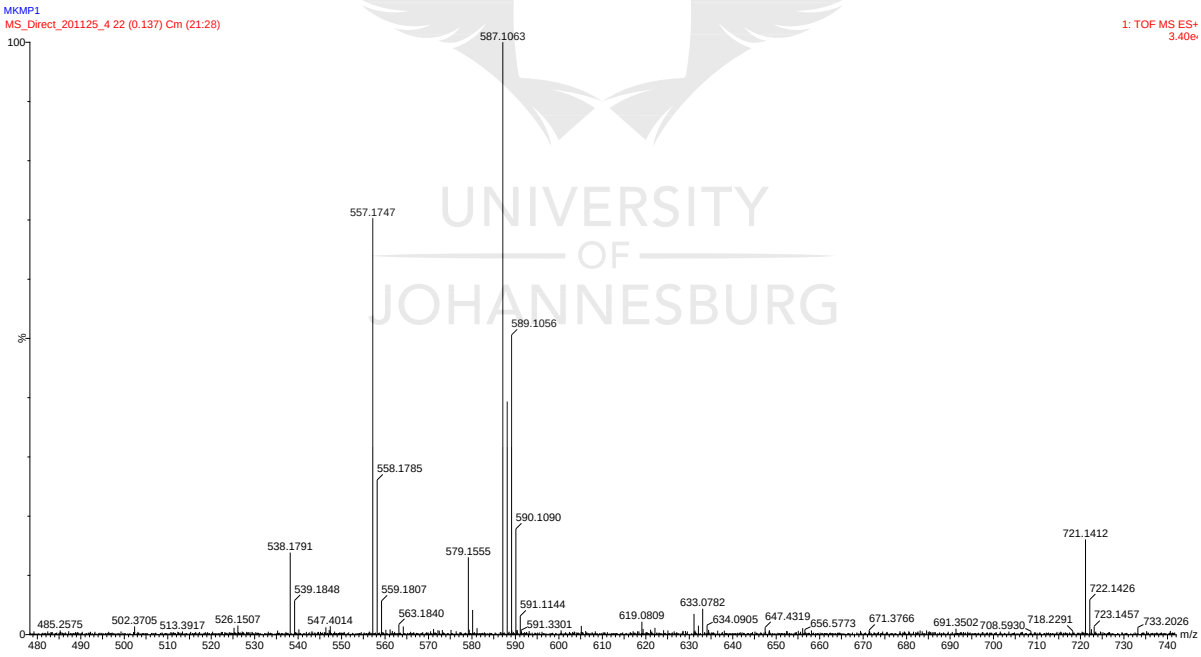

Figure A8 High resolution ESI-MS of $NiCl_2(PPh_3)_2$ recorded in the positive mode (positive): m/z = 619.0809 $[M\text{-}Cl+H]^+$.

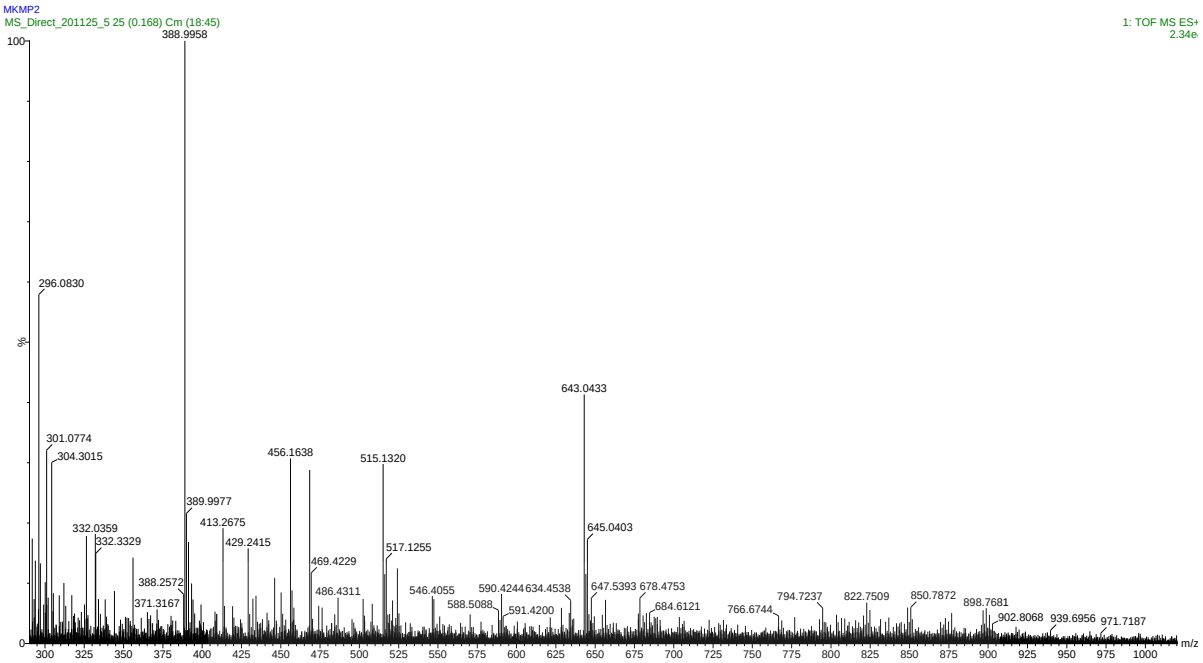

Figure A9 High resolution ESI-MS of compound (i) recorded in the positive mode (positive): m/z = 939.6956 $[M+H]^+$.